

U.S. DEPARTMENT OF COMMERCE  
National Technical Information Service

AD-A026 333

SGEMP PHENOMENOLOGY AND COMPUTER CODE DEVELOPMENT

INTELCOM R/D TECH

PREPARED FOR  
DEFENSE NUCLEAR AGENCY

11 NOVEMBER 1974

190083

 DNA 3653F

# SGEMP PHENOMENOLOGY AND COMPUTER CODE DEVELOPMENT

ADA 026333

Intelcom Rad Tech  
P.O. Box 81087  
San Diego, California 92138

11 November 1974

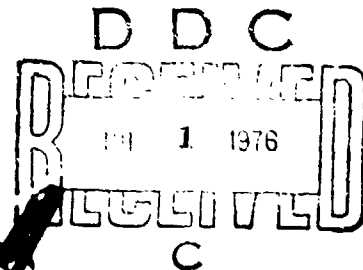
Final Report for Period October 1973—October 1974

CONTRACT No. DNA 001-74-C-0010

APPROVED FOR PUBLIC RELEASE,  
DISTRIBUTION UNLIMITED.

THIS WORK SPONSORED BY THE DEFENSE NUCLEAR AGENCY  
UNDER SUBTASK R99QAXEB089-44.

Prepared for  
Director  
DEFENSE NUCLEAR AGENCY  
Washington, D. C. 20305



REPRODUCED BY  
NATIONAL TECHNICAL  
INFORMATION SERVICE  
U. S. DEPARTMENT OF COMMERCE  
SPRINGFIELD, VA. 22161

UNCLASSIFIED

SECURITY CLASSIFICATION OF THIS PAGE (When Data Entered)

REPORT DOCUMENTATION PAGE		READ INSTRUCTIONS BEFORE COMPLETING FORM
1. REPORT NUMBER DNA 3653F	2. GOVT ACCESSION NO.	3. RECIPIENT'S CATALOG NUMBER
4. TITLE (and Subtitle)  SGEMP PHENOMENOLOGY AND COMPUTER CODE DEVELOPMENT		5. TYPE OF REPORT & PERIOD COVERED Final Report for Period October 1973—October 1974
		6. PERFORMING ORG. REPORT NUMBER INTEL-RT 8104-029
7. AUTHOR(s) Thomas N. Delmer                      Eric P. Wenaas Eugene P. dePlomb                      Andrew J. Woods		8. CONTRACT OR GRANT NUMBER(s)  DNA 001-74-C-0010
9. PERFORMING ORGANIZATION NAME AND ADDRESS Intelcom Rad Tech P.O. Box 81087 San Diego, California 92138		10. PROGRAM ELEMENT, PROJECT, TASK AREA & WORK UNIT NUMBERS NWED Subtask R99QAXEB089-44
11. CONTROLLING OFFICE NAME AND ADDRESS Director Defense Nuclear Agency Washington, D.C. 20305		12. REPORT DATE 11 November 1974
14. MONITORING AGENCY NAME & ADDRESS (if different from Controlling Office)		13. NUMBER OF PAGES <del>100</del> 112
		15. SECURITY CLASS. (of this report)  UNCLASSIFIED
		16a. DECLASSIFICATION/DOWNGRADING SCHEDULE
16. DISTRIBUTION STATEMENT (of this Report)  Approved for public release; distribution unlimited.		
17. DISTRIBUTION STATEMENT (of the abstract entered in Block 20, if different from Report)		
18. SUPPLEMENTARY NOTES  This work sponsored by the Defense Nuclear Agency under Subtask R99QAXEB089-44.		
19. KEY WORDS (Continue on reverse side if necessary and identify by block number) SGEMP                      DYNA2CYL                      Satellite Skin IEMP                      DYNASPHERE                      Currents Vulnerability                      Scaling SGEMP Experiments Calculational Methods                      Quasi-static, Dynamic E&M		
20. ABSTRACT (Continue on reverse side if necessary and identify by block number)  Two new computer codes, DYNA2CYL and DYNASPHERE, have been developed for use in system-generated EMP (SGEMP) and internal EMP (IEMP) problems.  The code DYNA2CYL solves Maxwell's equations dynamically and self-consistently in two dimensions (r and z) in the region between two concentric cylinders of finite length. The calculations are for end-on irradiation of the cylinders, which is simulated by specified emission of electrons		

DD FORM 1 JAN 73 1473

EDITION OF 1 NOV 65 IS OBSOLETE

UNCLASSIFIED

SECURITY CLASSIFICATION OF THIS PAGE (When Data Entered)

UNCLASSIFIED

SECURITY CLASSIFICATION OF THIS PAGE(When Data Entered)

20. ABSTRACT (Continued)

from either or both the outer and inner cylinders into the cylindrical cavity. The two cylinders can be isolated from one another or connected by an arbitrary load. The outputs of the code are fields and currents on the inner and outer cylinders, the potential difference between the two cylinders, and the current through the load between the cylinders.

The code DYNASPHERE solves Maxwell's equations dynamically and self-consistently in the region between two concentric spheres for specified electron emissions from the inner sphere into the cavity. The outputs of this code are similar to those from DYNA2CYL.

Parameter studies are performed, varying certain of the essential input parameters such as characteristic pulse time, fluence, dimensions, and emitted electron energy.

The codes have been further exercised to compare quasi-static solutions with the complete dynamic solutions. Ranges of validity of the quasi-static approximation are defined.

ia

UNCLASSIFIED

SECURITY CLASSIFICATION OF THIS PAGE(When Data Entered)

## CONTENTS

1. INTRODUCTION . . . . .	5
2. INCREASED COMPUTATIONAL CAPABILITY . . . . .	8
3. COMPUTER CODE VERIFICATION . . . . .	12
3.1 DYNA2CYL Code Checkout . . . . .	12
3.2 DYNA2CYL Double-Cylinder IEMP Study . . . . .	13
3.2.1 Introduction . . . . .	13
3.2.2 Problem Definition . . . . .	14
3.3 Results of Calculations . . . . .	14
3.3.1 Moderate-Fluence Results . . . . .	14
3.3.2 High-Fluence Results . . . . .	19
3.3.3 Summary of DYNA2CYL Results . . . . .	22
3.4 DYNASPHERE Code Checkout . . . . .	22
3.4.1 Comparison of DYNASPHERE and TSPHERE for SCL Conditions . . . . .	23
3.4.2 Comparison of DYNASPHERE and LFLUX for Short-Pulse Length Problem, NSCL . . . . .	26
4. APPLICATIONS AND PARAMETER STUDIES . . . . .	30
4.1 Applications . . . . .	30
4.2 Scaling Laws . . . . .	32
4.3 Parameter Study of Rise Time . . . . .	33
4.3.1 General Background . . . . .	33
4.3.2 Rise Time Variation . . . . .	38
4.4 Electron Velocity Variations . . . . .	40
4.5 Fluence Variations . . . . .	42
4.5.1 Peak Surface Currents . . . . .	42
4.5.2 Rise Times of Surface Currents . . . . .	42
4.6 Dimensional Variations . . . . .	45
5. COMPARISONS OF QUASI-STATIC AND FULLY DYNAMIC SOLUTIONS FOR ELECTROMAGNETIC FIELD CALCULATIONS IN A CYLINDRICAL CAVITY . . . . .	49
5.1 Introduction . . . . .	49
5.2 Dynamic Code . . . . .	49
5.3 Quasi-Static Approximation . . . . .	50
5.4 Code Results . . . . .	51
5.4.1 NSCL Solutions . . . . .	52
5.4.2 SCL Solutions . . . . .	60
5.5 Summary and Conclusions . . . . .	65
REFERENCES . . . . .	67
APPENDIX A — SCALING SGEMP EXPERIMENTS . . . . .	69
APPENDIX B — DYNASPHERE . . . . .	89
APPENDIX C — UPPER LIMIT FOR SGEMP-INDUCED SURFACE CURRENT ON A SPHERE, IN TERMS OF EMISSION CURRENT, FOR LONG-PULSE-WIDTH EXCITATION . . . . .	97

APPENDIX D -- DESCRIPTION OF THE PHYSICS AND MODELING USED IN THE CALCULATION OF THE ELECTRIC AND MAGNETIC FIELDS IN THE DYNACYL COMPUTER CODE . . . . .	99
APPENDIX E -- DESCRIPTION OF PHYSICS AND MODELING USED IN FIELDS AND CURRENTS IN THE TSPHERE COMPUTER CODE . . . . .	107

## FIGURES

2-1 Schematic representation of geometry for cylindrical code SGEMP calculations; missile compartment with equipment box. . . . .	9
2-2 Schematic representation of geometry for cylindrical code SGEMP calculations; configuration for SGEMP experiment . . . . .	9
3-1 Configuration used to determine the effects of the inner cylinder with the DYNA2CYL code. . . . .	15
3-2 Particle trajectories for cases of an empty cylinder, open-circuit inner cylinder, and short-circuited inner cylinder for low current density . . . . .	16
3-3 Electric field at the center of the emitting face of the exterior cylinder for three cases, low current density . . . . .	18
3-4 Magnetic field at the outer wall of the exterior cylinder at the end away from the emitting surface for three cases, low current density. . . . .	18
3-5 Particle trajectories for cases of a shorted inner cylinder and open-circuit inner cylinder, high current density . . . . .	20
3-6 Electric field at center of emitting face of the exterior cylinder for two cases, high current density . . . . .	21
3-7 Magnetic field at outer wall of exterior cylinder at the end away from the emitting surface for two cases, high current density . . . . .	21
3-8 Configuration for comparisons of the dynamic DYNASPHERE code with the quasi-static TSPHERE code and the low- fluence LFLUX code . . . . .	23
3-9 Surface currents at 90° versus time for DYNASPHERE and TSPHERE codes applied to long-pulse-length problem, low fluence. . . . .	25
3-10 Surface currents at 90° versus time for DYNASPHERE and TSPHERE codes applied to long-pulse-length problem, medium fluence . . . . .	27
3-11 Comparison of surface currents at 90° versus time from the IRT DYNASPHERE code and the Mission Research LFLUX code. . . . .	29

4-1	Resonant frequency of cavities associated with the TM modes of concentric spheres; inner radius fixed at 2 meters. . . . .	35
4-2	Surface currents at various locations on a 2-meter-radius sphere . . . . .	36
4-3	Surface current at 90° location on a 2-meter-radius sphere . . . . .	39
4-4	Surface current (normalized) at 90° for fast and slow photo-emitted electrons. . . . .	41
4-5	Surface current at 90° location on a 2-meter-radius sphere . . . . .	43
4-6	Peak surface current on a 2-meter-radius sphere. . . . .	44
4-7	Time of occurrence of peak surface current on a 2-meter-radius sphere . . . . .	44
4-8	Surface current at 90° on a 2-meter-radius sphere . . . . .	45
4-9	Surface current at 90° on a 2-meter-radius sphere . . . . .	46
4-10	Surface current at 90° on a 2-meter-radius sphere . . . . .	47
5-1	Electric fields as a function of time obtained from dynamic and quasi-static codes for parameters $\beta$ and $\eta$ which satisfy conditions for quasi-static approximation. . . . .	53
5-2	Electric fields as a function of time obtained from dynamic and quasi-static codes for parameters $\beta$ and $\eta$ which do not satisfy conditions for quasi-static approximation . . . . .	54
5-3	Ratio of peak axial electric field oscillations to peak axial electric field versus $\beta^2$ for different $\eta$ values. . . . .	56
5-4	Electric fields at the back face as a function of time obtained from dynamic and quasi-static codes for parameters $\beta$ and $\eta$ which satisfy conditions for quasi-static approximation . . . . .	57
5-5	Electric fields at the back face as a function of time obtained from dynamic and quasi-static codes for parameters $\beta$ and $\eta$ which do not satisfy conditions for quasi-static approximation. . . . .	58
5-6	Ratios of peak electric fields obtained from dynamic code to peak field obtained from quasi-static code . . . . .	59
5-7	Fractional transmitted currents versus time for different emission current levels. . . . .	61
5-8	Electric field at back versus time for low SCL case . . . . .	62
5-9	Electric field at back versus time for medium SCL case . . . . .	63
5-10	Electric field at back versus time for very high SCL case . . . . .	64

## 1. INTRODUCTION

This document describes continuing progress in the area of computer code developments, modeling, and applications for problems in internal EMP (IEMP) and system-generated EMP (SGEMP). This work is an outgrowth and extension of the effort on the quasi-static TEDIEM codes (Ref. 1 and Appendix E). The primary accomplishments are:

1. The addition of new geometries of particular interest to system-related assessments,
2. Conversion of the codes to a fully dynamic treatment,
3. Quantification of errors introduced by the quasi-static approximations,
4. A parameter exercise of the dynamic codes to determine variations of currents and fields as a function of relevant input parameters of interest.

The DYNA2CYL code was developed to treat coaxial cylinders of finite length, one located within the other. Electron emission can occur from the surface of either of the cylinders, and the two cylinders may be connected by an arbitrary load impedance. This geometry is useful for modeling satellite SGEMP as well as IEMP in cavities containing objects such as equipment boxes.

The DYNASPHERE code is similar to DYNA2CYL and was developed to treat the geometry consisting of concentric spheres with electron emission from the inner sphere. The two spheres may be either isolated or connected by a conductor. The solution technique consists of a finite-difference approach to the complete set of Maxwell's equations. Self-consistent particle motion is considered whereby the electron trajectories are altered by the electric field. The double-spherical geometry is particularly useful in the investigation of satellite SGEMP analysis and simulation studies.

**Preceding page blank**

The complete set of code geometries now available is shown in Table 1-1. These codes have been developed and refined over a period of several years and have been applied in the analysis of a number of systems of interest. Each of the geometries has been useful for different aspects of these studies, and the results have contributed significantly to the understanding of IEMP/SGEMP.

Table 1-1  
AVAILABLE CODES

Code	Geometry	Quasi-Static or Dynamic	Applications
DIODE	Parallel plate	Static	Fast-running code for pill-box geometries
SPARC	Parallel plate	Quasi-static	As above only quasi-static
TEDIEM-R0	Infinite cylinder, side-on illum.	Quasi-static	Long cylinders such as missile systems
TEDIEM-R2	Finite cylinder, end-on illum.	Quasi-static	Small cavities, equipment boxes, satellite equipment bays
TEDIEM-PC	Rod or cable over ground plane	Quasi-static	Perturbations provided by cables in space-charge region
DYNACYL	Single finite cyl. end-on illum.	Dynamic	As in TEDIEM-R2
DYNA2CYL	Concentric finite double cylinders	Dynamic	Most versatile; perturbations produced by objects within equipment bays or boxes, satellite SGEMP
DYNASPHERE	Concentric sphere	Dynamic	Satellite SGEMP
ABORC*	Arbitrary body of revolution code	Dynamic	Same as DYNA2CYL

\*Under development

The new dynamic capability of the DYNACYL code was used to determine the range of applicability of the quasi-static approximation by comparing results with the existing quasi-static TEDIEM-R2 code. Defining this range is important because this approximation is used extensively in system-related calculations, and because the quasi-static calculations are quite

straightforward and can be performed quickly on the back of the proverbial envelope to obtain quick, better than order-of-magnitude estimates

Finally, a number of parameter studies have been performed to demonstrate the code capabilities and to illustrate how fields and currents are affected by important input parameters. There are several basic input variables of interest, including:

- Pulse time history (e.g., rise time and pulse width),

- Electron energy (or velocity),

- Object size,

- Photon fluence (or magnitude of electron emission current).

It is necessary only to solve problems for a limited range of these variables. Scaling laws (Appendix A) can be applied to extend the results of the calculations to other dimensions and time histories, allowing a few studies to describe a wide range of parameters.

The remainder of this report is organized as follows.

- Section 2 - Increased Computational Capability

- Section 3 - Computer Code Verification

- Section 4 - Applications and Parameter Studies

- Section 5 - Comparisons of Quasi-Static and Fully Dynamic

  - Solutions for Electromagnetic Field Calculations  
in a Cylindrical Cavity

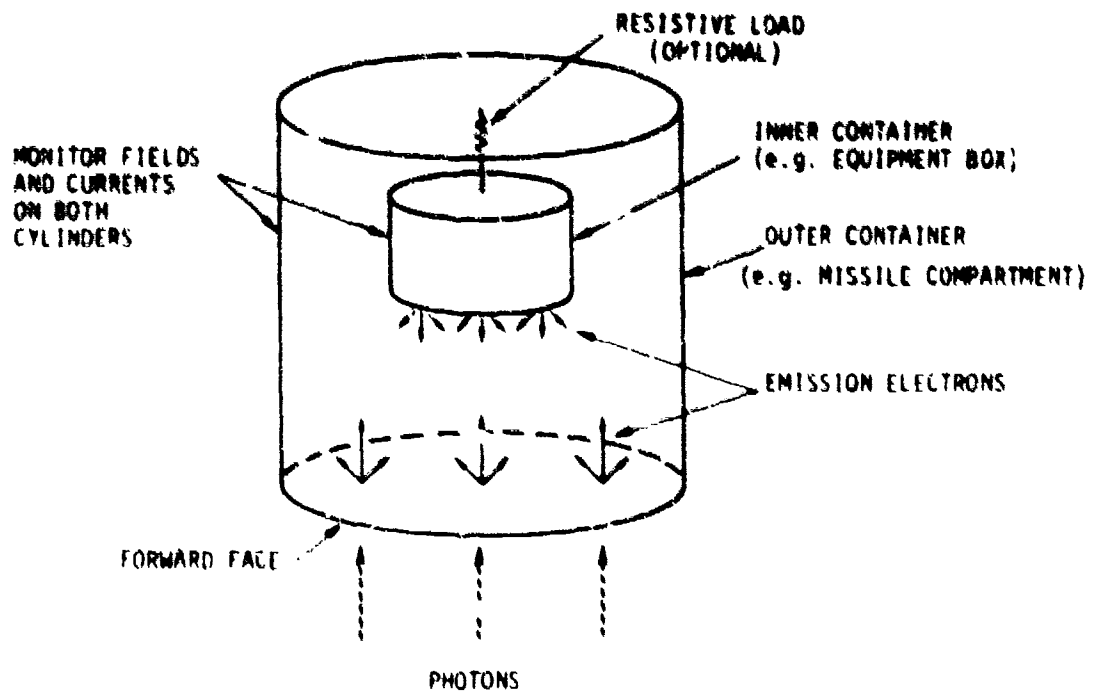
## 2. INCREASED COMPUTATIONAL CAPABILITY

The need to model increasingly complex physical situations exceeded the basic capabilities of former computer codes. Accordingly, two new codes have been generated for use in calculating electron motion and field generation. These add to our previous repertoire (Refs. 1,2 and Appendices F,E) in that they allow the solution to the full set of Maxwell's equations for geometries where there are two separate bodies. Both of the new codes are for rotationally symmetric situations, and therefore, consider two spatial dimensions. One of the codes is written in cylindrical geometry and the other in spherical geometry. Both codes require as inputs the emission characteristics of the electrons leaving the various surfaces.

The code DYNACYL, written in cylindrical geometry, is an extension of the DYNACYL code (Appendix B) to include an inner can. The numerics of the calculational procedure are very similar for the two. However, in the new version, the inner can is represented by a region of high conductivity, which is tantamount to setting the electric field to zero in a region of the inner space. A region of specified conductivity along the axis connects the inner and outer cans and allows the representation of a load between the two conductors.

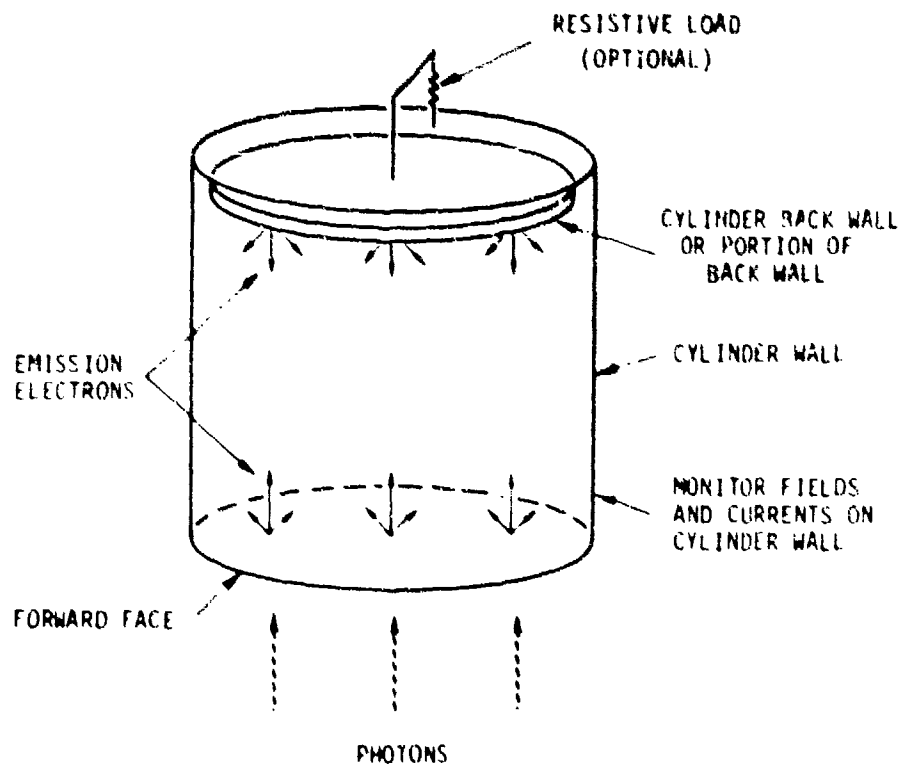
The main difference in the two cylindrical codes is in the sophistication of the inputs and outputs. Further complicating the situation is the fact that now emission can take place from either the inner or the outer can or from both. Particle tracking is also more difficult since there is now an inner region which will stop any incident electrons. However, a wide variety of problems of practical interest can be treated by using the increased capability.

Two typical problems of interest are shown schematically in Figures 2-1 and 2-2. Photons, being a typical cause of electron emission, are shown for illustrative purposes only, since the emission characteristics of the electrons are required as input.



RT-09318

Figure 2-1. Schematic representation of geometry for cylindrical code SGEMP calculations, missile compartment with equipment box



RT-09319

Figure 2-2. Schematic representation of geometry for cylindrical code SGEMP calculations; configuration for SGEMP experiment

Figure 2-1 shows the sort of situation one might expect to find when a structure is inside some container. The structure might be a satellite suspended in a test chamber for photon exposure, or it might be a piece of hardware in a compartment. In the former case, the load represents a cable monitoring the response of various systems, and in the latter case, the load represents wiring.

Figure 2-2 shows a situation where the interior cylinder has been distorted into a disk and placed at one of the outer cylinder. This configuration is of particular interest for an experimental situation where the end of a cavity may be isolated from the rest of the system by a load resistance to allow monitoring of the collected current. The influence of voltage build-up on the collector (in that it can change the current collected) is thus automatically accounted for.

The code DYNASPHERE, written in spherical geometry, is an extension of the TSPHERE code (Appendix E). The mathematical description of the code is given in Appendix B. In this case, the region between two perfectly conducting concentric spheres is treated. At present, emission is considered from the inner sphere only, and the capability of including a load between the spheres does not exist. Thus, in certain aspects, the code does not have the diversity of the DYNA2CYL code. However, as mentioned in Appendix B, the coordinate system for the field calculations is included in the program in a very general manner: the basic equations are written in general orthogonal coordinates. In practical terms, this means that variations in zone size are relatively easily incorporated. This is in contrast to the situation in DYNACYL and DYNA2CYL, where the constant zone size is built more deeply into the numerical differencing methods.

This ability to have varying zone sizes has been used to allow treatment of problems with high current densities. These cases are characterized by the fact that there are steep gradients near the emitting surface requiring fine grid spacing (small radial zone size) there, whereas this requirement does not hold far from the emitting surface.

The two computer codes have broadened our computational capability in several respects. With the ability to treat two cylinders connected by a load, we can describe many situations of interest for both prediction

purposes and experimental purposes. With the ability to consider variable zoning in the radial direction, we can describe cases where high current densities are of interest. In what follows, results of various applications of these capabilities are shown.

### 3. COMPUTER CODE VERIFICATION

Before the results of a computer code can be accepted, and prior to application of a code to systems studies, the code must be tested. These tests usually amount to comparison of results with analytical solutions where available, and comparison with other code results for regions where both codes are applicable.

The DYNA2CYL code is a relatively direct extension of DYNACYL as far as the physics involved is concerned. Verification of the new code is accomplished by comparing the results with the old code where possible. This comparison is presented below. Results are also presented and interpreted showing the logical consistency of the code. Finally, DYNASPHERE results are compared with those of two other codes. One of these is TSPHERE, which differs from the new code in that it uses a quasi-static solution to Maxwell's equations. The second of these, LFLUX, is valid only for low fluences but solves the full set of Maxwell's equations.

#### 3.1 DYNA2CYL CODE CHECKOUT

The DYNA2CYL code is a modification of DYNACYL in which an inner conducting cylinder has been placed within the simple cylindrical cavity treated by DYNACYL. Numerous checkouts have been performed to ensure proper code operation. Comparisons with DYNACYL (empty cavity) have been made for the case of increasingly smaller inner cylinders to ensure that the solutions approach the proper limit. Comparisons between the surface currents on the inner cylinder have been made with currents on the surface of a spherical-shaped object. The magnitudes and time histories (taking into account retardation) agreed well for low- and medium-fluence pulses having a 20-nsec FWHM. Comparisons were not made for high fluence, but good agreement is not expected for such cases since dynamic and geometric effects will be important due to the shortening of the effective pulse length by the space charge limiting.

## 3.2 DYNA2CYL DOUBLE-CYLINDER IEMP STUDY

### 3.2.1 Introduction

In modeling compartments of a missile or satellite for IEMP calculations, complex geometries are reduced to simple ones such as spheres or cylinders. Often a cavity which is cylindrical in shape may contain equipment boxes, greatly complicating the geometry. These equipment boxes may be connected to the outer cavity walls by circuits which have effective impedances varying from essentially short-circuit values to open-circuit values. Thus, the effect of these objects in the cavity can greatly complicate the IEMP response of the system. With the introduction of the double-cylinder IEMP capability of the DYNA2CYL code comes the opportunity to make predictions of the effects of objects in a cavity connected by arbitrary circuits to the cavity walls. The code is currently limited to an interior cylinder anywhere on the axis of the outer cylinder and connected by a resistive load to the outer cylinder (see Section 2). This geometry and circuitry can model many cases of interest with much greater accuracy than was formerly available.

Results of calculations performed with DYNA2CYL, presented in the following subsections, will show the effects on IEMP of placing an object such as an equipment box inside the cavity.

Results are presented for end-on irradiation for three cases:

1. An empty cylinder,
2. A cylinder within a cylinder (open-circuit)
3. A cylinder within a cylinder (short-circuit).

Results for both moderate and high space-charge limiting are presented. Moderate space-charge limiting occurs when the ratio of peak transmitted current reaching the rear face to the emitted current is approximately half the value at low-fluence emission. High space-charge limiting is the designation used when the ratio of transmitted to emitted current is less than 10% of the value at low levels.

The values chosen for cavity size, emitted electron energy, and time history are typical for IEMP. Although emission from all faces occurs in practical problems, forward emission from the outer cylinder face only is considered here. This facilitates the interpretation of the results and

is not unrealistic when reverse emission from objects within the cavity is less than the forward-emitted currents from the outer container walls.

### 3.2.2 Problem Definition

The basic test problem is a cylindrical cavity with a length and diameter equal to 40 cm. Monoenergetic electrons with a velocity of  $1 \times 10^8$  m/sec (20 keV) are emitted within the cavity, with a triangular pulse shape. A pulse rise time is chosen to be approximately 10 times the transit time for light across the cavity, a situation which will produce a quasi-static response at moderately low fluences and dynamic response at higher fluences. Hence, the pulse rise time is chosen to be approximately 10 nsec. Peak emission current density levels are 0.1 and 1 amp/cm<sup>2</sup>, corresponding to moderate and high space-charge limiting. For problems in which an inner cylinder is considered, a cylinder of 20 cm diameter and length has been chosen.

Fields and currents are predicted throughout the cavity. However, the electric field at the emitting face and the magnetic field at the rear surface are of particular interest. The entire problem geometry and field locations are shown in Figure 3-1.

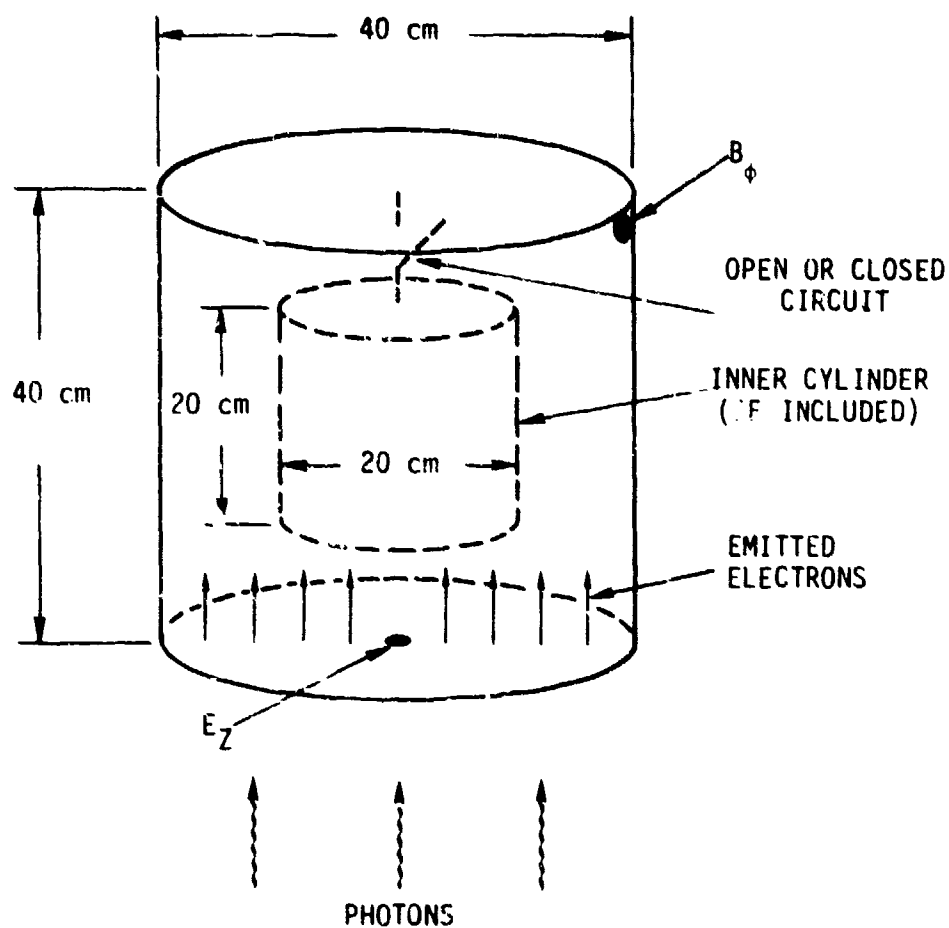
## 3.3 RESULTS OF CALCULATIONS

### 3.3.1 Moderate-Fluence Results

Results for an open- and short-circuited cylinder within a cylinder are compared to results obtained with an empty cylinder. Of primary interest is the electric field at the emitting surface and the magnetic field at the rear surface wall.

There exists a printout option in the DYNA codes which allows time-dependent tracking of electron trajectories. Electron trajectories for the three cases identified above are shown in Figure 3-2. Electron paths are shown for times near the peak of the emitted electron pulse. Because of the slow variation of the emitted electron pulse, the trajectories shown correspond to quasi-steady-state.

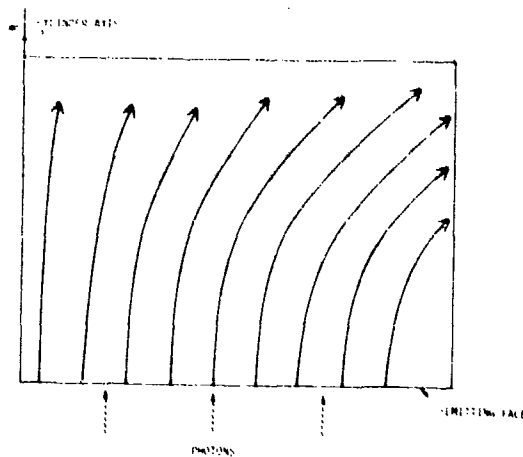
Brief comments about the cases follow.



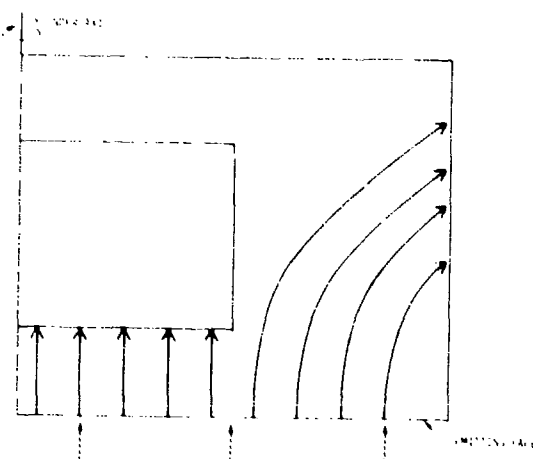
ELECTRON ENERGY = 20 keV  
 PULSE FWHM = 10 nsec  
 EMISSION CURRENT LEVELS = 0.1, 1 amp/cm<sup>2</sup>

RT-09320

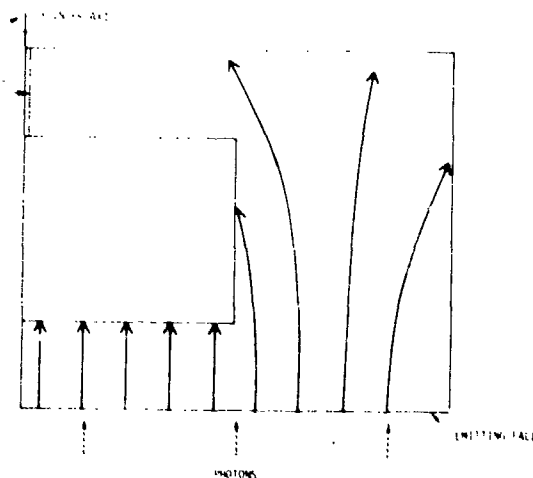
Figure 3-1. Configuration used to determine the effects of the inner cylinder with the DYNA2CYL code



Empty cylinder



Open circuit



Short circuit

Figure 3-2. Particle trajectories for cases of an empty cylinder, open-circuit inner cylinder, and short-circuited inner cylinder for low current density

a. Empty Cylinder

A modicum of space-charge limiting tends to bend electron trajectories towards the side of the can and reduce current transmitted to the rear face. In a strictly one-dimensional calculation, a fraction of the predicted charge would be returned (incorrectly) to the emitting face.

b. Open-Circuit Double Cylinder

Charge striking the inner cylinder cannot return to the emitting walls, and therefore, charge continually builds up. However, sufficient charge does not accumulate on the inner cylinder in the time frame of the pulse (moderate fluence only) to severely alter the electron trajectories.

c. Short-Circuit Double Cylinder

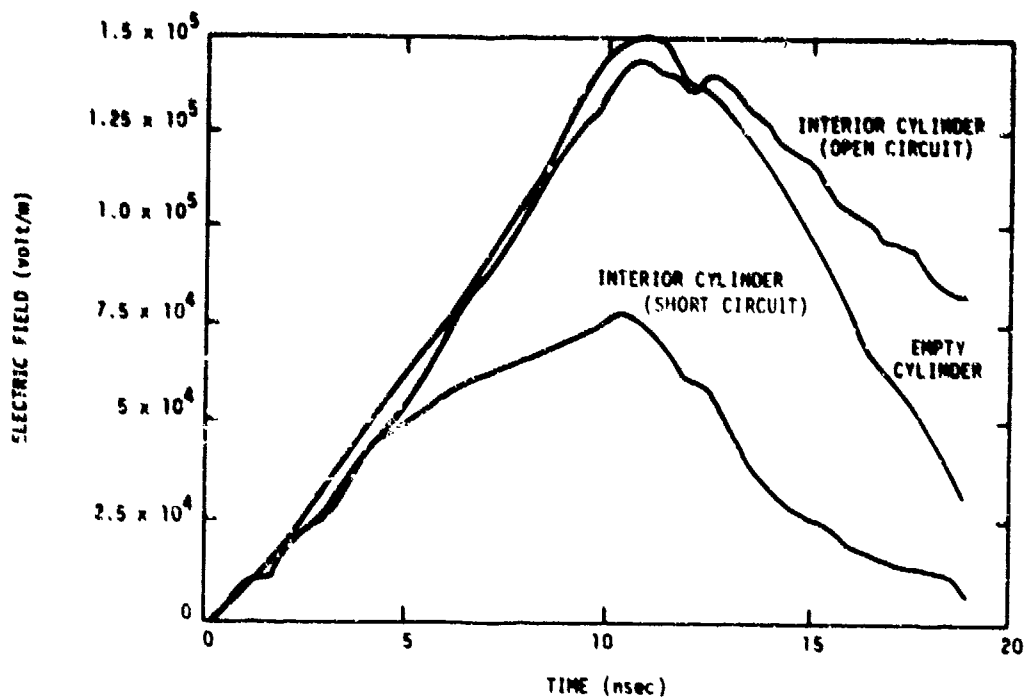
Short-circuiting the inner cylinder effectively reduces the potential at the center of the cavity, thus pulling electrons toward the center cylinder.

The electric and magnetic fields for each of the three cases are shown in Figures 3-3 and 3-4. Comments regarding differences in the fields follow.

Electric Fields

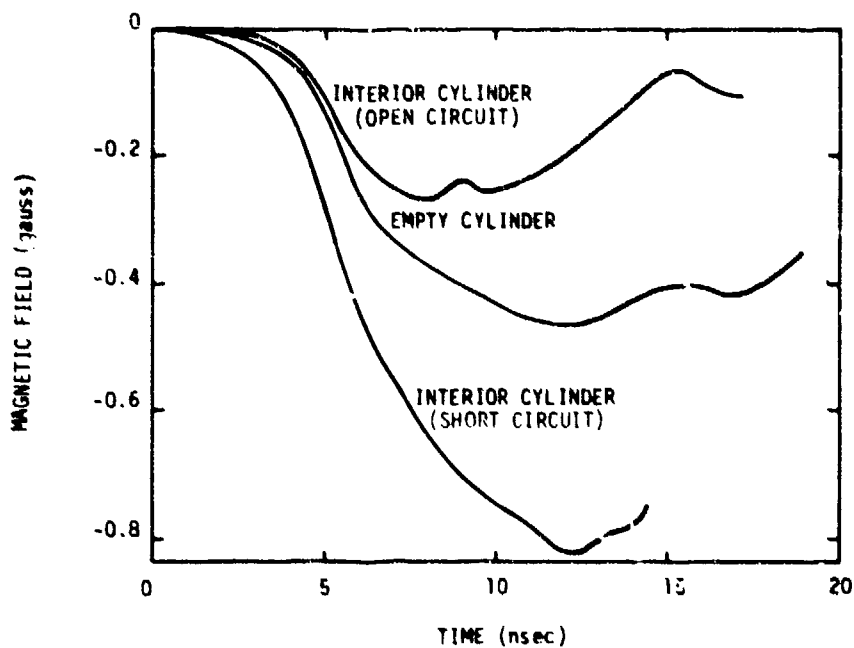
The electric fields for the empty cylinder and open-circuit cylinder are essentially the same for the first part of the pulse. The same amount of charge exists in the cavity regardless of whether it is in the free space or contained on the inner conducting cylinder. At late times, the charge in both cases tends to fall as electrons leave the cavity. However, the field remains at a significant level and in fact will reach a steady-state (non-zero) value at extremely late times for the open-circuit cylinder case. This is, of course, because charge is trapped on the isolated cylinder.

For the short-circuit cylinder, the electric field at the face increases for a time approximately equal to the electron flight time from the emitting face to the inner cylinder. After the charge strikes the inner cylinder, it quickly leaves the cavity (transit time for light is short compared to electron transit time in this problem), and the electric



RT-09324

Figure 3-3. Electric field at the center of the emitting face of the exterior cylinder for three cases, low current density



RT-09325

Figure 3-4. Magnetic field at the outer wall of the exterior cylinder at the end away from the emitting surface for three cases, low current density

field does not substantially increase thereafter, although there is some increase due to charge filling the remainder of the cavity.

#### Magnetic Fields

The magnetic field is considerably reduced for the open-circuit object within the cylinder when compared to the empty cylinder. The fields are reduced because the net current transmitted to the rear face is substantially reduced by the shadowing effect of the inner cylinder. On the other hand, the magnetic field is increased by almost a factor of two when the center cylinder is short-circuited to the rear face. The presence of the inner cylinder considerably reduces the space-charge limiting and causes more current to flow.

#### 3.3.2 High-Fluence Results

The same problem is now treated, except that the emission currents are increased by an order of magnitude to produce a high degree of space-charge limiting. Electron trajectories corresponding to the open and short-circuited inner cylinder cases are shown in Figure 3-5.

##### a. Open-Circuit Cylinder

Figure 3-5 shows electron trajectories for the open-circuit case for electrons emitted at 5 nsec, or half-way into the pulse. Charge initially strikes the inner cylinder and produces extremely high fields and potentials, causing the electrons to be deflected to either the emitting face or the side walls.

##### b. Short-Circuit Cylinder

The grounding of the inner cylinder permits the charge striking the cylinder to flow to ground. The corresponding low fields produce smaller perturbations in electron trajectories.

The electric and magnetic fields corresponding to these two cases are shown in Figures 3-6 and 3-7, and are discussed briefly below.

#### Electric Fields

The electric fields for the open- and short-circuit cases appear to be surprisingly similar. One would at first think that the electric field

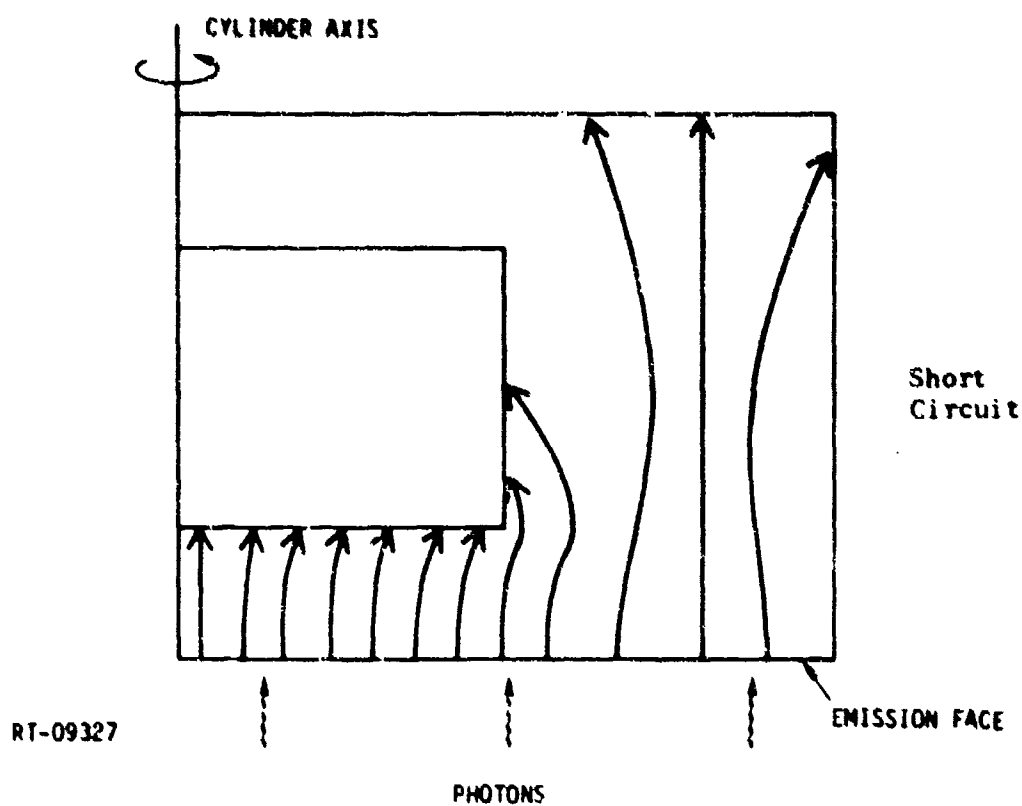
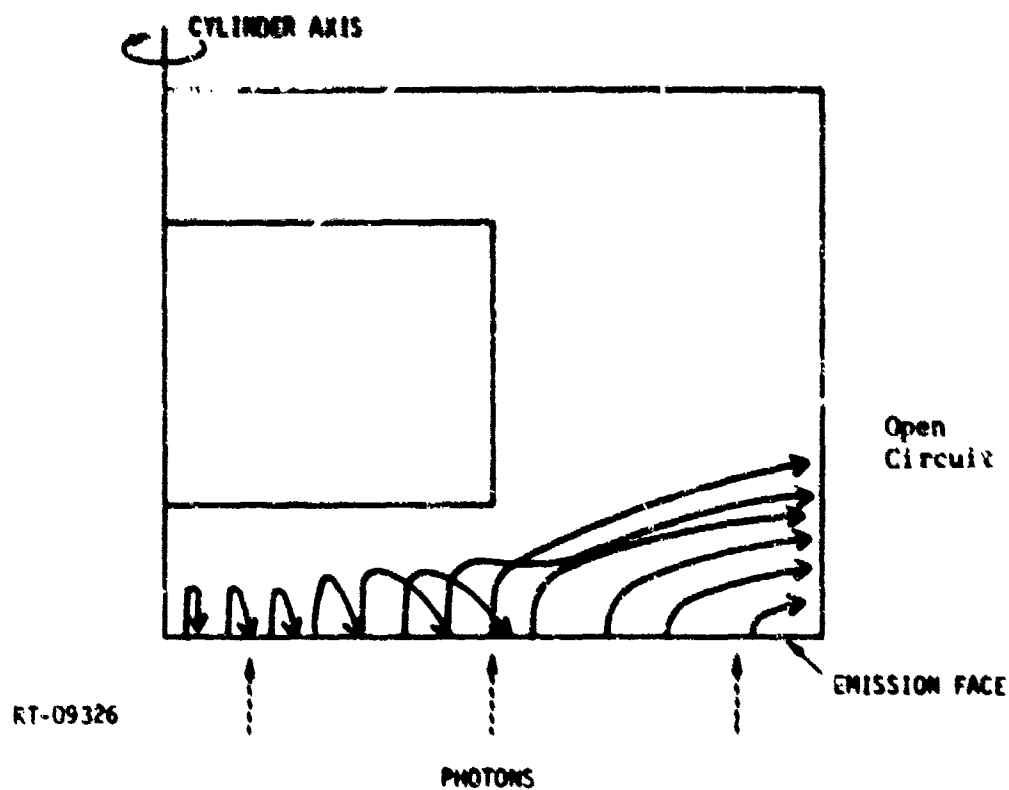
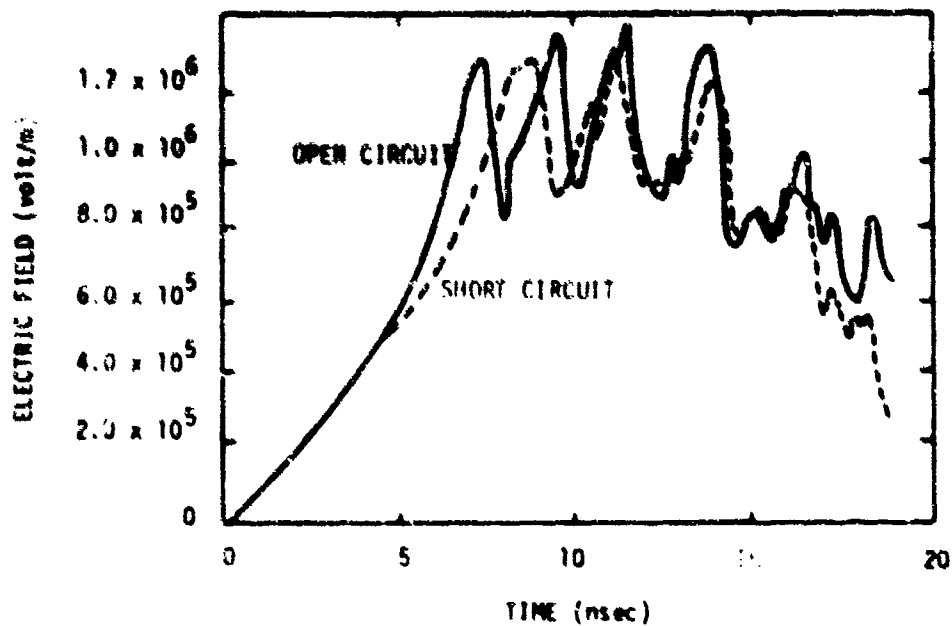
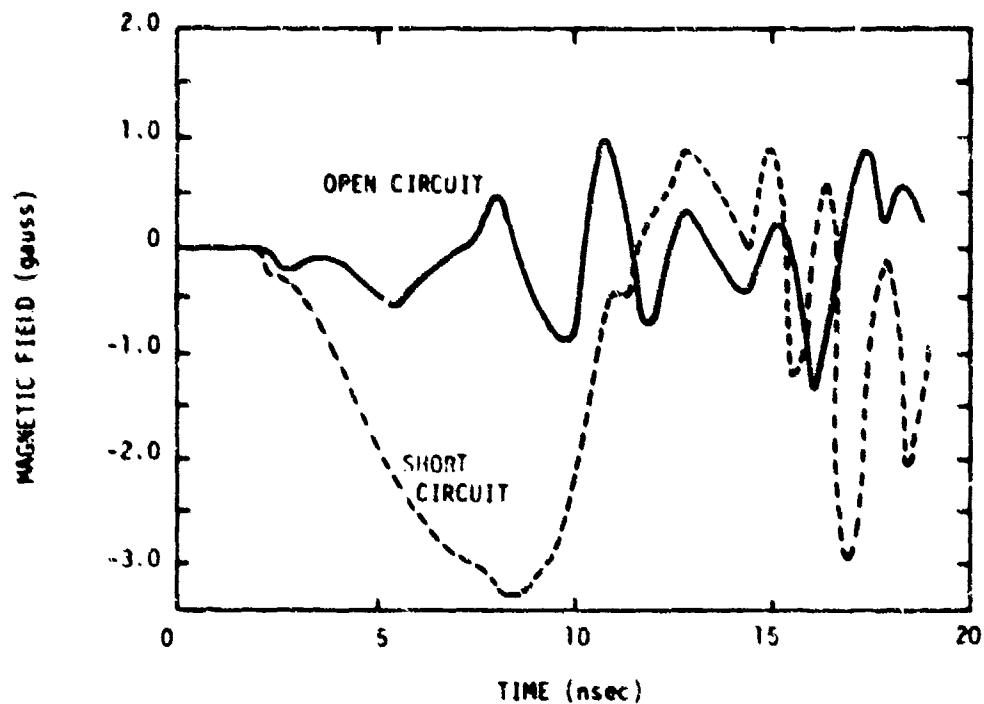


Figure 3-5. Particle trajectories for cases of a shorted inner cylinder and open-circuit inner cylinder for high current density



RT-09328

Figure 3-6. Electric field at center of emitting face of exterior cylinder for two cases, high current density



RT-09329

Figure 3-7. Magnetic field at outer wall of exterior cylinder at the end away from the emitting surface for two cases, high current density

for the short-circuit cylinder would be significantly smaller than that for the open-circuit cylinder. The fact is that, for highly limited conditions, the electric field at the emitting surface is quite insensitive to the conditions in the remainder of the cavity. The field distributions in space and potential differences between the emitting surface and points in the cavity do, however, depend strongly on the details in the cavity. Thus, the electric field at the emitting surface is not a good indicator of the degree of space-charge limiting.

The effective decrease in rise time due to the early onset of space-charge limiting excites resonant cavity modes and produces an oscillatory response in both electric and magnetic fields.

#### Magnetic Fields

Because of the high degree of space-charge limiting for the open-circuit cylinder, relatively small amounts of current are transmitted across the cavity. The magnetic fields are lower than for the short-circuit cylinder.

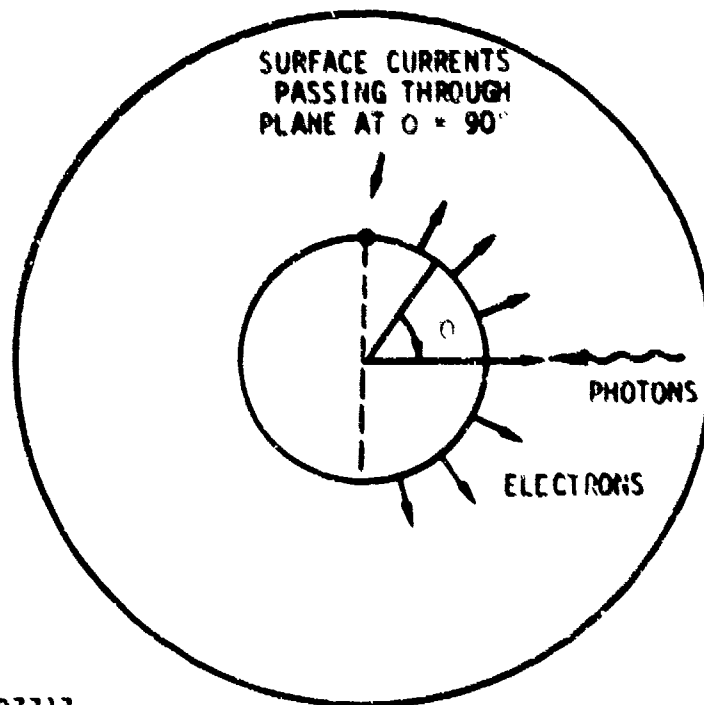
#### 3.3.3 Summary of DYNA2CYL Results

In summary, the fields and currents within a cavity equipment box, satellite, etc., can be significantly affected by the presence of objects and the grounding used for these objects. The response in terms of magnetic fields and transmitted currents can be significantly increased by the reduction of the space-charge barrier. On the other hand, highly space-charge-limited electric fields in the vicinity of emitting surfaces (e.g., where many systems cables may be located) are insensitive to objects within the cavity. There, a fairly accurate description of fields within the cavity may be possible even when the cavity is quite irregular.

#### 3.4 DYNASPHERE CODE CHECK-OUT

In this section, comparison is made between DYNASPHERE and the quasi-static code TSPHERE to check the accuracy of self-consistent routines. In the following subsections, comparison is made with the semi-analytic code LFLUX (Ref. 3) at low fluence where space-charge limiting is not a consideration.

The configuration used for comparison is shown in Figure 3-8, in which electrons are emitted from the inner half-sphere. Surface currents and electric fields are computed and compared in check-out problems. Comparisons are presented between the total surface current on the sphere passing across a plane through the sphere at  $90^\circ$  from the incident photon flux.



RT-07717

Figure 3-8. Configuration for comparisons of the dynamic DYNASPHERE code with the quasi-static TSPHERE code and the low-fluence LFLUX code

#### 3.4.1 Comparison of DYNASPHERE and TSPHERE for SCL Conditions

Surface currents obtained on the inner sphere of a concentric sphere geometry, using the newly developed DYNASPHERE code, have been compared with results obtained from the earlier TSPHERE code under both non-space-charge-limited (NSCL) and space-charge-limited (SCL) conditions. TSPHERE is a concentric-sphere SCMP code which is the forerunner to DYNASPHERE. A complete description of TSPHERE can be found in Reference 2. TSPHERE and DYNASPHERE treat similar geometries, but TSPHERE employs the quasi-static approximation to obtain electric fields and DYNASPHERE employs the full Maxwell's equation set to obtain the fields.

Results obtained with the two codes are expected to agree for long-pulse-length low-fluence problems where the quasi-static approximation has been shown to be valid. Comparisons were performed for a concentric spherical region with an inner radius of 2 meters and an outer radius of 5 meters. A slowly rising pulse with a long pulse width was chosen for purposes of comparing with the quasi-static code. The emission current pulse is triangular with 100-nsec rise and fall times. The pulse rise time is approximately equal to the electron flight time across the cavity. A spectrum of electrons with an average energy of 5 keV was emitted outward from the inner sphere with a level proportional to  $\cos \theta$ , falling off to zero at the side ( $\theta = 90^\circ$ ) of the inner sphere. Peak emission current densities of 0.42 and 4.2 amp/m<sup>2</sup> were chosen, corresponding to little space-charge limiting and moderate space-charge limiting.

Electrons were emitted from six points on the forward half of the inner sphere. TSPHERE employed 17 radial and six angular zones. The radial zones were finer near the inner sphere and coarser near the outer sphere. This zoning was used to describe the steep gradients which occur near the inner sphere under high-fluence conditions. DYNASPHERE employed 17 x 6 zoning grids with equal spacing everywhere for the low- and medium-fluence cases. Thirty radial and six angular zones equally spaced were employed for the high-fluence case. The emission electron energy spectrum was broken into 12 bins. Results were obtained for the first 350 nsec of the pulse.

#### a. Low-Fluence Results

Results for the surface currents on the inner sphere at  $90^\circ$  to the incident photon direction are shown in Figure 3-9. Agreement between the codes for the low-fluence case seems to be good. This agreement is expected because of the long pulse length and lack of fields affecting particle trajectories. Note the time labelled  $\pi R/2c$  on the graphs. This is the time required for light to travel from the  $\theta = 0$  position to the  $\theta = 90^\circ$  position on the inner sphere. The DYNASPHERE surface current displays a time lag evidenced by its values being somewhat lower than TSPHERE results during this time interval. TSPHERE does not take this retardation into account, so its surface currents rise more steeply at the beginning of the pulse.

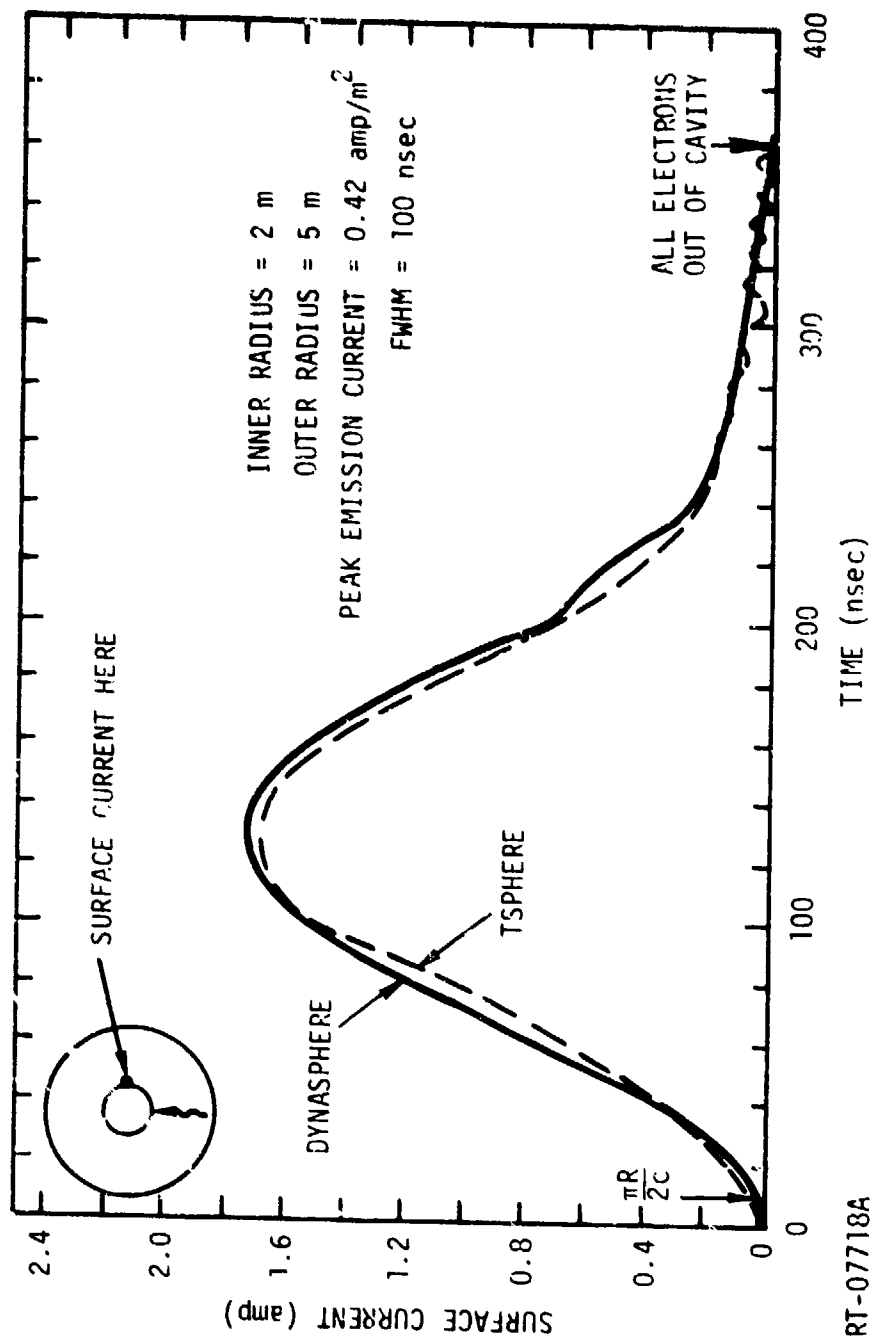


Figure 3-9. Surface currents at 90° versus time for DYNASPHERE and TSPHERE codes applied to long-pulse-length problem, low fluence

Note that the peak of the surface current occurs at a time later than the peak of the emitted current pulse. The reason for this is that the electrons must move out almost one spherical radius before they induce the maximum current on the sphere. Thus, the lag between the emission current peak and the surface current peak is approximately equal to the time required for the electron to move out to a large fraction of the sphere's radius.

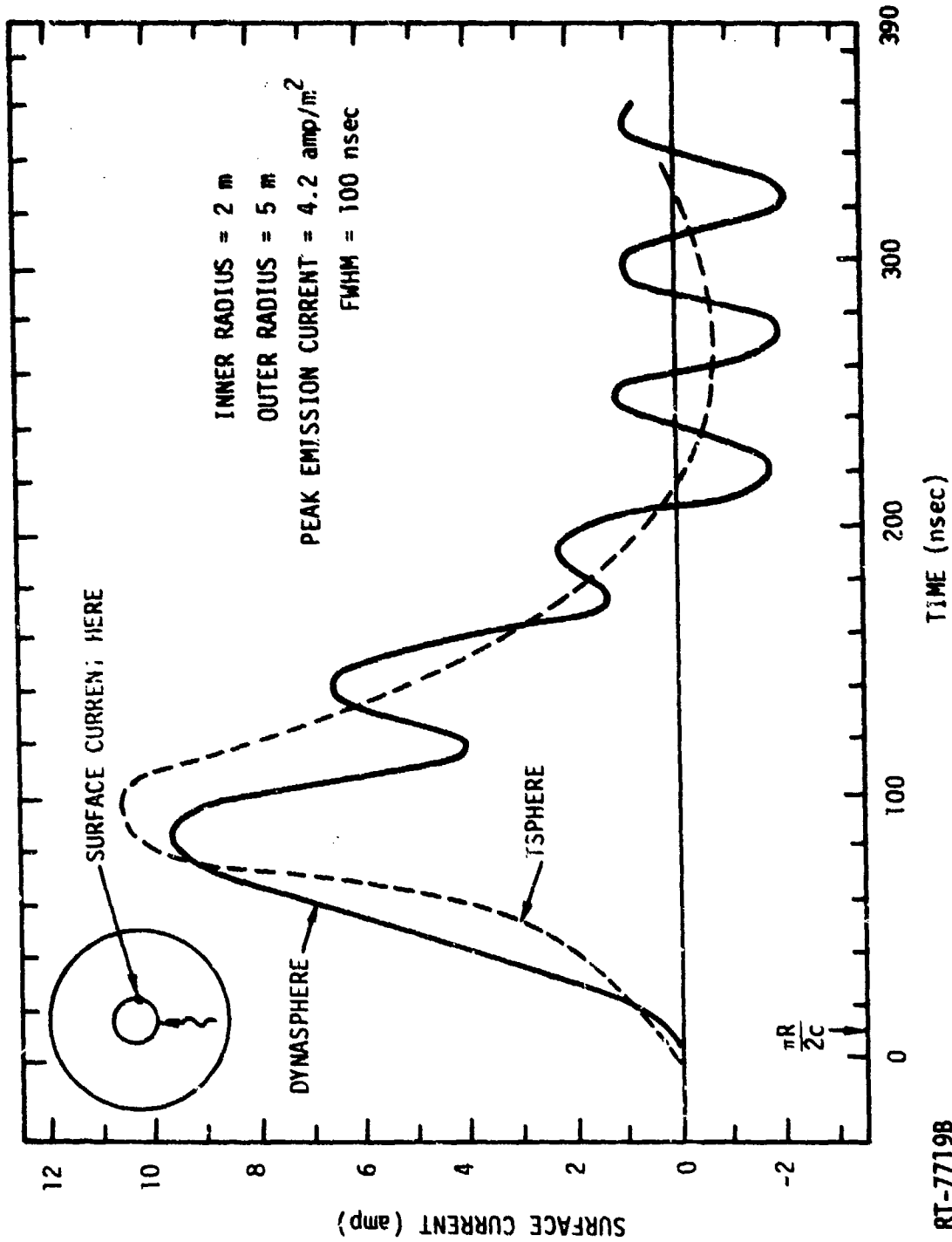
#### b. Moderate-Fluence Case

At higher fluences there is space-charge limiting. The emitted pulse of current begins rising until a point is reached at which the currents pulled back to the sphere are approximately equal to the emitted currents.

The currents induced on the sphere do not substantially increase after this point, and therefore, the effective rise time of the driving function (emitted electrons) is decreased. When this happens, cavity oscillations may be introduced. This is the case here, and the oscillations are shown in Figure 3-10. Note that both the quasi-static TSPHERE and dynamic DYNASPHERE show the decreased pulse rise time (compare rise times in Figures 3-9 and 3-10), but that the DYNASPHERE code displays an oscillating solution characteristic of the dynamic response of the cavity, whereas TSPHERE does not. The theoretical characteristic period of oscillation for a double spherical cavity (radii 2 and 5 meters) is approximately 50 nsec, a value which compares favorably with the results of Figure 3-10.

#### 3.4.2 Comparison of DYNASPHERE and LFLUX for Short-Pulse-Length Problem, NSCL

The comparison of DYNASPHERE with an existing SGEMP code reported in the previous section was valuable for testing the new code for consistency with earlier methods for long-pulse-length problems and space-charge-limited currents. That comparison does not provide a test of the dynamic capabilities of the new code, however. To obtain this check-out, DYNASPHERE was compared with the existing LFLUX code on a moderately short-pulse-length problem. LFLUX is a concentric-sphere SGEMP code in which electron motion is not consistent with the electric and magnetic fields. Therefore, its results are valid only for low-fluence conditions.



RT-7719B

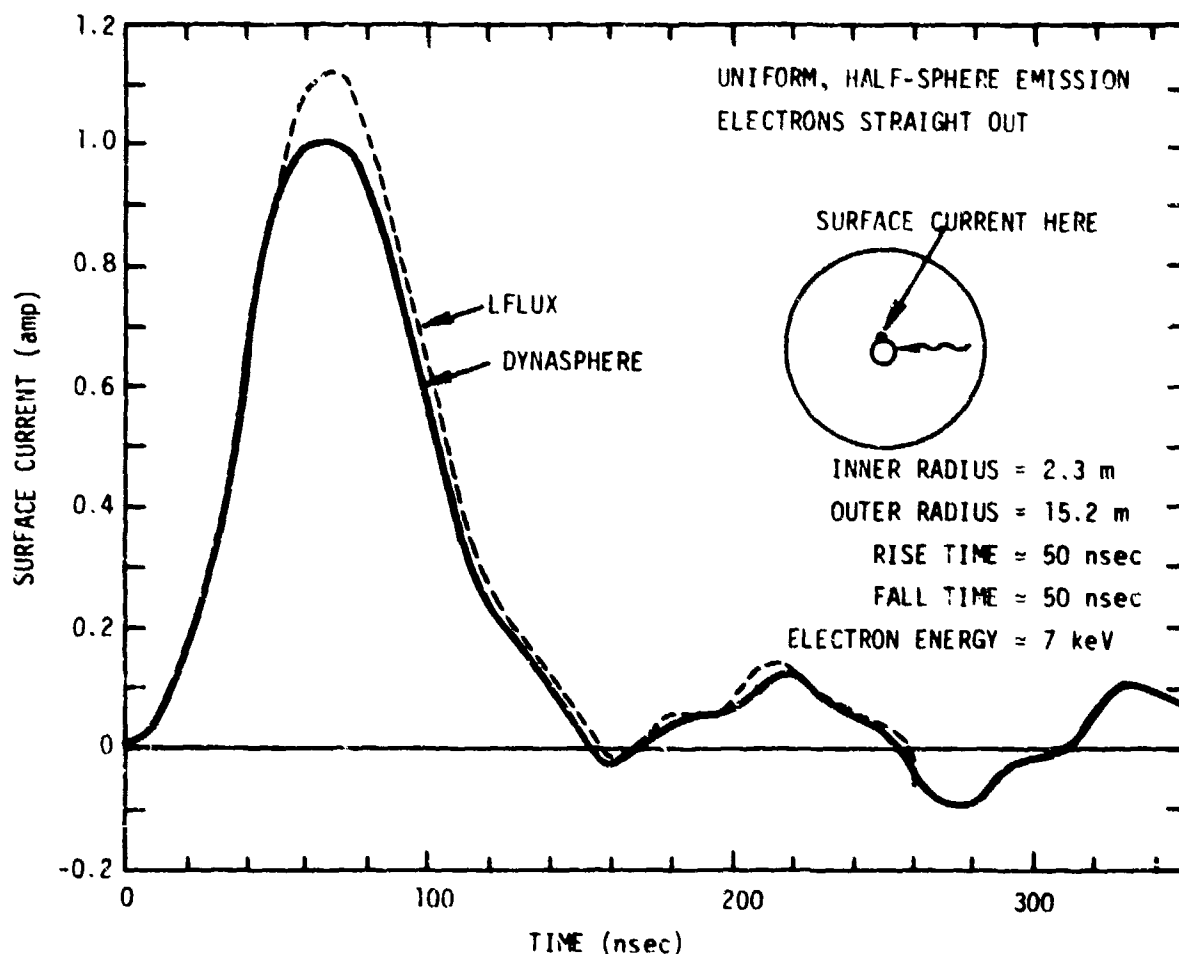
Figure 3-10. Surface currents at 90° versus time for DYNASPHERE and TSPHERE codes applied to long-pulse-length problem, medium fluence

The comparison of DYNASPHERE with LFLUX was made on a low-fluence problem in which the pulse width was comparable to the  $L/c$  time of the cavity. The  $L/c$  time is the characteristic time for light to traverse the cavity. Studies made with the IRT DYNACYL code for the solution of Maxwell's equations in finite cylinders have shown that pulse widths comparable to the photon flight time can cause large effects directly attributable to the dynamic terms in Maxwell's equations (see Section 5). This test problem should, therefore, be a good check-out of the dynamic capabilities of the DYNASPHERE code.

The configuration of the test problem is illustrated in Figure 3-8 and in the inset of Figure 3-11. The inner and outer sphere radii were 2.3 and 15.2 meters, respectively. Electrons of 7-keV energy were emitted straight out from the forward half of the inner sphere with a uniform spatial distribution. The pulse had a 45-nsec rise time, 10-nsec flat top, and 45-nsec fall time. The photon and electron flight times were roughly 40 and 200 nsec, respectively. The peak emission current density was  $0.11 \text{ amp/m}^2$ , which resulted in no effect of the fields on electron trajectories.

In the DYNASPHERE runs, the region between the spheres was broken into 45 radial and 10 angular zones of equal spacing. Electrons were emitted from the centers of the angular zones, which were in the forward direction. The time step employed was 5 nsec, which allowed for a reasonable description of the emission-electron pulse shape without causing large computer costs. LFLUX employed approximately 120 radial zones. The angular dependence in LFLUX is done semi-analytically, employing Legendre polynomials. In this case, the first five were used, which was equivalent to six angular zones in the direct-differencing method. The time step was 1.33 nsec. The velocity of the electrons is  $5 \times 10^7 \text{ m/sec}$ . A quick calculation will show that both the DYNASPHERE and LFLUX time steps were consistent with their radial zone sizes in that the electrons moved approximately one zone each time step. DYNASPHERE zoning is somewhat rougher than LFLUX zoning because its capability to handle the entire fluence range requires particle-following to obtain currents as opposed to analytically specifying them. This increased capability results in higher computer costs.

The results of the comparison are shown in Figure 3-11. Surface currents at  $90^\circ$  on the inner sphere obtained from the two codes are plotted versus time. Agreement is seen to be excellent. The minor disagreements may be attributable to the rougher grid sizes employed by DYNASPHERE. Both codes show roughly the same values for the peak surface current and also the peak values in the oscillations due to cavity resonances. Also, the period of the resonances is the same in both codes. This period corresponds roughly to the time for light to traverse the cavity, which is the period expected for the oscillations.



RT-07721A

Figure 3-11. Comparison of surface currents at  $90^\circ$  versus time from the IRT DYNASPHERE code and the Mission Research LFLUX code. Medium-pulse-length case with pulse length  $\ll$  electron flight time, low fluence.

#### 4. APPLICATIONS AND PARAMETER STUDIES

Dynamic, time-dependent codes now exist to treat several geometries of interest for systems and phenomenology studies. These codes have been exercised over a range of parameters of interest to investigate the characteristics of the solutions and sensitivities to the various input parameters. A number of results from these parameter studies are presented here.

The primary input parameters of interest are:

1. Emitted electron energy (or velocity) spectrum,
2. Dimensions,
3. Pulse time history,
4. Emitted current levels (or photon fluence).

Many variations are possible, including spatial distribution of emitted electrons, geometry variations, emissions from various surfaces, time-dependent emitted-electron energy spectra, effects of time-phasing electron emission (i.e., angle of incidence effects), etc. The study reported here is restricted to the four basic input variables identified above because they appear to be the most fundamental as well as the most interesting. Also, certain of the parameter variations mentioned above (such as effects of emitted angular distribution) were reported previously (Ref. 3).

##### 4.1 APPLICATIONS

Two fundamentally different types of problems can be treated by either the DYNACYL or DYNASPHERE code. One consists of the "outside problem," in which electrons are emitted from the surface of the inner object towards the outside surface. The inner object is representative of an isolated body such as a satellite, while the outer object can be representative of a satellite test chamber. The external response of the object in free space may be investigated by moving the outer boundary out to a very large distance, thereby approximating a surface at infinity.

The second type of problem is the "inside problem," consisting of emission from the outer wall towards the inside in which there might or might not be an inner object. If present, the inner object might or might not be connected to the outer boundary wall. The outer cavity wall is representative of an equipment box, an electronics box, or a missile cavity, while the inner object might be an equipment box or other structural element.

The outside problem described above has become known as the system-generated electromagnetic pulse (SGEMP) problem, while the inside problem has retained the name of internal electromagnetic pulse (IEMP) problem. The nomenclature is admittedly confusing, and the distinction between the two problems diminishes as the cavity becomes more and more open to the outside.

In this section, we consider only the outside problem and treat the inside problem in the next section. The DYNASPHERE code is exercised using a wide range of variables.

In the following studies, calculations were made for a 2-meter-radius sphere with electron emission occurring from one-half the sphere, as shown in Figure 3-8. The electron energy distribution is approximately Maxwellian with an average velocity of 0.1 to 0.2c unless otherwise noted. Pulse time histories are triangular, with rise times equal to the pulse widths. Electron fluence levels are variable and have been adjusted to correspond to either low, medium, or high space-charge limiting. "Low-fluence" solutions correspond to emission levels where there is no space-charge limiting and the solution is essentially linear. All charge emitted from the inner sphere is transmitted to the outer sphere. "Medium fluence" corresponds to the situation where a modicum of limiting occurs and approximately 10% of the emitted charge is able to escape from the inner sphere to the outer sphere. "High fluence" corresponds to a great deal of limiting whereby only 1% or less of the emitted charge escapes.

In all cases, the response parameter of interest has been chosen to be the surface current crossing a plane which passes through the sphere at an angle  $\theta$  as shown in Figure 3-8.

Before presenting the results of the parameter study, a few remarks about scaling laws will be made to indicate how the results of the present study can be generalized.

#### 4.2 SCALING LAWS\*

A detailed discussion of scaling laws is given in Appendix A. A summary of these results follows.

Solutions can be obtained directly for a whole class of problems from a single solution obtained for one set of parameters. Thus, the solution for a single set of parameters has a wider range of applicability than for the particular set of parameters chosen. Solutions are identical if the input parameters are changed by the following factors.

$$\begin{aligned}t' &= t/\alpha && \text{(time)} \\R' &= R/\alpha && \text{(dimension)} \\I' &= \alpha I && \text{(fluence)} \\v' &= v && \text{(electron velocity)}\end{aligned}$$

The solution scales if the time and dimensions are compressed by  $\alpha$ , the incident fluence (or total number of electrons) is increased by the same factor  $\alpha$ , and the electron velocity (energy) is unchanged. When the input parameters are varied in this first fashion, the electromagnetic field quantities will change in the following way.

$$\begin{aligned}E' &= \alpha E && \text{(electric field)} \\H' &= \alpha H && \text{(magnetic field strength)} \\V' &= V && \text{(potential)} \\I' &= I && \text{(current)} \\J' &= \alpha^2 J && \text{(current density)} \\\rho' &= \alpha^2 \rho && \text{(charge density)}\end{aligned}$$

As an example, consider the solution to a problem obtained with a pulse of characteristic time  $\tau$ , dimension  $L$ , peak current density  $J_p$ , and electron velocity  $v$ . The solutions obtained for this problem are denoted by  $E$ ,  $H$ ,  $V$ ,  $I$ ,  $J$ , and  $\rho$ . For problems in which the pulse characteristic time is shortened by  $\alpha$ , the dimensions made smaller by  $\alpha$ , and the peak

---

\*The work described in Section 4.2 and in Appendix A was carried out at IRT, supported by IR&D funds.

emission current density increased by  $a^2$  (one factor of  $a$  for the increase in fluence and one factor for the decrease in pulse width), the solutions will be  $aE$ ,  $aH$ ,  $I$ ,  $a^2J$ , and  $a^2p$ .

The solutions presented in the following sections were obtained for a specific set of parameters characteristic of those found in certain problems of interest. However, these results can be directly scaled to obtain solutions for many other ranges of parameters of interest.

### 4.3 PARAMETER STUDY OF RISE TIME

#### 4.3.1 General Background

A parameter study of pulse rise time has been performed in which the rise time and pulse width (e.g., primary frequency components) are varied through a range where dynamic or resonant effects may be important. Resonances are usually excited when the excitation pulse has significant energy content in the frequency range of the structural resonances. Generally, this occurs when the pulse has a rise time and pulse width shorter than the transit time of light across the object of dimension  $L$ ,

$$t_r \lesssim L/c.$$

Higher-order modes, of course, can be excited with pulses of shorter rise times (higher-frequency content).

The lowest-order mode for a sphere of radius  $R$  is approximately

$$\omega = \frac{0.8c}{R},$$

which corresponds to a frequency of  $0.8c/2\pi R$ . The lowest-order mode for the sphere can be strongly excited with a pulse having a characteristic time in the range\* of

$$t_r \approx \frac{0.34}{f} = \frac{0.27R}{c}.$$

Thus, a pulse of approximately 16-nsec rise time and width may couple efficiently to the 2-meter-radius sphere considered in this parameter study.

---

\*A pulse of rise time  $t_r$  has a significant amount of energy close to the frequency  $f = 0.34/t_r$ .

The previous discussion pertains to an isolated sphere in free space. However, DYNASPHERE solutions are obtained with an outer spherical boundary. This boundary will not perturb the solution for the isolated sphere for the period of time required for light to traverse to the outer wall and back to the inner surface. This period of time is designated "clear time" and is simply

$$t_c = \frac{2(R_0 - R)}{c},$$

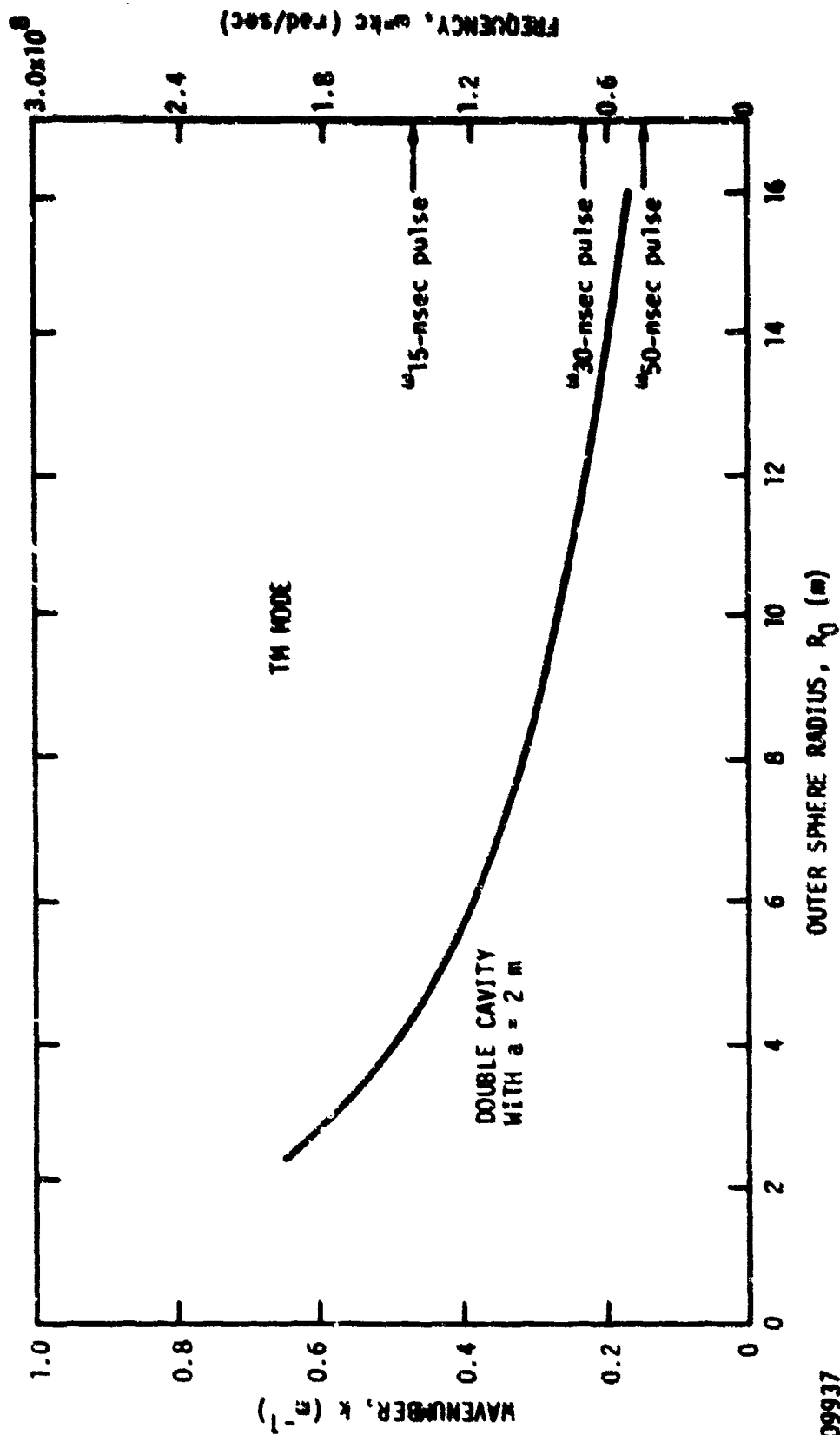
where  $R_0$  is the outer boundary wall radius.

Resonant frequencies for concentric spheres are shown in Figure 4-1 as a function of outer spherical radius for an inner sphere radius of 2 meters. The primary frequency content in 50-, 30-, and 15-nsec pulses are marked on the vertical scale for comparison.

Surface currents for a 2-meter sphere (outer boundary radius of 10 meters) as a function of time are shown in Figure 4-2 for various angular slices around the sphere. The pulse width and rise time of the emitted electron pulse is 50 nsec. It is evident from Figure 4-1 that such a pulse has a frequency content below the lowest-order mode associated with the double-spherical cavity and, therefore, should not strongly excite the cavity. Indeed, the solutions shown in Figure 4-2 do not display any oscillatory behavior.

We now point out several characteristics of these solutions. Note that the peak in surface current occurs at approximately 20 nsec after the peak of the emitted electron pulse. This delay time cannot be attributed to the finite speed of light between  $\theta = 0$  and  $\theta = 90^\circ$ , which is only on the order of  $t_d = (\pi/2)(R/c) = 10$  nsec. Furthermore, if it were due to light delay, the surface currents would peak at different times for the different angles.

The delay is caused by the finite time required for the electrons to move away from the sphere a sufficient distance to induce maximum surface currents on the sphere. If we consider a single electron moving away from a sphere, we find that the maximum surface current is induced immediately after the electron leaves the surface. However, if we consider a stream of electrons moving away from the surface, we find that each electron



RT-09937

Figure 4-1. Resonant frequency of cavities associated with the TM modes of concentric spheres; inner radius fixed at 2 meters

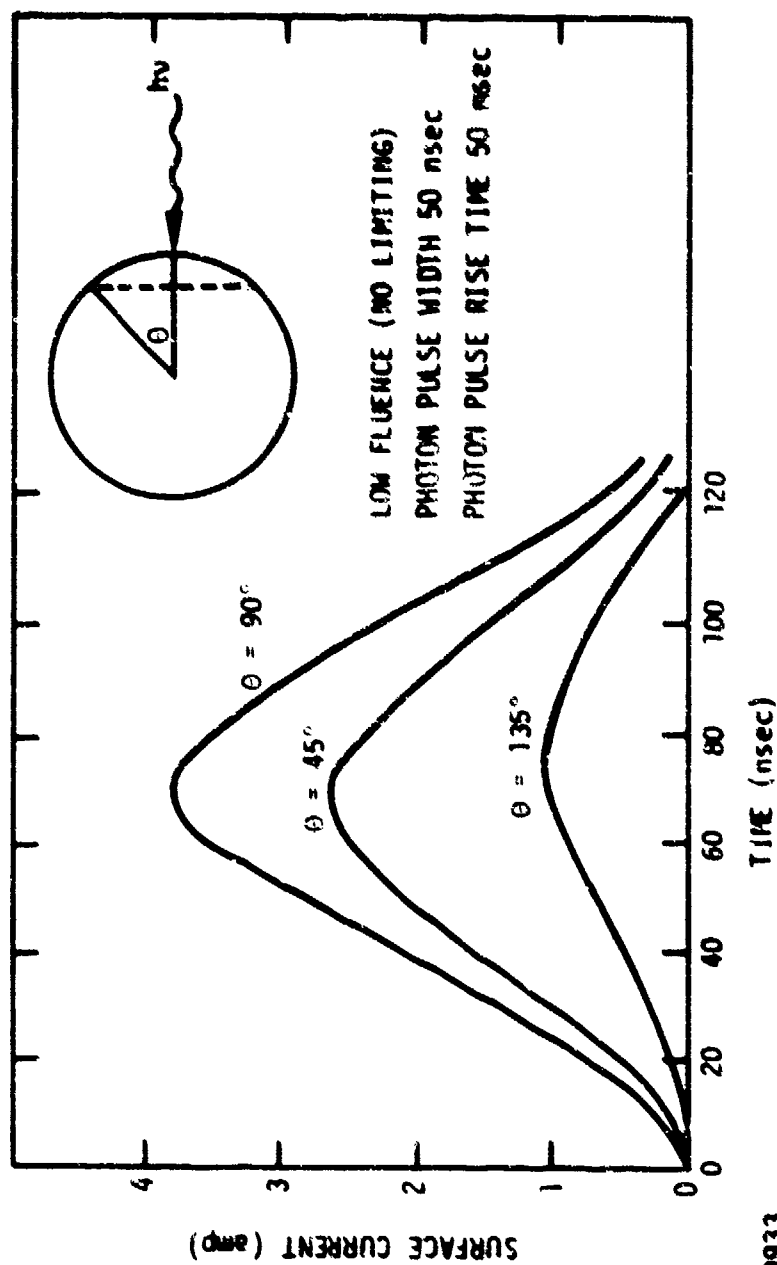


Figure 4-2. Surface currents at various locations on a 2-meter-radius sphere

contributes significantly to the surface current until it reaches 1/2 to 3/4 of a radius. The surface current continues to rise as electrons are emitted until the electron stream reaches 1/2 to 3/4 of a radius, at which point the surface current reaches its peak. Thus, the delay time between the emission peak and the surface current peak is simply the time required for the electron to reach a distance of approximately 1/2R.

For the example problem, we are considering this delay time as

$$t_d = \frac{R/2}{v_e} = \frac{1.0}{0.15c} = 20 \text{ nsec}.$$

Thus, a delay time of 20 nsec added to the 50-nsec pulse rise time results in a peak surface current at approximately 70 nsec, as shown.

A second characteristic of interest is the ratio of peak emitted current to peak surface current. We define the peak emitted current  $I_{em}$  to be the sum of all peak surface current densities; i.e.,

$$I_e = \int \vec{J}_p(\vec{r}, t_p) d\vec{s},$$

where  $t_p$  is the time at which the local emission current density is peak. The peak surface current is the total peak current flowing across a plane at the angle where the maximum current flows; i.e.,

$$I_{surf}(\theta_m) = \int \vec{K}_{surf}(\theta_m, t_p) d\vec{l}.$$

The angle  $\theta_m$  at which the peak surface current flows is dependent upon the assumed emission pattern. For half-sphere emission assumed in these studies, the maximum occurs close to 90°. It is evident in Figure 4-2 that the surface currents at  $\theta = 45^\circ$  and  $135^\circ$  are lower than the current at  $\theta = 90^\circ$ .

The ratio of peak surface current to peak emission current is dependent on several factors including total emitted charge, pulse rise time, and electron velocity. For highly space-charge-limited problems, the ratio can be  $10^{-4}$  or less. Even for low-emission-level situations where no charge returns, the ratio can be significantly less than unity for fast pulses and slow electrons. The ratio can approach 0.5 for half-sphere emission when the pulse rise time is long compared to the time

required for the electrons to travel to 1/2 to 3/4 of the spherical radius\* (see Appendix C).

$$t_r \geq \frac{R}{v_e}.$$

For the present example in which there is no space-charge limiting, the rise time would have to be greater than 2 meters divided by  $v_e \approx 0.1c$ , or 66 nsec, for the ratio  $I_{\text{surf}}/I_{\text{em}}$  to approach 1/2. The rise time is 50 nsec, and therefore, the ratio should be somewhat less than 0.45. The actual ratio is  $\approx 3.85/14.5$ , or 0.27.

#### 4.3.2 Rise Time Variation

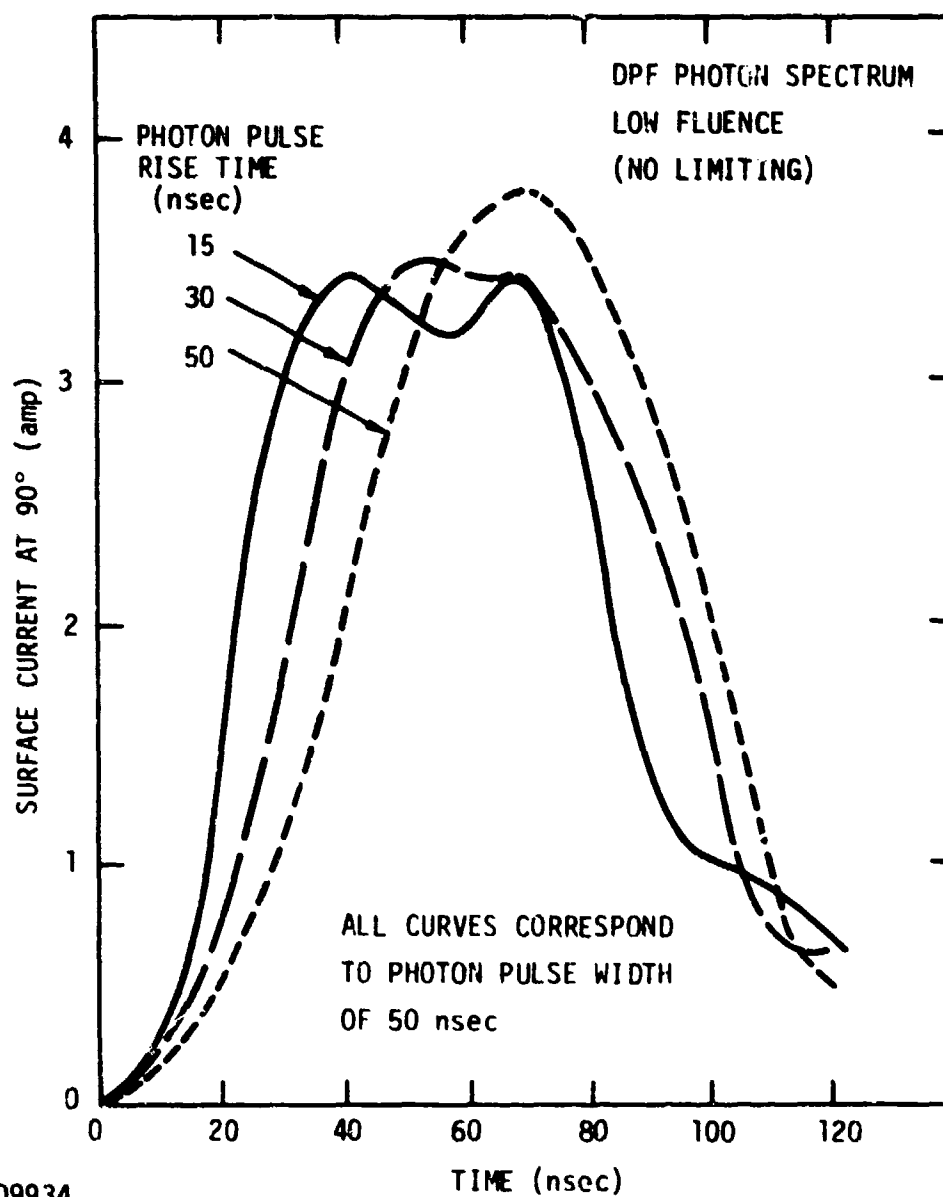
Surface currents at  $\theta = 90^\circ$  are shown together in Figure 4-3 for pulse rise times of 50, 30, and 15 nsec. The pulse width is fixed at 50 nsec, and the peak emission current density is identical for all three. We note that the rise time of the surface current decreases with decreasing photon pulse rise times. The delay time between the peak in surface current and the peak in emitted current remains on the order of 20 to 25 nsec for all three cases.

Resonance begins to appear as the pulse rise time is decreased from 50 to 15 nsec. This resonance is associated with the presence of the outer sphere rather than an isolated sphere. Note the slight increase in current at a time slightly later than the time required for the wave to travel to the outer wall and back to the inner sphere.

Strong resonances are not excited for any of the pulses due to the slow velocity of the electrons. It must be remembered that the peak surface current does not occur before the electrons move out approximately 1/2 to 3/4 of a radius regardless of pulse rise time. For slow electrons ( $v \approx 0.1c$ ), this minimum time is greater than the time required to excite resonances. Thus, we see evidence that the quasi-static solution prevails when the electron transit time across a characteristic dimension of interest ( $\sim R$ ) is slow compared to the transit time for light, even when the pulse rise time is fast. This result is demonstrated in the next section.

---

\*The point at which the electrons no longer effectively contribute to the flow of surface current.



RT-09934

Figure 4-3. Surface current at 90° location on a 2-meter-radius sphere; constant pulse width and fluence, various rise times

#### 4.4 ELECTRON VELOCITY VARIATIONS

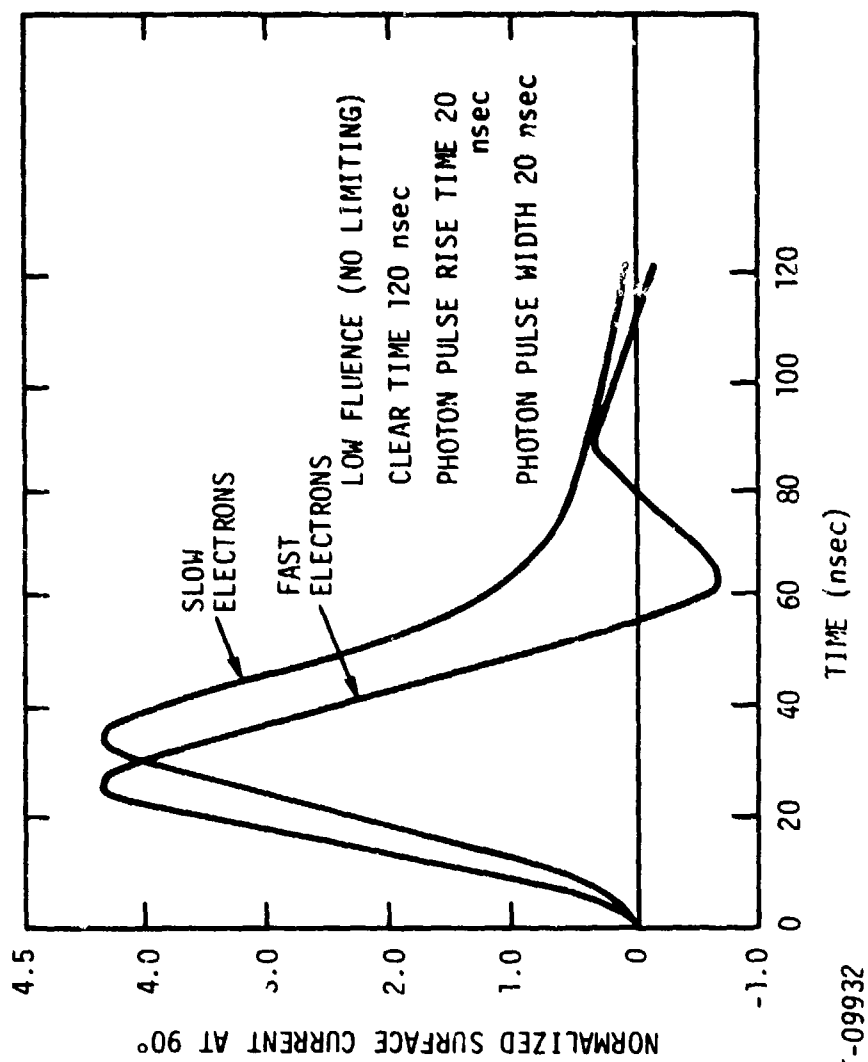
In the previous section, it was stated that the electron velocity is a controlling factor in determining resonance effects. In this section, we explicitly demonstrate this fact by comparing two sample calculations for which the mean electron speed has values of  $\sim 0.15c$  and  $\sim 0.9c$ , with all other parameters the same.

A 20-nsec pulse width and rise time were chosen. A low emission current density was chosen so that neither problem would be space-charge-limited. The only difference in the input parameters to the two problems is the velocity distribution of the photo-emitted electrons.

An outer boundary radius of 22 meters was chosen so that enough clear time ( $\sim 120$  nsec) is available to observe resonances of an isolated sphere. The results of this exercise are shown in Figure 4-4. It is evident that the surface current corresponding to the lower-velocity electrons does not exhibit an oscillatory response, whereas the current corresponding to the fast electrons is clearly oscillatory. Note also that the delay between the peak of the surface current and the peak of the pulse is diminished for the high-velocity electron problem; the electrons reach  $1/2$  to  $3/4$  of a radius sooner. The surface current responses in Figure 4-4 are normalized to the same peak value to emphasize the difference in the oscillatory behavior. The actual peak value for the "fast" electrons exceeds that of the "slow" electrons by about a factor of three.

The preceding results would be much more pronounced for an emitter with a geometry associated with high-Q resonances. It is well known that sphere resonances are highly radiation-damped, whereas, for example, dumbbell-shaped objects resonate with a much lower frequency, in proportion to their characteristic dimensions, and ring down relatively slowly compared to the sphere case. It is not our purpose here to demonstrate extreme resonance effects, but rather to present the fundamental physics of SGEMP-induced surface current resonances.

An important point worth repeating is that the characteristic time for determining the effective spectral content of an SGEMP excitation is related to the time required for the photo-emitted electrons to move out an effective distance from the system, in addition to the rise time of the photon pulse.



RT-09932

Figure 4-4. Surface current (normalized) at 90° for fast and slow photo-emitted electrons; fast and slow curves are normalized to the same peak value.

## 4.5 FLUENCE VARIATIONS

All the previous parameter variations have been performed for low-fluence electron emission where virtually no space-charge limiting occurs. In the next series of problems, we begin with a low fluence and progressively increase the fluence while holding all other input parameters constant. A pulse width and rise time of 20 nsec have been chosen. The inner radius is 2 meters and the outer radius 10 meters, corresponding to a clear time of approximately 50 nsec. Emission currents vary from a low of  $3.2 \text{ amp/m}^2$  up to a high of  $3.2 \times 10^4 \text{ amp/m}^2$ . The corresponding surface currents are shown in Figure 4-5. Oscillatory behavior after 50 nsec is associated with electromagnetic waves between the inner and outer walls, while oscillatory behavior before 50 nsec, exhibited at the higher fluences, is associated with the inner sphere alone.

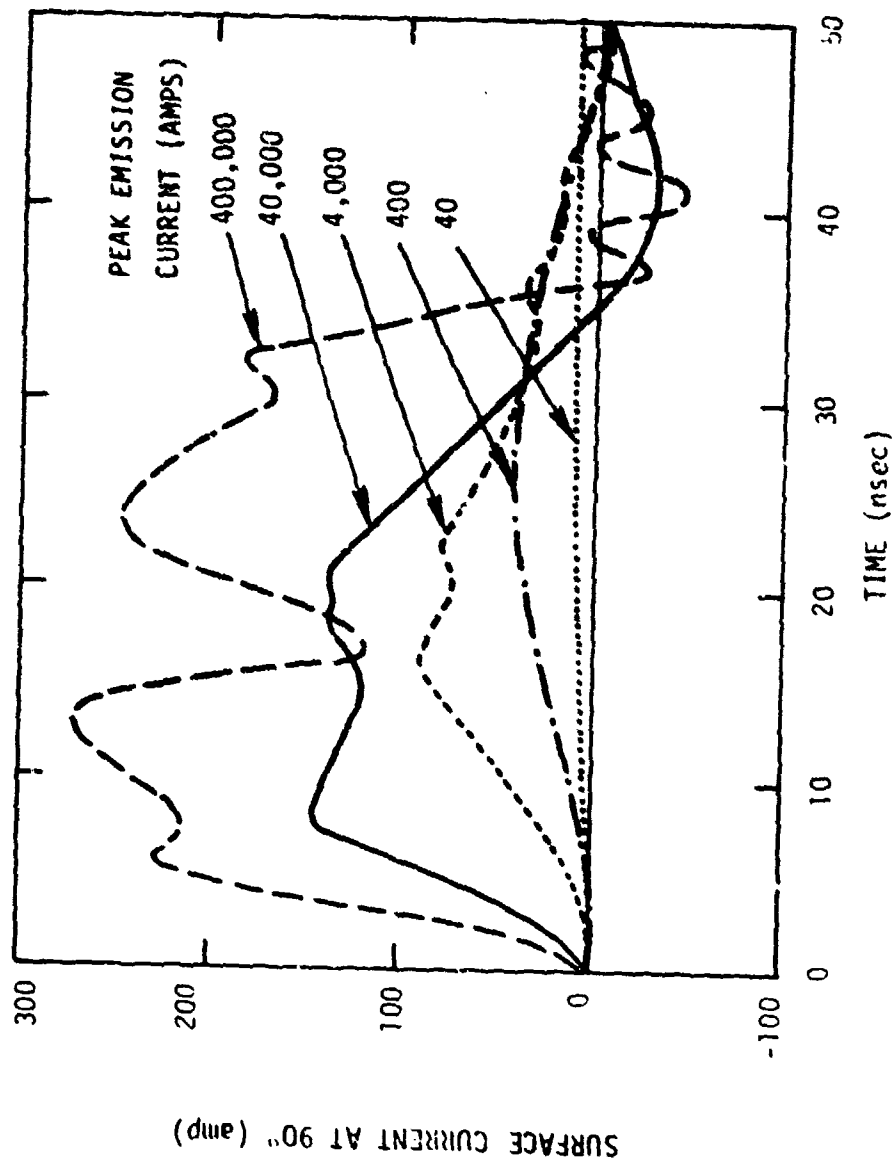
We note several interesting aspects of these solutions in the following subsections.

### 4.5.1 Peak Surface Currents

The peak surface current as a function of emission current is shown in Figure 4-6. The onset of space-charge limiting occurs at an emission current of several  $\text{amp/m}^2$ , and a further increase of 4 orders of magnitude in emission current results in an increase of a factor of 50 in surface current. Thus, space-charge limiting is very effective in limiting the replacement currents flowing on an object.

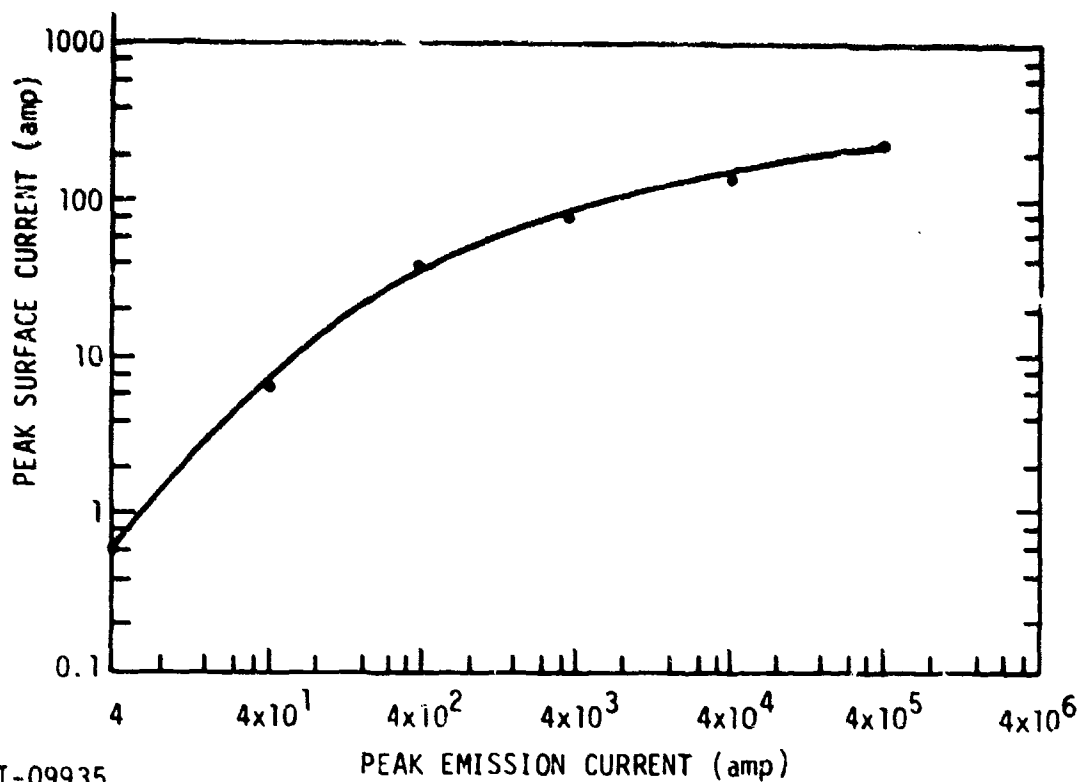
### 4.5.2 Rise Times of Surface Currents

It is interesting to note the effective decrease in response rise time as the fluence is increased. The time at which the peak surface current occurs is shown as a function of fluence in Figure 4-7. Note that the effective rise time of the response can be significantly shorter than the rise time of the emitted electron pulse. This shortening of the surface current rise time occurs because the space-charge-limited electrons do not travel far from the surface before they are turned around and returned to the surface. The response is, therefore, significantly



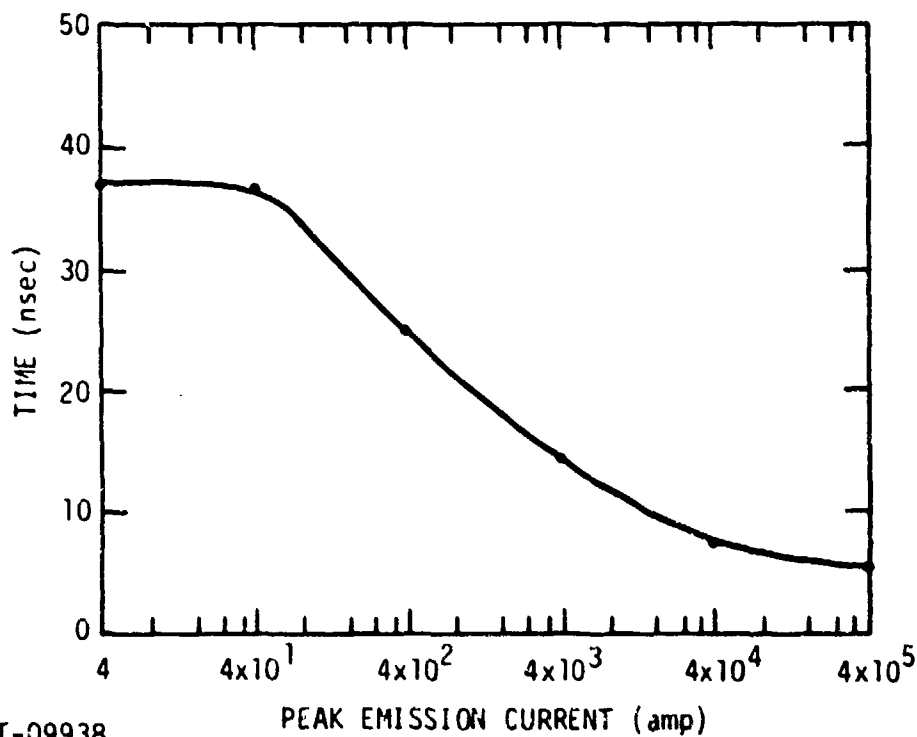
RT-09920

Figure 4-5. Surface current at 90° location on a 2-meter-radius sphere



RT-09935

Figure 4-6. Peak surface current on a 2-meter-radius sphere



RT-09938

Figure 4-7. Time of occurrence of peak surface current on a 2-meter-radius sphere

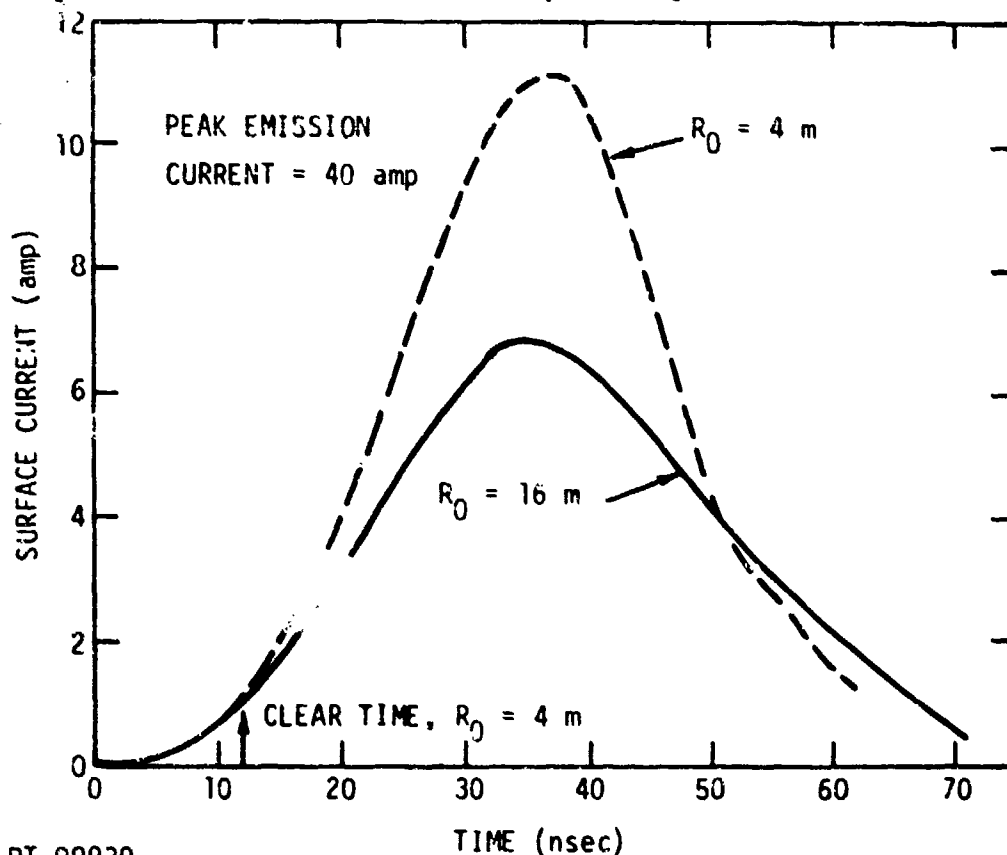
smaller than it would be in the absence of space-charge limiting, and it is also significantly faster (with more high-frequency spectral content).

#### 4.6 DIMENSIONAL VARIATIONS

All previous solutions have been obtained with an inner sphere of 2 meters. Solutions for other dimensions can be obtained directly by using the scaling laws described in Section 4.2 and Appendix A. In this section, we investigate effects arising from changing the ratio of inner spherical radius to outer radius.

Solutions have been obtained for an inner sphere of 2 meters and an outer sphere of 4, 16, and 22 meters at low fluences. Solutions have also been obtained for an outer radius of 4 and 10 meters at medium and high fluences. The clear times are marked on each figure, and it is evident when the wave reflected from the outer sphere returns to the inner sphere.

Figure 4-8 shows the surface current response at  $90^\circ$  on a 2-meter-radius sphere for radiation from a DPF photon spectrum with rise time and

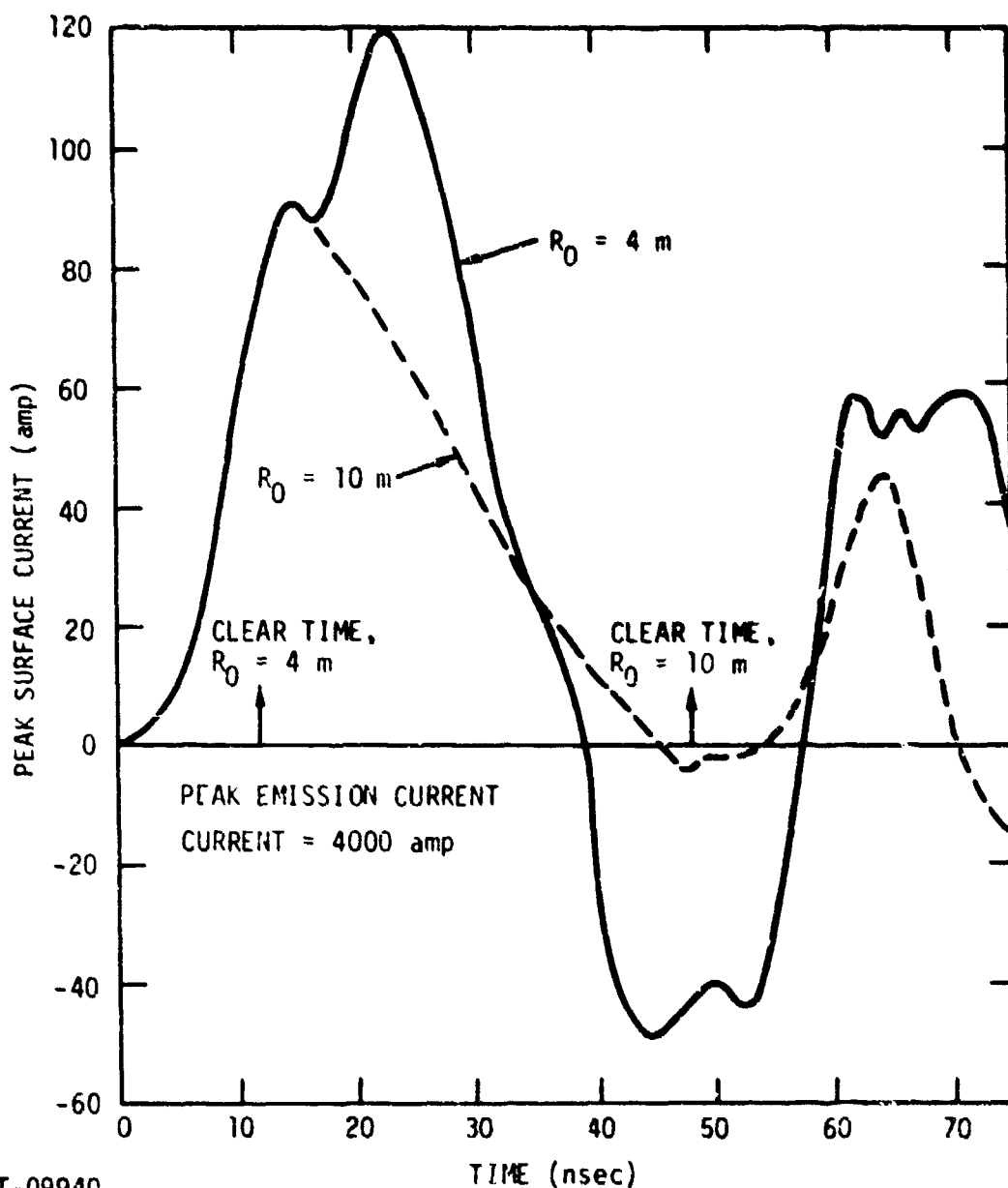


RT-09939

Figure 4-8. Surface current at  $90^\circ$  on a 2-meter-radius sphere

pulse width both arbitrarily set equal to 20 nsec. The small outer sphere, with 4-meter radius, corresponds to a clear time of only 12 nsec. The large outer sphere corresponds to an 84-nsec clear time. Clearly, the surface current amplitude is enhanced by about 50% by the interactions with the small outer sphere. Note that virtually no hint of oscillatory behavior is seen.

Figure 4-9 shows the same problem as that of Figure 4-8 except for an outer sphere of 10 meters and a higher photon fluence, corresponding to

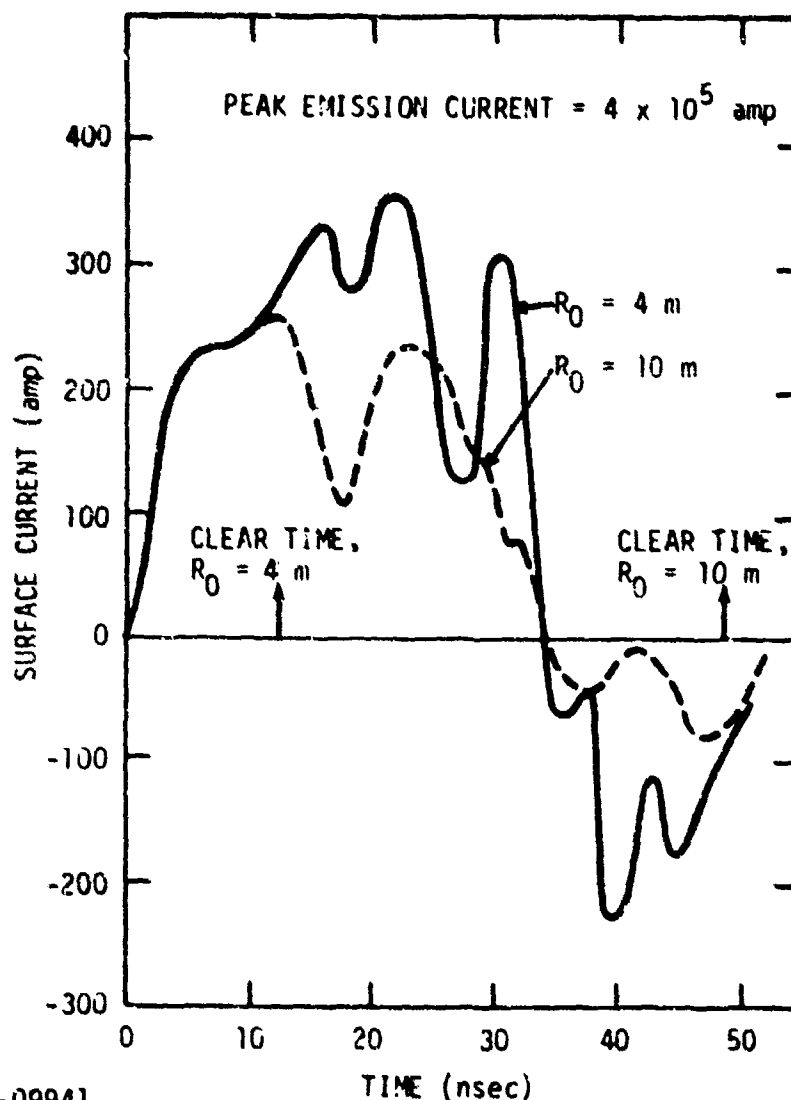


RT-09940

Figure 4-9. Surface current at  $90^\circ$  on a 2-meter-radius sphere

moderate space-charge limiting. (The peak emission current is about 4000 amperes in this example.) Dynamic effects are apparent after the occurrence of each clear time. The small outer chamber ( $R_0 = 4$  m) produced about a 50% amplification of the peak response, with a corresponding overshoot between 40 and 60 nsec that should significantly enhance the high-frequency spectral content of the surface current.

At a higher photon fluence level corresponding to  $4 \times 10^5$  amperes, the same example is repeated in Figure 4-10. In this case, the charge density just outside the emitting surface is great enough to produce plasma oscillations in interaction with the rapidly changing electric fields near



RT-09941

Figure 4-10. Surface current at  $90^\circ$  on a 2-meter-radius sphere

the surface. It appears that such plasma oscillations could be producing the shorter time scale oscillations in the surface current curve in Figure 4-10. The dynamic interactions again introduce about a 50% increase in the peak surface current, and a substantial overshoot between 35 and 50 nsec, in this case. Therefore, the medium- and high-fluence dynamic interactions are qualitatively the same except for the apparent plasma oscillations in the high-fluence case. Table 4-1 summarizes the dynamic effects shown in Figures 4-8, 4-9, and 4-10.

Table 4-1  
SUMMARY OF DYNAMIC INTERACTIONS BETWEEN A 2-METER-RADIUS SPHERE  
AND A SMALL OUTER CHAMBER ( $R_0 = 4$  m)

Photon Fluence	Peak Surface Current Amplification	Time Dependence of the Response
Low	About 50%	Monopolar - no oscillations
Medium (moderate limiting)	About 50%	Bipolar - cavity period apparent
High (extreme limiting)	About 50%	Bipolar - cavity period apparent - plasma oscillations apparently superimposed on cavity ringing

## 5. COMPARISONS OF QUASI-STATIC AND FULLY DYNAMIC SOLUTIONS FOR ELECTROMAGNETIC FIELD CALCULATIONS IN A CYLINDRICAL CAVITY

### 5.1 INTRODUCTION

The quasi-static approximation has been used extensively in the past in many calculations and computer programs for the solution of electromagnetic fields and currents resulting from radiation exposure of cavities of different geometries. A number of qualitative arguments have been used to justify the use of the quasi-static approximation, but no quantitative results have been reported to identify the range of applicability of the quasi-static approach or the magnitude of the errors introduced by the approximation. The fully dynamic code DYNACYL (Appendix D) has been applied to a number of situations to identify the ranges of validity for the quasi-static approximation.

### 5.2 DYNAMIC CODE

The dynamic code was developed to treat a geometry consisting of two finite concentric cylinders, each of arbitrary length. The fields are calculated for a cylindrically symmetric region enclosed in a perfectly conducting can. The laws governing the generation of the fields are Maxwell's equations, and solutions are obtained by a finite-differencing scheme.

Maxwell's equations are solved in cylindrical coordinates, assuming rotational symmetry about the cylinder axis and symmetry as far as direction of rotational motion is concerned. The rotational symmetry is similar to assuming that all derivatives with respect to azimuthal angle are zero. However, this still leaves the possibility of currents in the azimuthal direction (toroidal currents). The assumption that there is no preferred direction of rotation eliminates this possibility. The form of the reduced equations is

$$\frac{\partial \epsilon_0 E_r}{\partial t} = - \frac{\partial H_\phi}{\partial z} - J_r ,$$

$$\frac{\partial \epsilon_0 E_z}{\partial t} = \frac{1}{r} \frac{\partial (r H_\phi)}{\partial r} - J_z ,$$

and

$$\frac{\partial \mu_0 H_\phi}{\partial t} = \frac{\partial E_z}{\partial r} - \frac{\partial E_r}{\partial z} .$$

These equations, expressed here in MKS units, are solved for the radial and axial components of the electric field ( $E_r$ ,  $E_z$ ) and the azimuthal magnetic field ( $H_\phi$ ). The medium in which the fields are generated has the same permittivity and permeability as a vacuum. The region of interest is surrounded by perfectly conducting walls. It is assumed that all fields are initially zero, so the three equations above imply the divergence equations

$$\nabla \cdot \epsilon_0 \mathbf{E} = \rho$$

and

$$\nabla \cdot \mu_0 \mathbf{H} = 0$$

if the charge density  $\rho$  is determined by

$$\frac{\partial \rho}{\partial t} = - \frac{1}{r} \frac{\partial (r J_r)}{\partial r} - \frac{\partial J_z}{\partial z} .$$

From the form of the equations, it is clear that they represent the time evolution of the fields driven by the current. Thus, it is the current which must be specified to determine the fields.

### 5.3 QUASI-STATIC APPROXIMATION

There are a number of ways to view the quasi-static approximation, which ignores retarded potentials. Solutions are obtained by assuming that the charge density is quasi-stationary and that the fields have reached their equilibrium values. Mathematically, the assumption is equivalent to the assumption that the curl of the electric field is negligible.

Ranges of validity of the quasi-static approximation can be estimated analytically by rearranging the full set of Maxwell's equations in terms of the electric field and source charge, nondimensionalizing the resulting equation, and comparing terms with the quasi-static Poisson equation. Two important parameters emerge from such a comparison:

$$\beta = v/c$$

and

$$\eta = t_r/(L/c) ,$$

where  $v$  is the electron velocity,  $L$  is the cavity dimension,  $c$  is the speed of light, and  $t_r$  is the rise time of the emitted pulse of electrons. Thus,  $\beta$  is the ratio of electron speed to the speed of light, while  $\eta$  is the ratio of pulse rise time to the time required for light to traverse the cavity.

By requiring that the terms in Maxwell's equations contributing to the fully dynamic solution be small relative to the quasi-static terms, inequalities result:

$$\eta^2 \gg 1$$

and

$$\eta \gg \beta .$$

Both inequalities must hold if the problem is predominantly quasi-static. Because  $\beta$  is always less than unity, the second inequality is automatically satisfied when the first is satisfied. The second one is listed to illustrate that  $\beta$  becomes an important parameter when the first is not satisfied. Subsequent results will demonstrate this behavior.

These inequalities represent the conditions under which the quasi-static solution is valid; however, they do not give an indication of the magnitude of error involved when these conditions are not met.

#### 5.4 CODE RESULTS

A number of fully dynamic and quasi-static computer calculations were performed for a wide range of parameters for which the quasi-static conditions were not always met. In general, the dynamic solutions vary from the quasi-static in three important respects:

Peak amplitude variations,  
Oscillatory response characteristics of cavity,  
Delay time due to finite velocity of light.

Code results were obtained for space-charge-limited and non-space-charge-limited cases. SCL situations are of great interest because SCL can significantly alter the time history of the currents in the cavity in a way which cannot readily be ascertained from inspection of the emitted current. Thus, a problem with a particular pulse time history (and associated parameter  $\eta$ ) for which static approximation is valid in the absence of limiting may require the fully dynamic treatment when SCL occurs. Calculations are performed on a cylindrical cavity with electrons uniformly emitted from the front face of the cavity, with a triangular time history defined by the full width at half maximum (FWHM). Dimensions and other parameters used in specific calculations are indicated on each of the figures. Monoenergetic electrons are used for NSCL calculations, while Maxwellian energy distributions are used for SCL calculations.

#### 5.4.1 NSCL Solutions

5.4.1.1 Oscillatory Response. The first set of response calculations has been selected to illustrate the time history variations between quasi-static and dynamic calculations for several parameter values of  $\beta$  and  $\eta$ . Typical results for the electric fields at the front of the cylindrical cavity are shown in Figures 5-1 and 5-2.

The conditions for the cylinders shown in Figure 5-1 are such that  $\beta = 0.27$  and  $\eta \approx 3$ . The inequalities  $\eta^2 \gg 1$  and  $\eta \gg \beta$  are well satisfied, and the solution is essentially quasi-static.

The conditions for the cylinder shown in Figure 5-2 are such that  $\beta = 0.27$  and  $\eta \approx 0.6$ . The inequality  $\eta^2 \gg 1$  is not satisfied and dynamic aspects of the solution appear. Note that the dynamic solution for the peak electric field at the spatial position chosen is greater than the quasi-static solution, and that the late-time solution contains ringing which is characteristic of the cavity. This trend is generally followed by solutions for the electric and magnetic fields throughout the cavity. The frequency of oscillation is approximately equal to

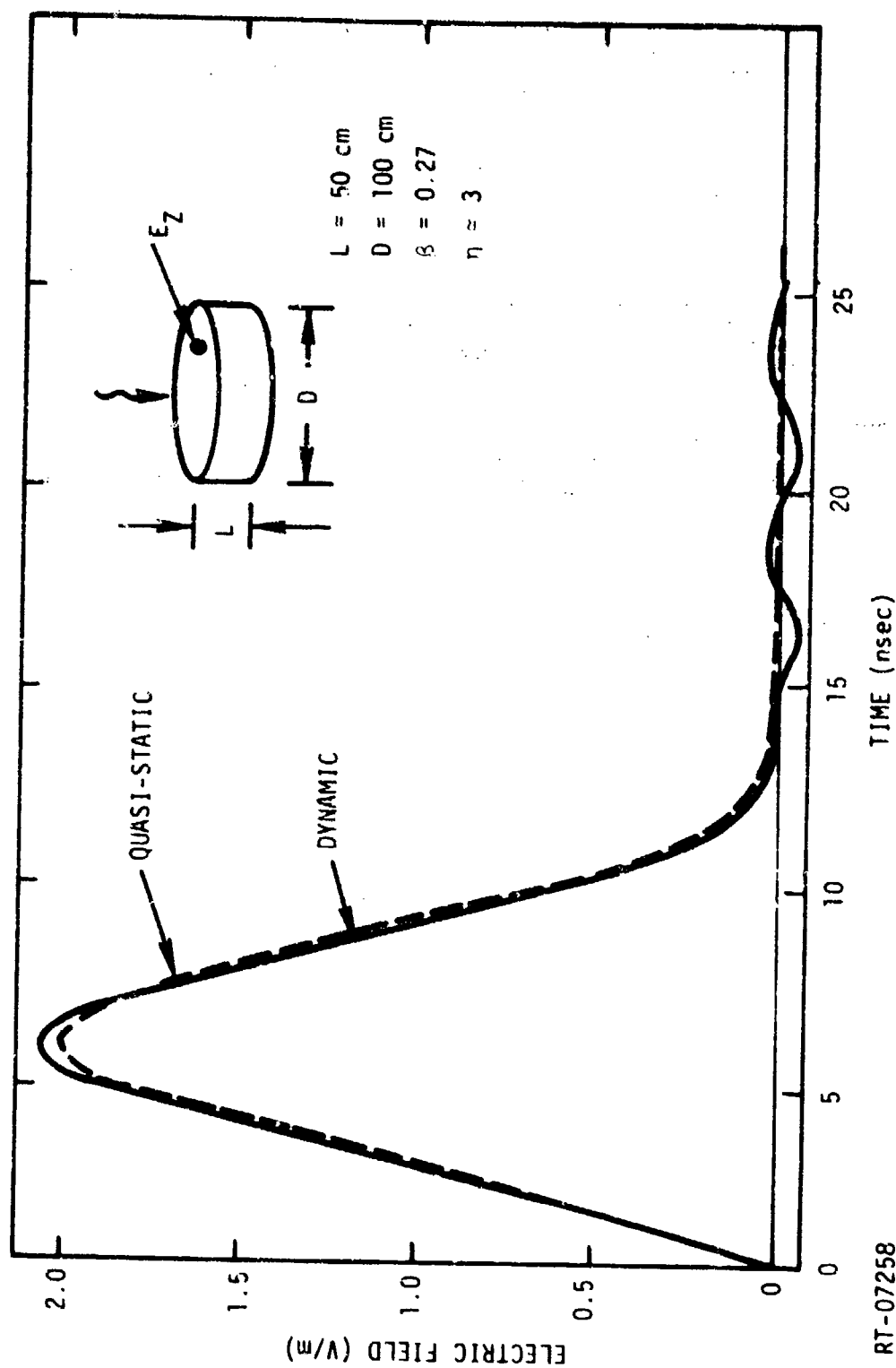
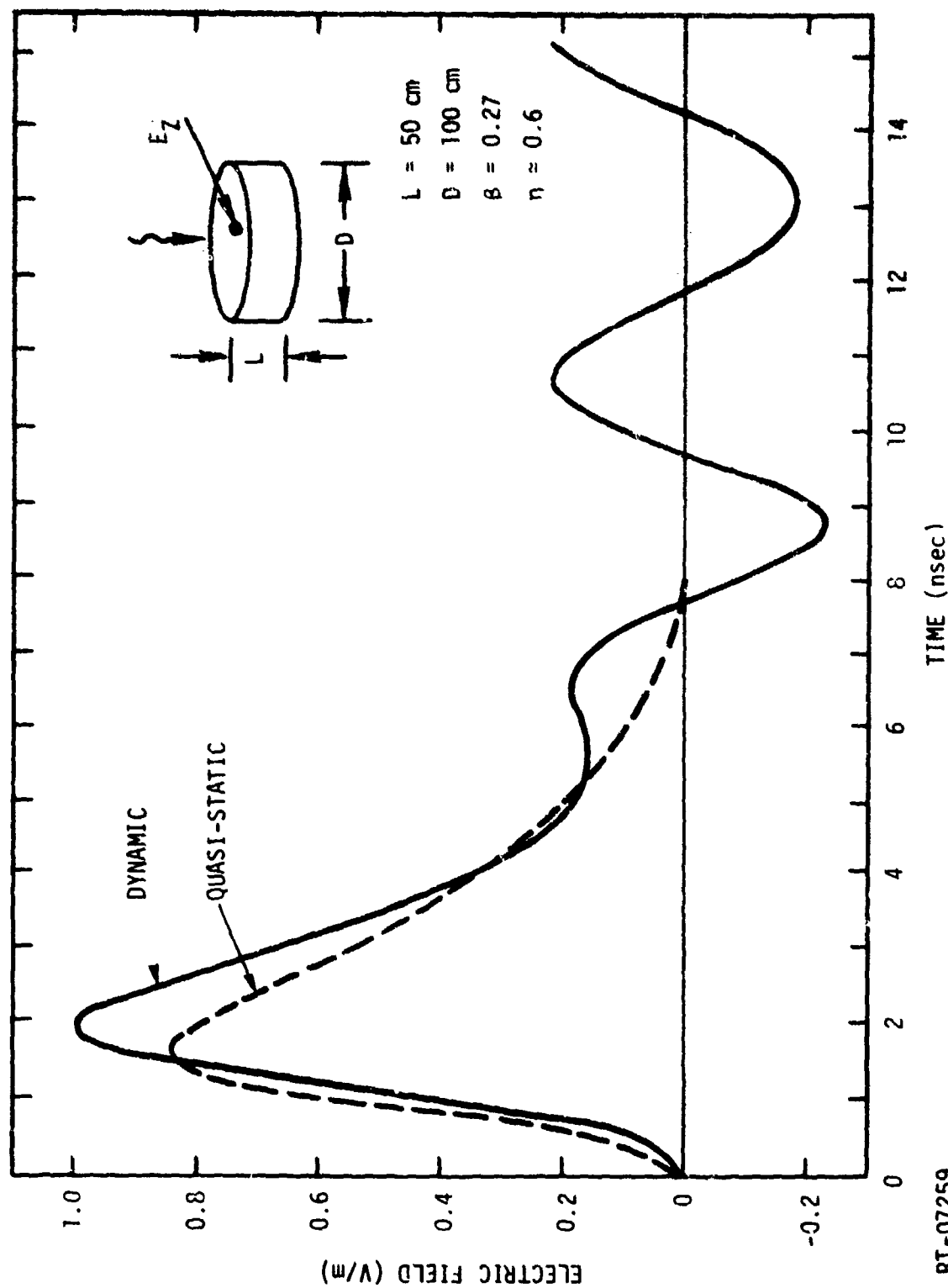


Figure 5-1. Electric fields as a function of time obtained from dynamic and quasi-static codes for parameters  $\beta$  and  $\eta$  which satisfy conditions for quasi-static approximation



RT-07259

Figure 5-2. Electric fields as a function of time obtained from dynamic and quasi-static codes for parameters  $\beta$  and  $\eta$  which do not satisfy conditions for quasi-static approximation

$$f = \frac{2.29 \times 10^8}{L} = \frac{c}{\sqrt{2}L}$$

as expected.

A number of calculations were performed as a function of the two parameters  $\beta$  and  $\eta$  to determine the ratio  $R$  of the amplitude of the late-time oscillatory response to the peak amplitude. This ratio is indicative of the amount of energy in the primary pulse which has been coupled into the cavity. The peak amplitude of late-time oscillatory response is essentially constant in these calculations because no damping has been considered. The ratio  $R$  is shown in Figure 5-3 for a number of parameters  $\beta$  and  $\eta$ .

**5.4.1.2 Response Delay.** One shortcoming of the quasi-static solution is that retarded potentials are neglected and, therefore, the response throughout the cavity is essentially instantaneous. This delay time is not obvious in the dynamic field solutions of Figures 5-1 and 5-2 because the fields are calculated at the source of the electron emission. The fields at the back of the cavity, however, are delayed by a time approximately equal to  $L/c$ , as illustrated in Figures 5-4 and 5-5.

Note that when quasi-static conditions prevail, the delay time is insignificant, as shown in Figure 5-4. As the solutions become more dynamic in nature, the delay becomes increasingly more prominent, as shown in Figure 5-5.

**5.4.1.3 Peak Amplitude.** In general, the dynamic solutions yield larger peak fields than the quasi-static solutions. A parametric study of the parameters  $\beta$  and  $\eta$  was performed to determine deviations from the quasi-static solutions. The peak electric field at the side of the cavity wall was chosen as the basis of comparison. The ratio of the peak electric field obtained from the full set of Maxwell's equations is compared with results from the quasi-static solution in Figure 5-6. The trends are consistent with the two inequalities involving parameters  $\beta$  and  $\eta$ . Note how the results are much more sensitive to  $\beta$  when  $\eta$  is not much larger than unity. Note also that for small  $\eta$ , the solutions tend to be quasi-static regardless of the electron velocity. However, for large  $\eta$ , the velocity of the electron becomes important in determining whether the solution is quasi-static.

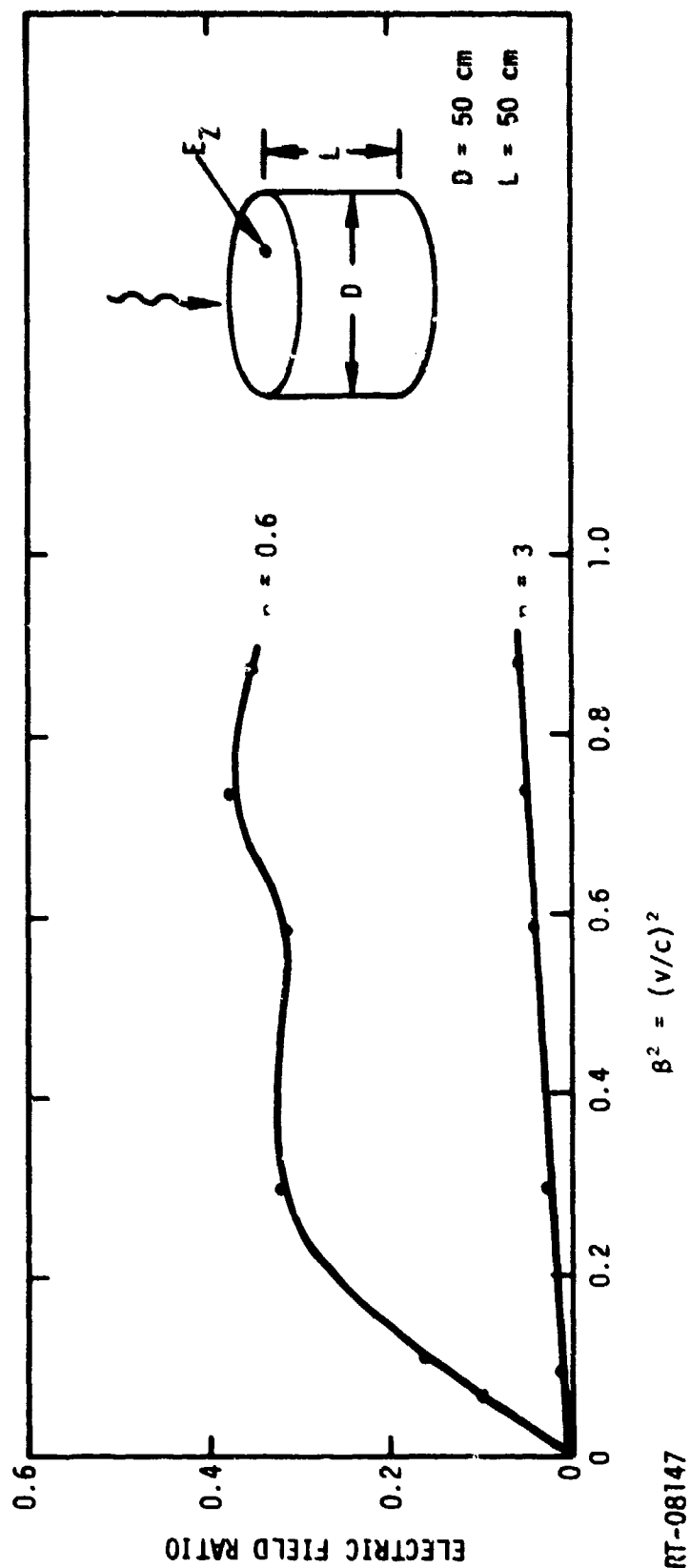
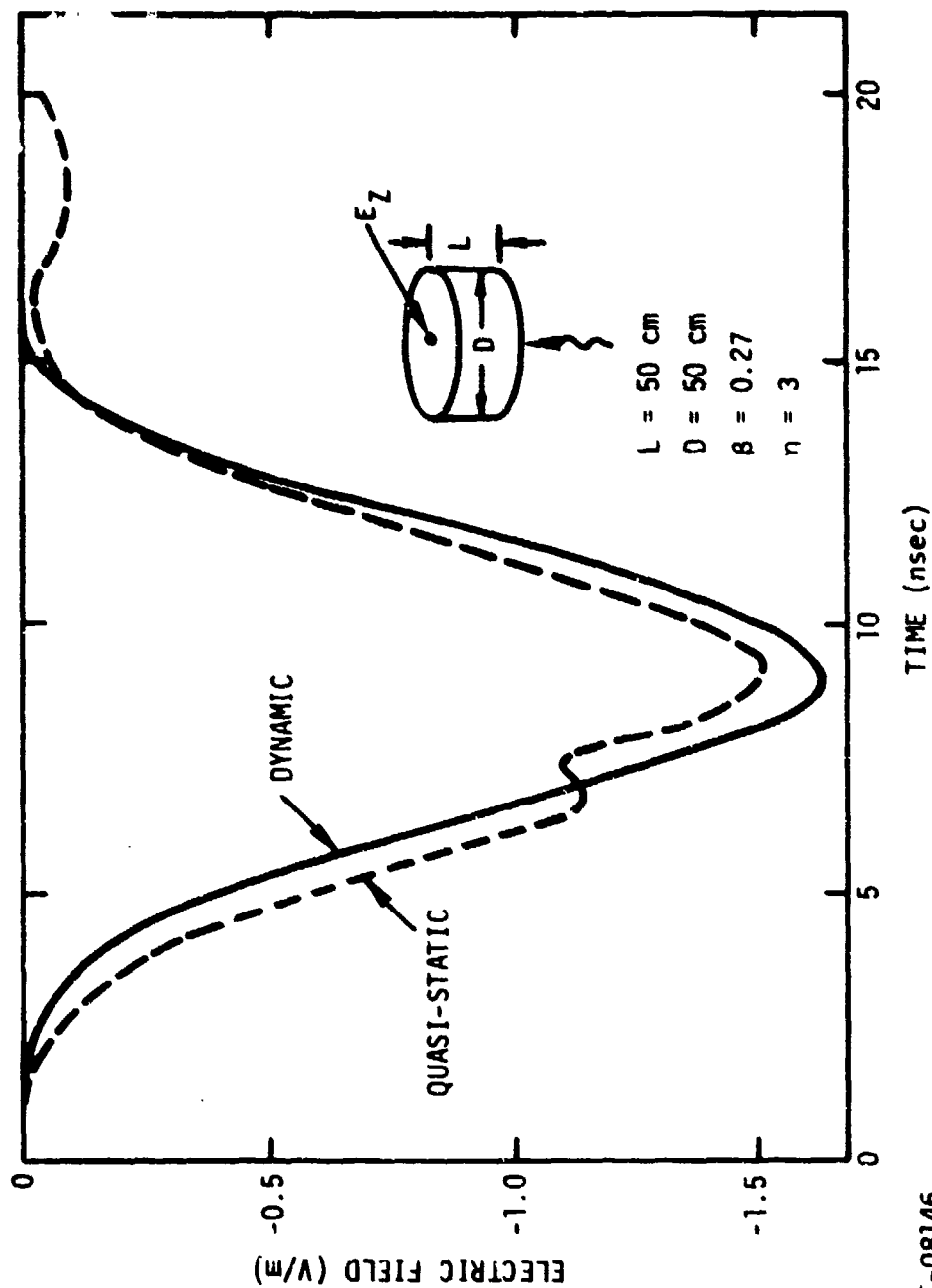
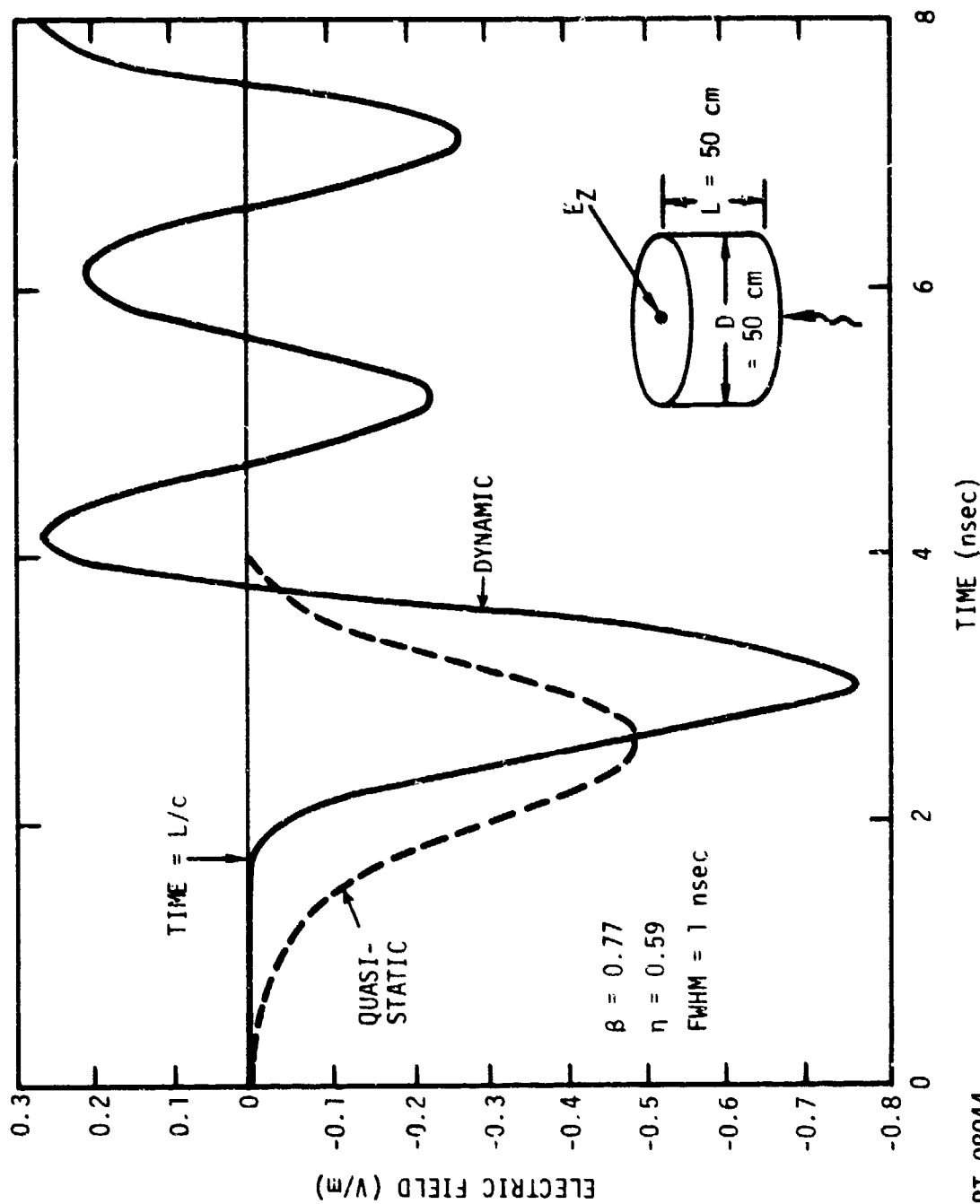


Figure 5-3. Ratio of peak axial electric field oscillations to peak axial electric field versus  $\beta^2$  for different  $\eta$  values;  $\beta$  is the ratio of electron speed to the speed of light;  $\eta$  is the ratio of pulse rise time to  $L/c$ .



RT-08146

Figure 5-4. Electric fields at the back face as a function of time obtained from dynamic and quasi-static codes for parameters  $\beta$  and  $\eta$  which satisfy conditions for quasi-static approximation



RT-08044

Figure 5-5. Electric fields at the back face as a function of time obtained from dynamic and quasi-static codes for parameters  $\beta$  and  $\eta$  which do not satisfy conditions for quasi-static approximation

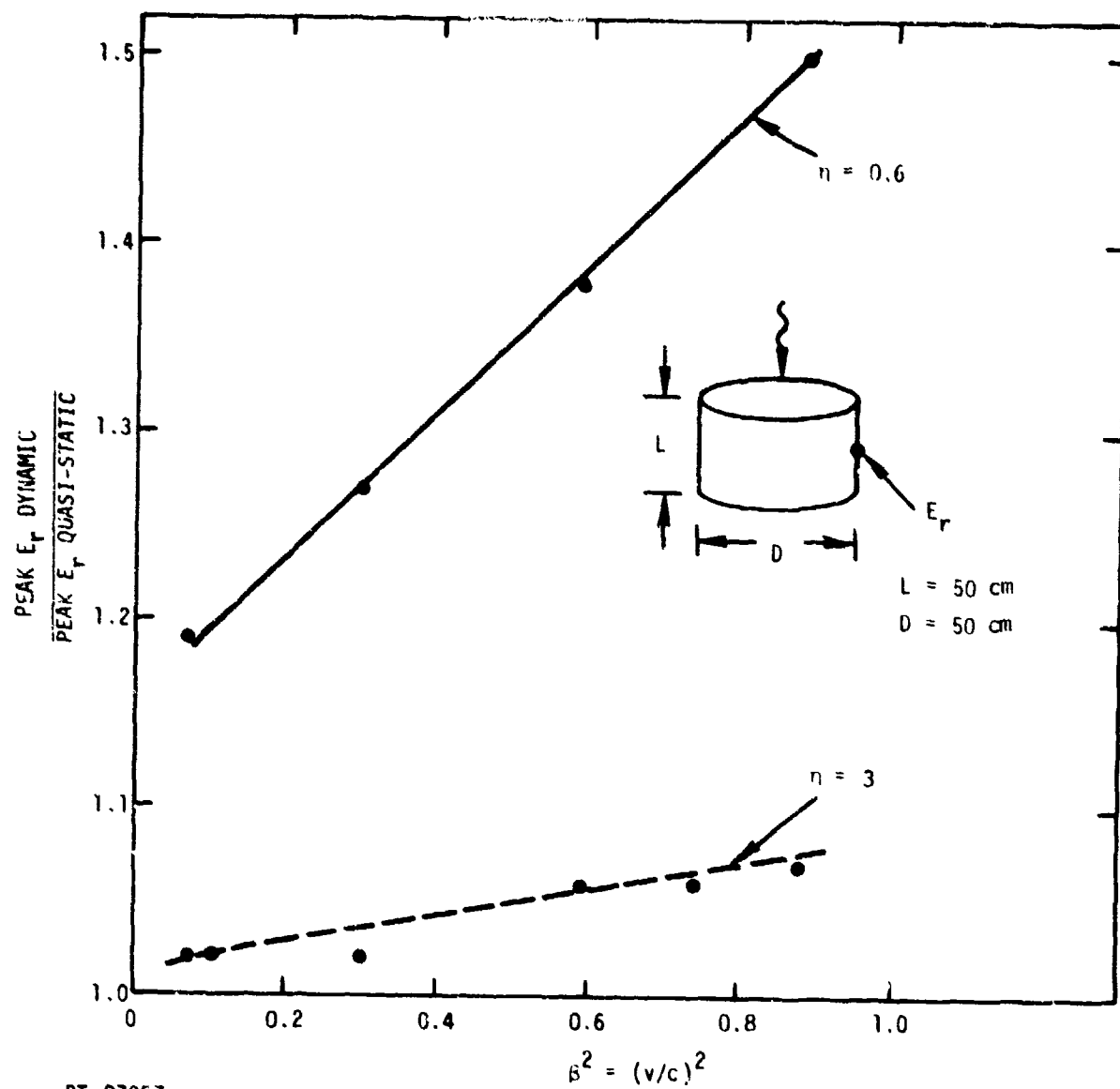


Figure 5-6. Ratios of peak electric fields obtained from dynamic code to peak field obtained from quasi-static code

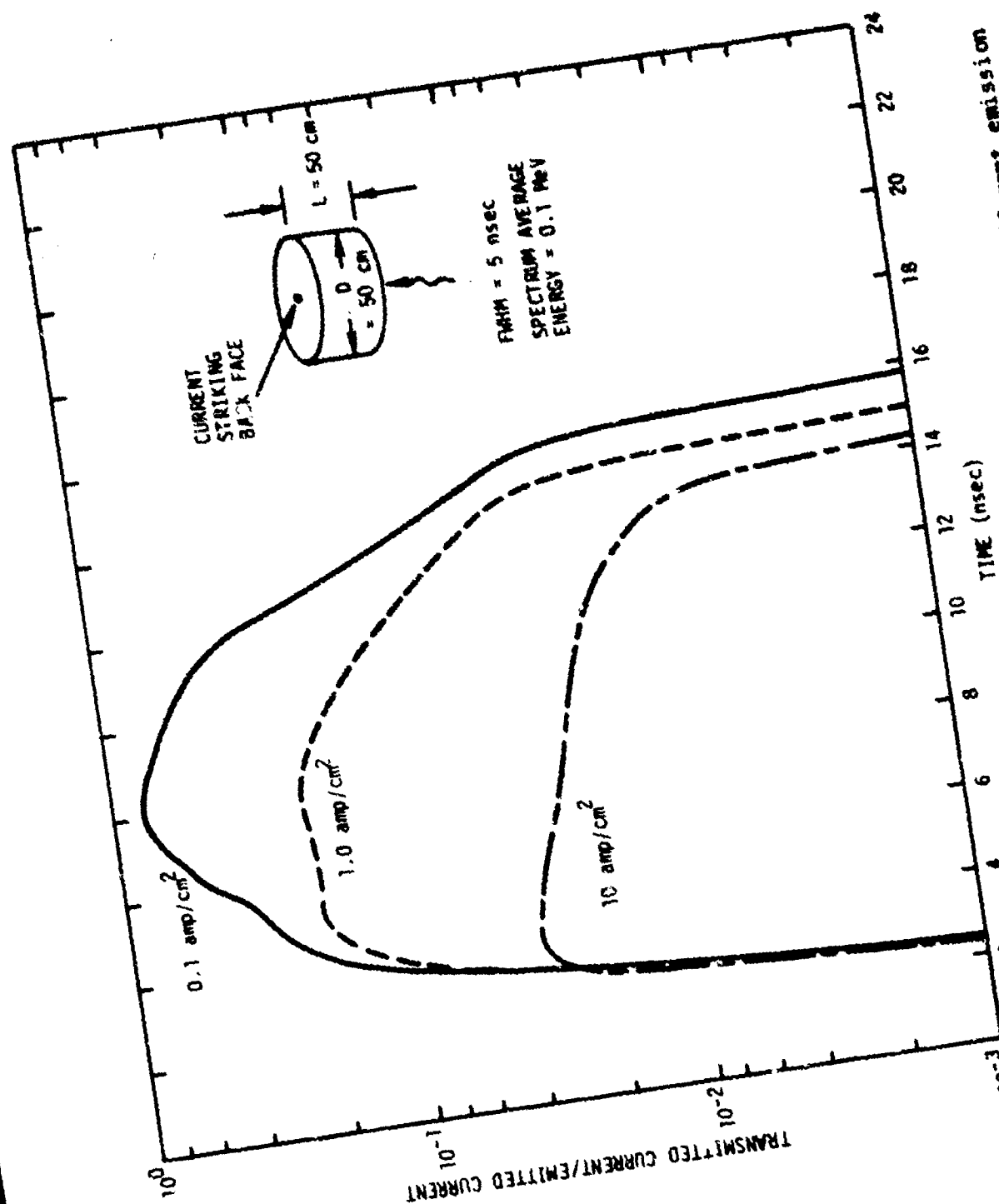
#### 5.4.2 SCL Solutions

Dynamic and quasi-static code calculations were also performed for cases in which the electron currents were space-charge limited. The following calculations are intended to demonstrate how a situation with a particular pulse shape can be essentially quasi-static when there is no SCL but may require a full dynamic treatment when SCL occurs. This situation arises because the fields alter the electron trajectories in such a way that the effective current pulse shape at locations within the cavity is significantly different from the emission current pulse shape. The frequency content associated with the emission current pulse shape might well satisfy the quasi-static requirements for  $\beta$  and  $\eta$ , but the effective current pulse shape which determines cavity fields may not. Such a case is treated in this section.

Electrons are emitted uniformly from one face of a pillbox cavity with a length-to-diameter ratio of unity. The emitted electron time history is triangular, with rise and fall times equal to 5 nsec. The emitted electron energy distribution is proportional to  $\exp(-|E-E_0|/E_0)$  where  $E_0$  is selected such that the average electron energy is 0.1 MeV. Emission current levels of 0.1, 1.0, and 10 amp/cm<sup>2</sup> were chosen, roughly corresponding to small, medium, and large amounts of SCL.

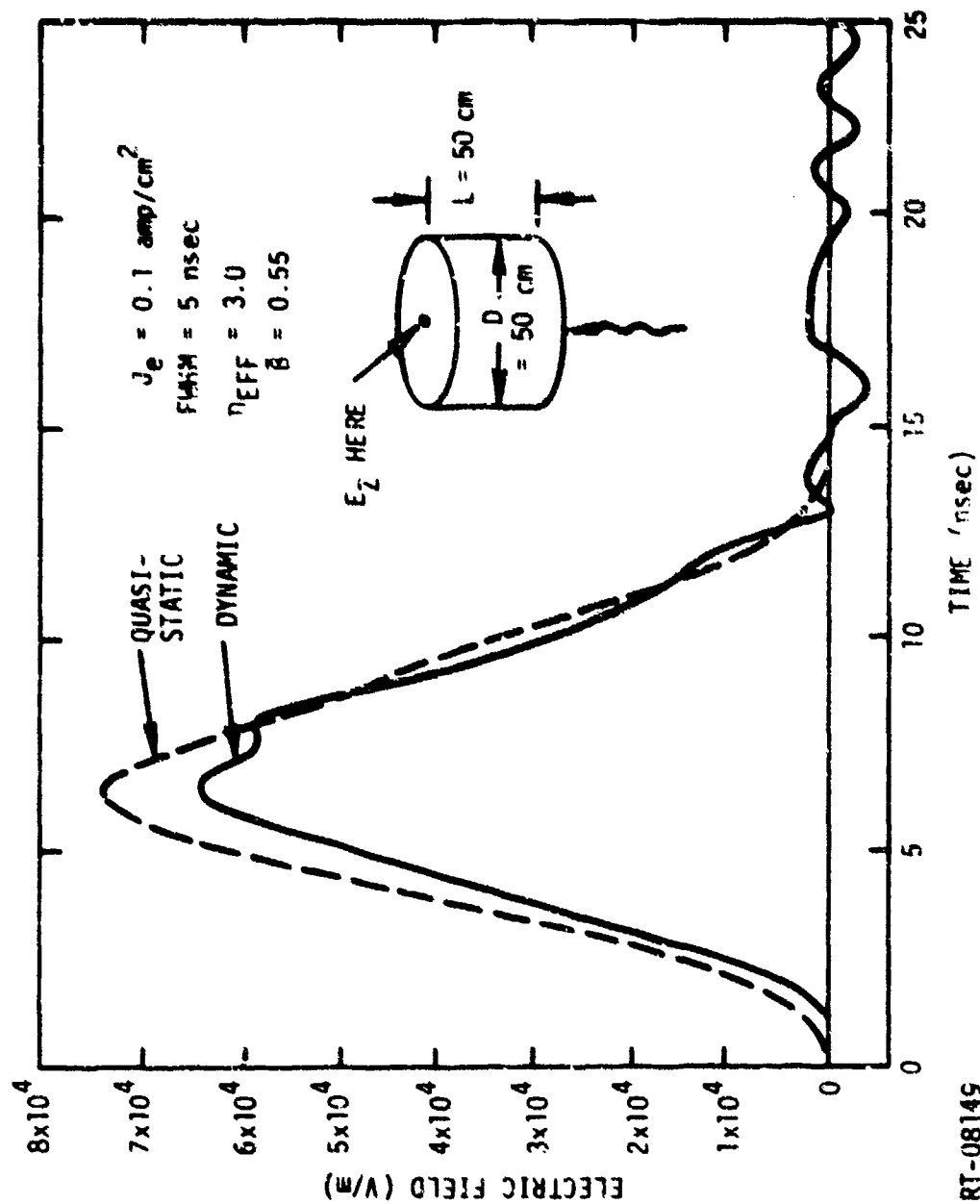
The amount of SCL can be quantitatively gauged by the fractional amount of emitted current which reaches the opposite side of the cavity, as shown in Figure 5-7 for each of the three cases.

Based on the emitted current, the parameters  $\eta^2$  and  $\beta$  have values of 9 and 0.55, and the solutions might, therefore, appear to be essentially quasi-static. The electric fields at the back of the cavity, as shown in Figures 5-8, 5-9, and 5-10 for the three cases, indicate that the solution is quasi-static only for the NSCL solution, and that the dynamic aspects of the solution become more apparent as the amount of SCL increases. This result is not surprising since the fields throughout the majority of the cavity are more dependent on the transmitted current than on the emitted current. The effect of SCL is to decrease the effective pulse rise time. It would, therefore, appear that an effective value of  $\eta$  should be defined based on the rise time of the transmitted current rather than on the emitted



RT-08148

Figure 5-7. Fractional transmitted currents versus time for different emission current levels



RT-08149

Figure 5-8. Electric field at back versus time for low SCL case

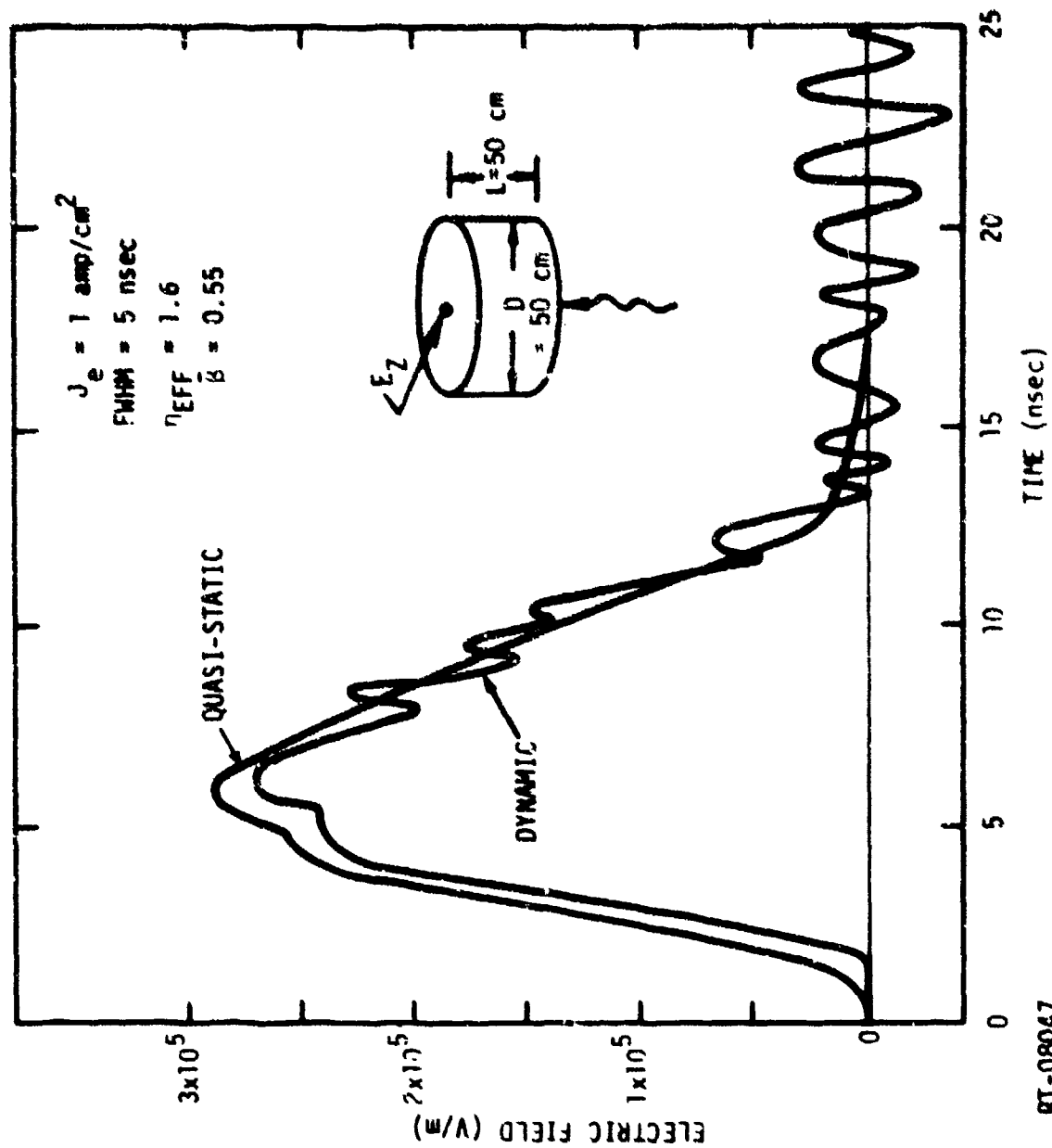
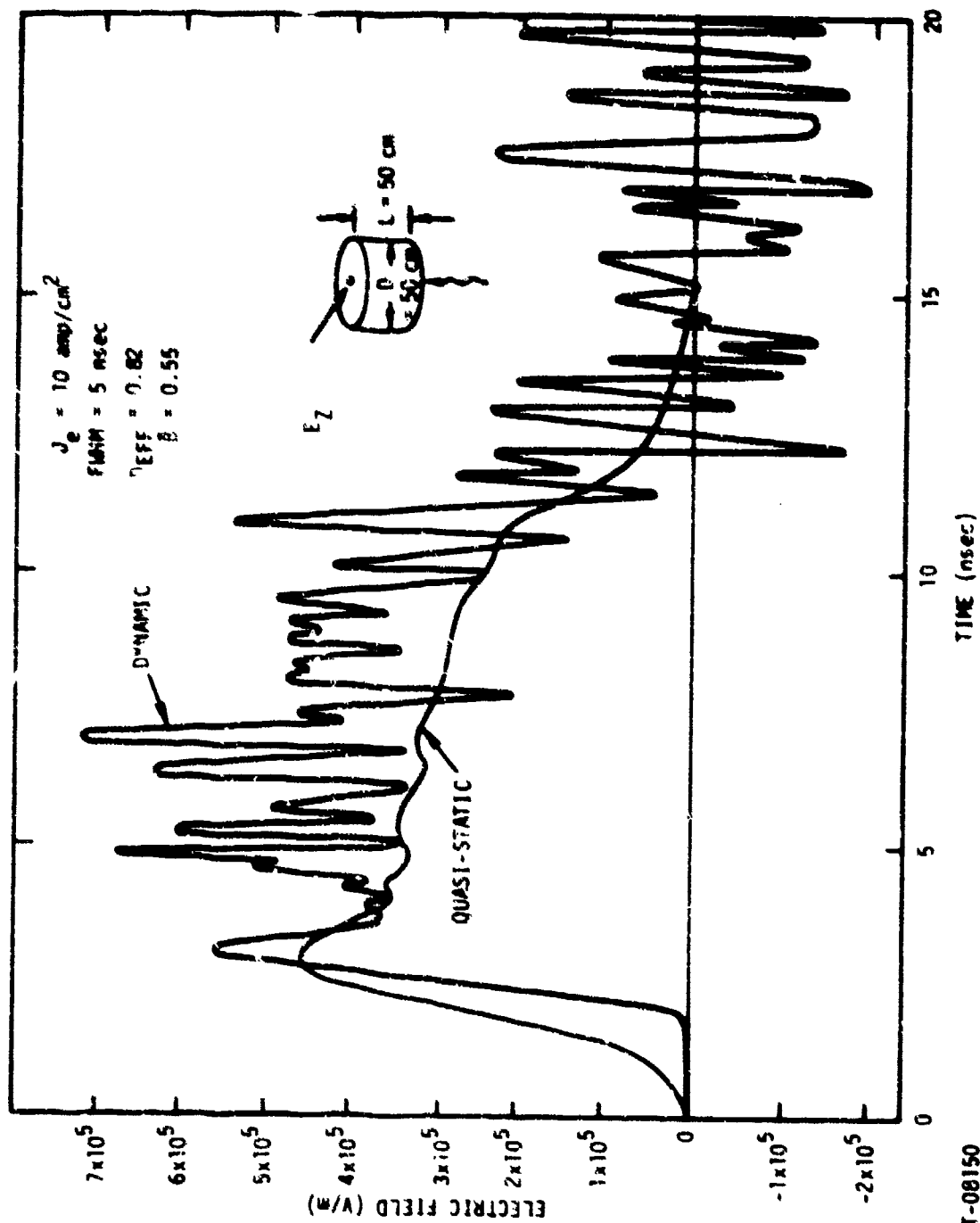


Figure 5-9. Electric field at back versus time for medium SCL case



RT-08150

Figure 5-10. Electric field at back versus time for very high SCL case

current. Effective values of  $\beta$  and  $\eta$  based on the transmitted current are shown in Table 5-1. It is evident that the solutions should be essentially quasi-static for the first two cases but not for the third.

Table 5-1  
PARAMETERS  $\beta$  AND  $\eta$  FROM RESULTS OF THREE DIFFERENT  
EMISSION CURRENT RUNS WITH SPACE-CHARGE-LIMITING

Emission Current Level (amp/cm <sup>2</sup> )	$\beta$	Rise Time (nsec)	$\eta_{\text{EFF}}$	$\eta^2_{\text{EFF}}$	$\eta_{\text{EFF}}/\beta$
0.1	0.55	5.0	3.0	9.0	16
1.0	0.55	2.8	1.6	2.6	4.7
10.0	0.55	1.4	0.82	0.66	1.2

$\beta$  is the average value of electron velocity over the speed of light.

$\eta_{\text{EFF}}$  is rise time of transmitted current pulses divided by  $L/c$  time of the cavity.

Quasi-static solutions require  $\eta^2 \gg 1$ ;  $\eta/\beta \gg 1$ .

## 5.5 SUMMARY AND CONCLUSIONS

A fully dynamic, self-consistent IEMP code, DYNACYL, has been developed and exercised to determine the range of validity of previously developed quasi-static calculations. Solutions for the dynamic treatment vary from the quasi-static approach in three important respects. The dynamic solutions generally display higher peak field values than quasi-static solutions, are delayed in time due to the finite speed of light, and contain oscillatory late-time solutions characteristic of resonances associated with the particular geometry of interest.

Two parameters have been defined which determine whether the solution to a particular problem will display dynamic effects or will be essentially quasi-static. It has been found that problems which are essentially quasi-static without SCL may display highly dynamic behavior under SCL conditions. The SCL causes fields and currents to reach maximum values much sooner than the emitted pulse and thereby increases the frequency content of the effective driving function.

Finally, it has been determined that the quasi-static solutions yield essentially the same results (to within a factor of two) as dynamic solutions over virtually the entire range of interest of IEMP problems, with the notable exception of the late-time response after the end of the emitted pulse. This portion of the response is electromagnetic in nature and cannot be determined from the quasi-static approach.

#### REFERENCES

1. E. P. dePlomb and A. J. Woods, "TEDIEM-RZ and -RΘ: Two Dimensional Time-Dependent IEMP Computer Codes," DNA 3140F, March 10, 1973.
2. E. P. Wenaas et al., "Topics in SGEMP Analysis," INTEL-RT 0001-080, February 25, 1974.
3. Dan Higgins, Mission Research Corp., private communication, February 1974.

## APPENDIX A

### SCALING SGEMP EXPERIMENTS\*

#### 1. INTRODUCTION

In many system-related experiments dealing with SGEMP effects, it may be necessary or desirable to scale one or more of the many variables available to the experimenter. Insight into scaling laws is necessary to design meaningful experiments, choose proper excitation sources, and relate results to systems of interest. The effort described in this note is a first attempt at putting down a number of obvious relationships between scaling parameters.

We begin first by listing the important quantities which can most readily be varied by the experimenter:

$t$  = time (varied by changing the time history of the photon pulse)

$r$  = dimension (characteristic dimension of test object)

$\gamma$  = incident photon fluence

$v$  = electron velocity

There are also a number of ancillary quantities which cannot readily be varied:

$q$  = electron charge

$m$  = electron mass

$\epsilon$  = permittivity of free space

$\mu$  = permeability of free space

$\sigma$  = conductivity

We seek information on how the important variables of *time*, *dimension*, *fluence*, and *electron velocity* will affect the electromagnetic quantities of interest, which include:

$E$  = electric field

$H$  = magnetic field strength

$I$  = current

$\rho$  = charge density

$J$  = current density

$\Delta V$  = potential difference

---

\*Work performed under IRT-sponsored IR&D program.

It is convenient to relate the scaled quantities denoted by a (') from the unscaled quantities with the following relationships:

$$t' = t/\tau$$

$$r' = r/R$$

$$\gamma' = \Gamma\lambda$$

$$v' = \beta v$$

where the factors  $\tau$ ,  $R$ ,  $\Gamma$ , and  $\beta$  are the dimensionless scaling factors. We assume that  $q$ ,  $m$ ,  $\mu$ , and  $\epsilon$  do not scale and that  $\sigma$  is infinite.

In this note, we determine the scaling laws for the linear problem (Section 2) and the nonlinear problem (Section 3). Our solutions, strictly speaking, apply to the space surrounding perfect conductors, as well as to currents flowing on the conductors. Coupling to cables and objects with dielectrics is briefly discussed in Section 4. Solutions for several example problems using the nonlinear DYNASPHERE SGEMP code are presented in Section 5 for illustrative purposes. Finally, system implications are discussed in Section 6, the summary.

## 2. LINEAR SCALING

In this section we apply the scaling laws to Maxwell's equations to determine how the electromagnetic quantities of interest scale for linear problems in which the electron motion is not perturbed by the fields. The emitted current becomes

$$J'_e = f \frac{dy'}{dt} = f \Gamma \tau \frac{dy}{dt} ,$$

$$J'_e = \Gamma \tau J_e . \quad (1)$$

The charge density at the emitting surfaces located at point  $R_0$  for each velocity increment becomes

$$J'_e = \rho'_v(R'_0) v' ,$$

$$\rho'_v(R'_0) = \frac{J'_e}{v'} ,$$

$$\rho_v'(R_0') = \frac{\Gamma \tau J_e}{\beta v} = \frac{\Gamma \tau}{\beta} \rho_v(R_0) . \quad (2)$$

The scaled equation of motion for the electron in the linear region, where the electron trajectory is unaffected by the electron and magnetic fields, is

$$r_e'(t') = v't' + R_0' , \quad (2A)$$

where  $R_0'$  is the position of the electron on the emitting surface. Substituting for  $v'$ ,  $t'$ , and  $R_0'$ ,

$$r_e'(t') = \beta v \frac{t}{\tau} + \frac{R_0}{R} .$$

The solution scales if the following relationships hold.

$$\boxed{\frac{\tau}{\beta} = R} \quad (3)$$

and

$$r_e' = \frac{1}{R} [vt + R_0] = \frac{r_e}{R} . \quad (4)$$

The position of the electron scales; therefore, the ratio of the charge density at a point in space to the charged density at the emitting surface in the scaled geometry equals the same ratio in the unscaled geometry for electrons of velocity  $v$ .

$$\frac{\rho_v'(R_0')}{\rho_v'(r')} = \frac{\rho_v(R_0)}{\rho_v(r)} .$$

From Eq. 2,

$$\rho_v'(r') = \rho_v(r) \frac{\rho_v'(R_0')}{\rho_v(R_0)} = \rho_v(r) \frac{\Gamma \tau}{\beta} . \quad (5)$$

This result holds for charge as a result of any emitted velocity increment and, therefore, holds for all velocity increments. The total charge density due to all velocity increments scales properly provided all velocity increments scale as  $\beta$  (the velocity or energy distribution remains unchanged). Thus,

$$\boxed{\rho'(r') = \rho(r) \frac{\Gamma \tau}{\beta} .} \quad (6)$$

Substituting these results into the set of Maxwell's equations yields

$$(a) \quad \nabla' \cdot E' = \frac{\rho'}{\epsilon_0} . \quad (7)$$

Noting that  $\nabla' = R \nabla$  ,

$$R \nabla \cdot E' = \frac{\Gamma \tau \rho}{\beta \epsilon} ,$$

$$\nabla \cdot E' \frac{\beta R}{\Gamma \tau} = \frac{\rho}{\epsilon} ,$$

or

$$E = \frac{E' \beta R}{\Gamma \tau} .$$

Thus,

$$\boxed{E' = E \frac{\Gamma \tau}{\beta R}} . \quad (8)$$

$$(b) \quad \nabla' \times H' = \rho' v' + \epsilon \frac{dE'}{dt} ,$$

$$R \nabla \times H' = \frac{\Gamma \tau}{\beta} \rho v + \epsilon \tau \frac{d}{dt} \left( \frac{\Gamma \tau E}{\beta R} \right) .$$

Using the necessary condition 3,  $\tau/\beta = R$ .

$$R \nabla \times H' = \Gamma \tau \rho v + \tau \Gamma \epsilon \frac{dE}{dt}$$

or

$$\nabla \times \frac{R H'}{\Gamma \tau} = \rho v + \epsilon \frac{dE}{dt} .$$

Thus,

$$H = \frac{R H'}{\Gamma \tau}$$

or

$$\boxed{H' = \frac{\Gamma \tau}{R} H} . \quad (10)$$

$$(c) \quad \nabla' \times E' = \frac{-dB'}{dt} = \frac{-1}{\mu} \frac{dH'}{dt} , \quad (11)$$

$$R \nabla \times E' = \frac{-1}{\mu} \tau \frac{\Gamma \tau}{R} \frac{dH}{dt} ,$$

$$R^2 \nabla \times \frac{\mathbf{E}'}{\Gamma \tau^2} = \frac{-1}{\mu} \frac{d\mathbf{I}}{dt}.$$

Therefore,

$$\frac{R^2 \mathbf{E}'}{\Gamma \tau^2} = \mathbf{E},$$

or

$$\mathbf{E}' = \frac{\Gamma \tau^2}{R^2} \mathbf{E}.$$

Using condition 3,  $\beta = \tau/R$ ,

$$\boxed{\mathbf{E}' = \frac{\Gamma \tau \beta \mathbf{E}}{R}} \quad (12)$$

The expression for the scaled electron field given by Eq. 12 is inconsistent with Eq. 8 unless

$$\boxed{\beta = 1} \quad (13)$$

Thus, we see that proper scaling can be achieved only if the electron velocity is not scaled.

The potential difference between any two points is given by

$$\Delta V'(r') = - \int_{y=R_0'}^{y=r'} E'(y) dy \quad (14)$$

$$= - \int_{y=R_0/R}^{y=r/R} E'(y) dy$$

$$= - \int_{y=R_0}^{y=R} E'(y) \frac{dy}{R}$$

$$= - \frac{1}{R} \int_{y=R_0}^{y=R} \frac{\Gamma \tau E}{R} dy = \Delta V(r) \frac{\Gamma \tau}{R^2}$$

$$\boxed{\Delta V'(r') = \frac{\Gamma \tau}{R^2} \Delta V(r)} \quad (15)$$

The total currents scale as follows.

$$I' = \oint H' dl' = \oint \frac{\Gamma \tau}{R} H \frac{dl}{R} \quad (16)$$

$$I' = \frac{\Gamma \tau}{R^2} I \quad (17)$$

Condition 13, along with condition 3, requires

$$\tau = R \frac{1}{2} \alpha, \quad (18)$$

where  $\alpha$  is defined as the primary scaling factor for both time and space.

Scaling results are summarized in Table B-1.

Table A-1

Scaling Factors	Scaling Requirements
$t' = t/\tau$	$\alpha \triangleq R = \tau$
$r' = r/R$	$\beta = 1$
$v' = \beta v$	
$\gamma' = \Gamma \gamma$	

Scaling Results

$$\begin{aligned} J' &= \alpha \Gamma J_e \\ \rho' &= \alpha \Gamma \rho \\ E' &= \Gamma E \\ H' &= \Gamma H \\ \Delta V' &= \frac{\Gamma}{\alpha} \Delta V \\ I' &= \frac{\Gamma}{\alpha} I \end{aligned}$$

In summary, scaling is possible for a linear matrix of electrons in free space in the presence of perfect conditions if the relationships in Table A-1 are satisfied. The various quantities will scale as shown. The development here does not treat dielectrics or imperfect conductors.

If we require that the potential at the scaled point  $r'$  be the same as that at the unscaled point  $r$ , then we require that

$$\Gamma = \alpha, \quad (19)$$

a condition which we will show in Section 3 is necessary for proper scaling of the nonlinear solution.

### 3. NONLINEAR SCALING

Scaling for cases in which the electron trajectories are perturbed by the fields can be treated by replacing Eq. 2A by

$$r'(t') = \int_{\eta=0}^{\eta=t'} \int_{\xi=0}^{\xi=\eta} F[r'(\xi), \xi] d\xi d\eta + \int_{\xi=0}^{\xi=t'} v'(r', \xi) d\xi + R'_0 \quad (20)$$

where

$$F' = q(E' + v' \times B') \quad (21)$$

We first replace  $t'$  by  $t/\tau$  on the right side:

$$r'(t') = \int_{\eta=0}^{\eta=t/\tau} \int_{\xi=0}^{\xi=\eta} F[r'(\xi), \xi] d\xi d\eta + \int_{\xi=0}^{\xi=t/\tau} v'(r', \xi) d\xi + R'_0.$$

Now replace the arbitrary integration variable  $\eta$  by  $\eta/\tau$ :

$$r'(t') = \int_{\eta=0}^{\eta=t} \int_{\xi=0}^{\xi=\eta/\tau} F'[r'(\xi), \xi] d\xi \frac{d\eta}{\tau} + \int_{\xi=0}^{\xi=t/\tau} v'(r', \xi) d\xi + R'_0.$$

Next replace the arbitrary integration variable  $\xi$  by  $\xi/\tau$  and the coordinate  $R'_0$  by  $R_0/R$ :

$$r'(t') = \int_{\eta=0}^{\eta=t} \int_{\xi=0}^{\xi=\eta} F'[r'(\xi/\tau), \xi/\tau] \frac{d\xi}{\tau} \frac{d\eta}{\tau} + \int_{\xi=0}^{\xi=t} v'(r', \xi/\tau) \frac{d\xi}{\tau} + \frac{R_0}{R}.$$

Using the expression for  $E'$  and  $H'$  in Table A-1, Eq. 21 becomes

$$F' = q(E' + v' \times B') = q(\tau E + \tau v \times B) = \tau F,$$

and the equation of motion becomes

$$r'(t) = \frac{r}{\tau} \int_0^t \int_0^\eta F \, d\xi \, d\eta + \frac{1}{\tau} \int_0^t v \, d\xi + \frac{R_0}{R}.$$

The position  $r'(t)$  will scale properly if

$$\frac{r}{\tau} = \frac{1}{\tau} = \frac{1}{R}.$$

But  $\tau = R = \alpha$ , so that

$$\frac{r}{\alpha} = \frac{1}{\alpha} = \frac{1}{\alpha}.$$

Therefore, for the position of the electron to scale properly, the following relation must hold.

$$\boxed{r = \alpha}.$$

This condition is equivalent to condition 19, requiring that the potential at the scaled point  $r'$  equal that at the unscaled point  $r$ .

We summarize the scaling requirements for the linear and nonlinear cases in Table A-2.

Table A-2

Scaling Parameters	Scaling Factors
$t' = t/\tau$	$\tau = \alpha$
$r' = r/R$	$R = \alpha$
$v' = \beta v$	$\beta = 1$
$\gamma' = \Gamma \gamma$	$\Gamma = \alpha$
<u>Scaled Field Quantities</u>	
$J' = \alpha^2 J$	
$\rho' = \alpha^2 \rho$	
$E' = \alpha E$	
$H' = \alpha H$	
$\Delta v' = \Delta v$	
$I' = I$	

#### 4. SAMPLE PROBLEMS

To verify the scaling laws discussed in the previous several chapters, we have exercised the DYNASPHERE SCEMP code for several problems of interest. The conditions for the two sets of problems shown in Table A-3 were chosen so that one set would be linear and one set would be space-charge-limited and, therefore, nonlinear.

Magnetic fields, electric fields, and surface currents on a spherical surface were calculated at the following points.

$$E_r \text{ at } \theta = 0^\circ$$

$$B_\phi \text{ at } \theta = 90^\circ$$

$$I \text{ through a plane at } \theta = 90^\circ$$

Results are shown in Table A-4 and graphically illustrated in Figures A-1 through A-6.

Note that the results are plotted as a function of  $E \times R$ ,  $H \times R$ , and  $I$  versus  $t/(2\pi R/c)$  for a triangular pulse of rise time and full width at half maximum of  $\pi R/c$ . While the scales at first seem abstract, the results are quite general in that they apply to any sphere with radius  $R$  excited by a pulse with rise time  $\pi R/c$ .

Table A-3  
SCALING PROBLEM SET CHARACTERISTICS

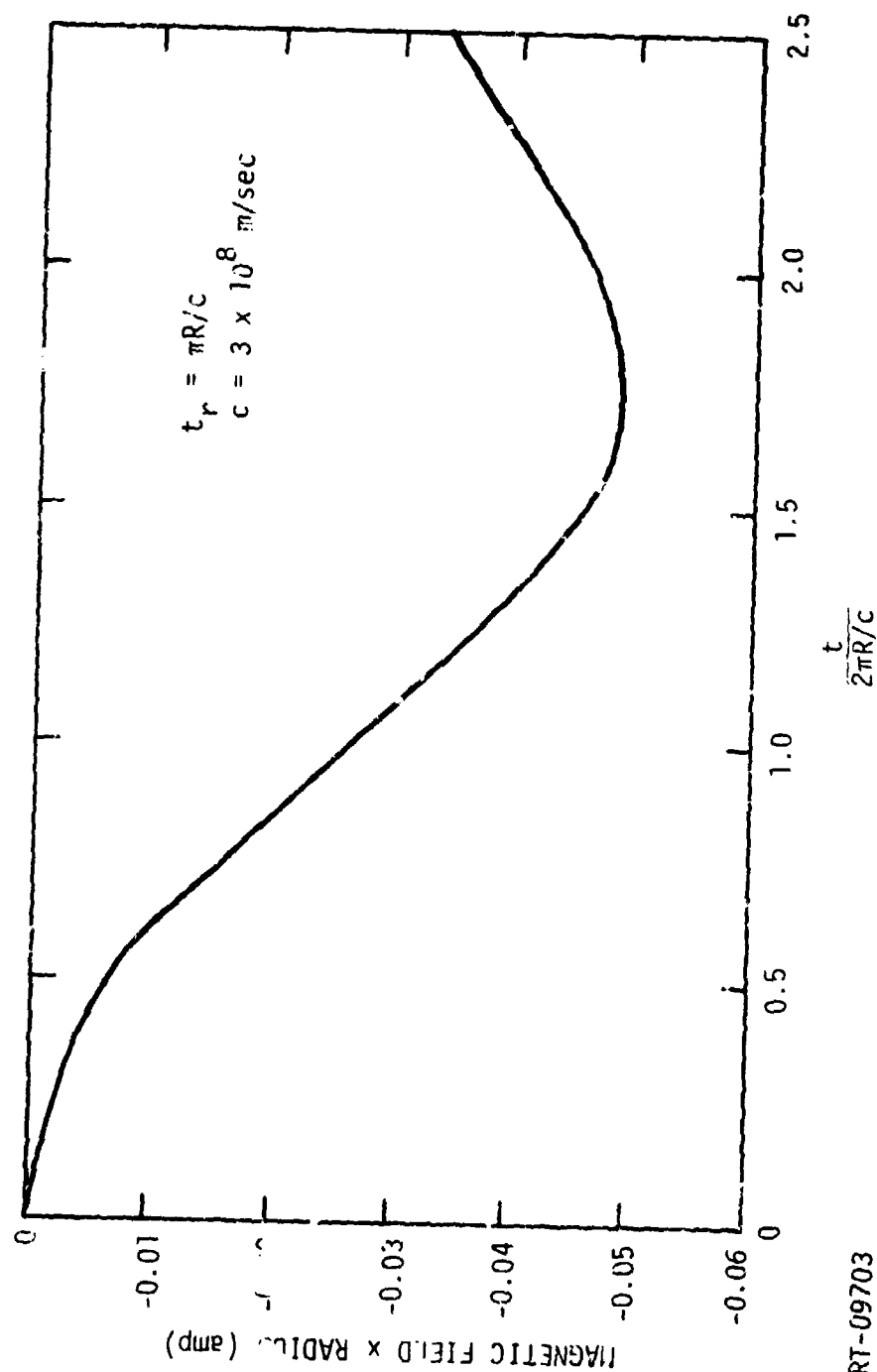
Range	Sphere Size, $R_0$ (m)	Emitted Charge (coulomb)	Pulse Rise Time (nsec)	Pulse FWHM (nsec)	Average Electron Energy (keV)
Linear	Large sphere (2)	$4.8 \times 10^{-8}$	20	20	10
	Small sphere (0.2)	$4.8 \times 10^{-9}$	2	2	10
Nonlinear	Large sphere (2)	$2.6 \times 10^{-4}$	20	20	10
	Small sphere (0.2)	$2.6 \times 10^{-5}$	2	2	10

Table A-4  
TABULATED RESULTS FOR TWO PROBLEM SETS

Time (nsec)	$J_e$ (amp/m <sup>2</sup> )	E (0°) (volt/m)	H (90°) (amp/m)	Surface Current (90°) (amp)
Inner radius 0.2 m; peak emission current = 10 amp/m <sup>2</sup> ; $t_r = 2$ nsec				
1	4.75	$2.736 \times 10^2$	$-6.006 \times 10^{-2}$	$-7.454 \times 10^{-2}$
2	9.75	$1.063 \times 10^3$	$-2.668 \times 10^{-1}$	$-3.3112 \times 10^{-1}$
3	5.25	$1.714 \times 10^3$	$-4.565 \times 10^{-1}$	$-5.6660 \times 10^{-1}$
4	$2.5 \times 10^{-1}$	$1.646 \times 10^3$	$-4.643 \times 10^{-1}$	$-5.7627 \times 10^{-1}$
5	0	$1.271 \times 10^3$	$-3.349 \times 10^{-1}$	$-4.1566 \times 10^{-1}$
Inner radius = 2 m; peak emission current 0.1 amp/m <sup>2</sup> ; $t_r = 20$ nsec				
10	$4.75 \times 10^{-2}$	$2.736 \times 10^1$	$-6.004 \times 10^{-3}$	$-7.4522 \times 10^{-2}$
20	$1 \times 10^{-1}$	$1.066 \times 10^2$	$-2.670 \times 10^{-2}$	$-3.3140 \times 10^{-1}$
30	$5.2500 \times 10^{-2}$	$1.716 \times 10^2$	$-4.573 \times 10^{-2}$	$-5.6753 \times 10^{-1}$
40	$2.5 \times 10^{-3}$	$1.648 \times 10^2$	$-4.648 \times 10^{-2}$	$-5.7689 \times 10^{-1}$
50	0	$1.273 \times 10^2$	$-3.357 \times 10^{-2}$	$-4.1666 \times 10^{-1}$
Inner radius = 0.2 m; peak emission current = $5 \times 10^4$ amp/m <sup>2</sup> ; $t_r = 2$ nsec				
0.5	$1.1875 \times 10^4$	$3.257 \times 10^5$	$-4.962 \times 10^1$	$-6.584 \times 10^1$
1	$2.4375 \times 10^4$	$1.291 \times 10^6$	$-2.335 \times 10^2$	$-2.8982 \times 10^2$
1.5	$3.6875 \times 10^4$	$2.019 \times 10^6$	$-2.672 \times 10^2$	$-3.3169 \times 10^2$
2	$4.9375 \times 10^4$	$1.961 \times 10^6$	$-1.502 \times 10^2$	$-1.8642 \times 10^2$
2.5	$3.8125 \times 10^4$	$1.838 \times 10^6$	$-1.114 \times 10^2$	$-1.3831 \times 10^2$
3	$2.5625 \times 10^4$	$1.625 \times 10^6$	$-8.582 \times 10^1$	$-1.0652 \times 10^2$
3.5	$1.3125 \times 10^4$	$1.306 \times 10^6$	$-1.394 \times 10^2$	$-1.7301 \times 10^2$
4	$6.25 \times 10^2$	$7.963 \times 10^5$	$-7.442 \times 10^1$	$-9.2373 \times 10^1$
4.5	0	$4.54 \times 10^5$	$1.251 \times 10^2$	$1.5523 \times 10^2$
5.0	0	$3.937 \times 10^5$	$1.950 \times 10^2$	$2.4201 \times 10^1$

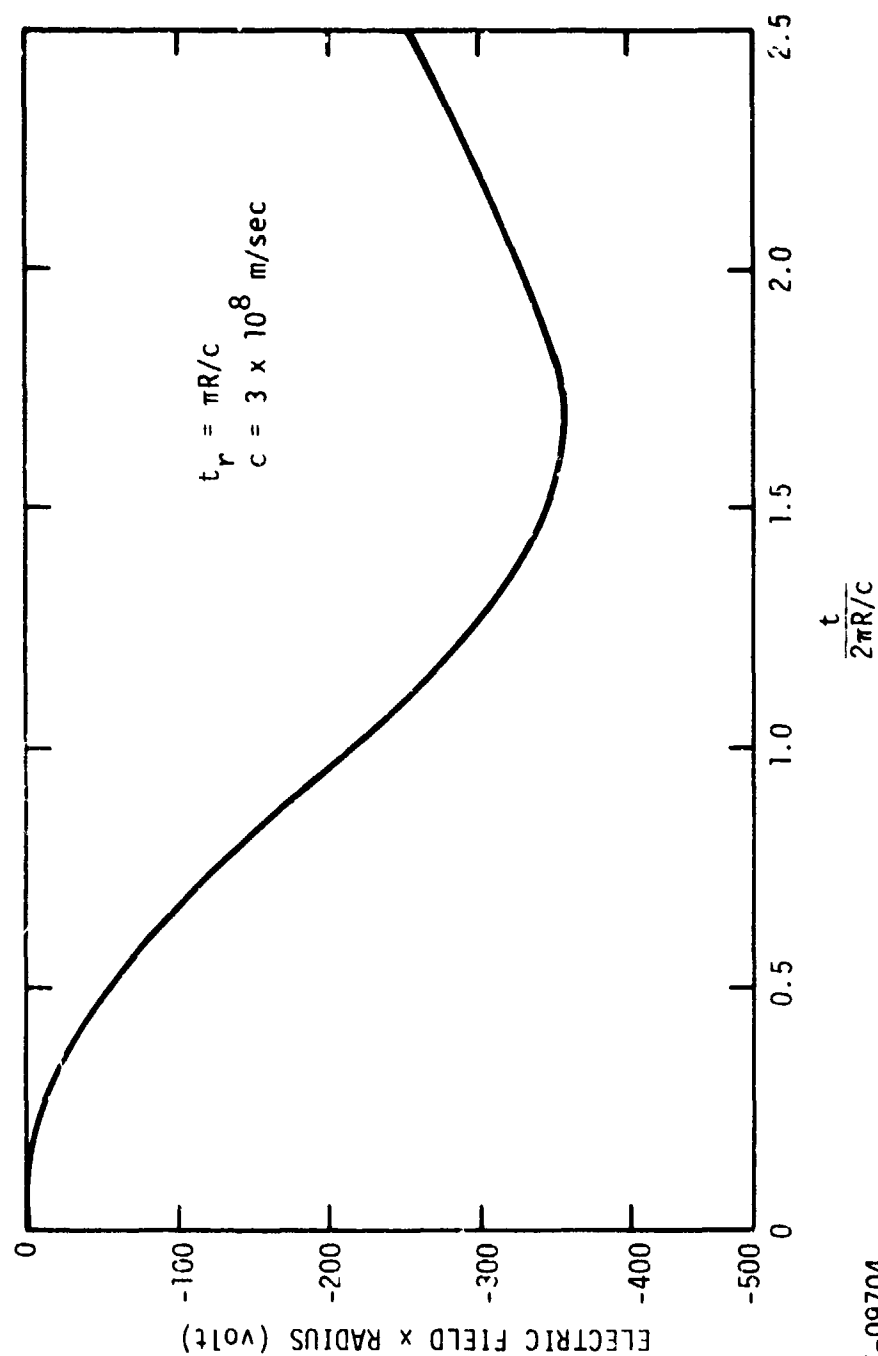
Table A-4 (continued)

Time (nsec)	$J_e$ (amp/m <sup>2</sup> )	E (0°) (volt/m)	H (90°) (amp/m)	Surface Current (90°) (amp)
Inner radius = 2 m; peak emission current = $5 \times 10^2$ amp/m <sup>2</sup> ; $t_r = 20$ nsec				
5	$1.875 \times 10^2$	$3.257 \times 10^4$	-4.9561	$-6.5464 \times 10^{-1}$
10	$2.4375 \times 10^2$	$1.291 \times 10^5$	$-2.334 \times 10^1$	$-2.8972 \times 10^2$
15	$3.6875 \times 10^2$	$2.019 \times 10^5$	$-2.672 \times 10^1$	$-3.3168 \times 10^2$
20	$5 \times 10^2$	$1.963 \times 10^5$	$-1.502 \times 10^1$	$-1.8645 \times 10^2$
25	$3.8125 \times 10^2$	$1.838 \times 10^5$	$-1.118 \times 10^1$	$-1.3882 \times 10^2$
30	$2.5625 \times 10^2$	$1.626 \times 10^5$	-8.492	$-1.0540 \times 10^2$
35	$1.3125 \times 10^2$	$1.306 \times 10^5$	$1.401 \times 10^1$	$-1.7393 \times 10^2$
40	6.25	$7.962 \times 10^4$	-7.441	$-9.235 \times 10^{-1}$
45	0	$4.54 \times 10^4$	$1.261 \times 10^1$	$1.5655 \times 10^2$
50	0	$3.935 \times 10^4$	$1.933 \times 10^1$	$2.3993 \times 10^2$



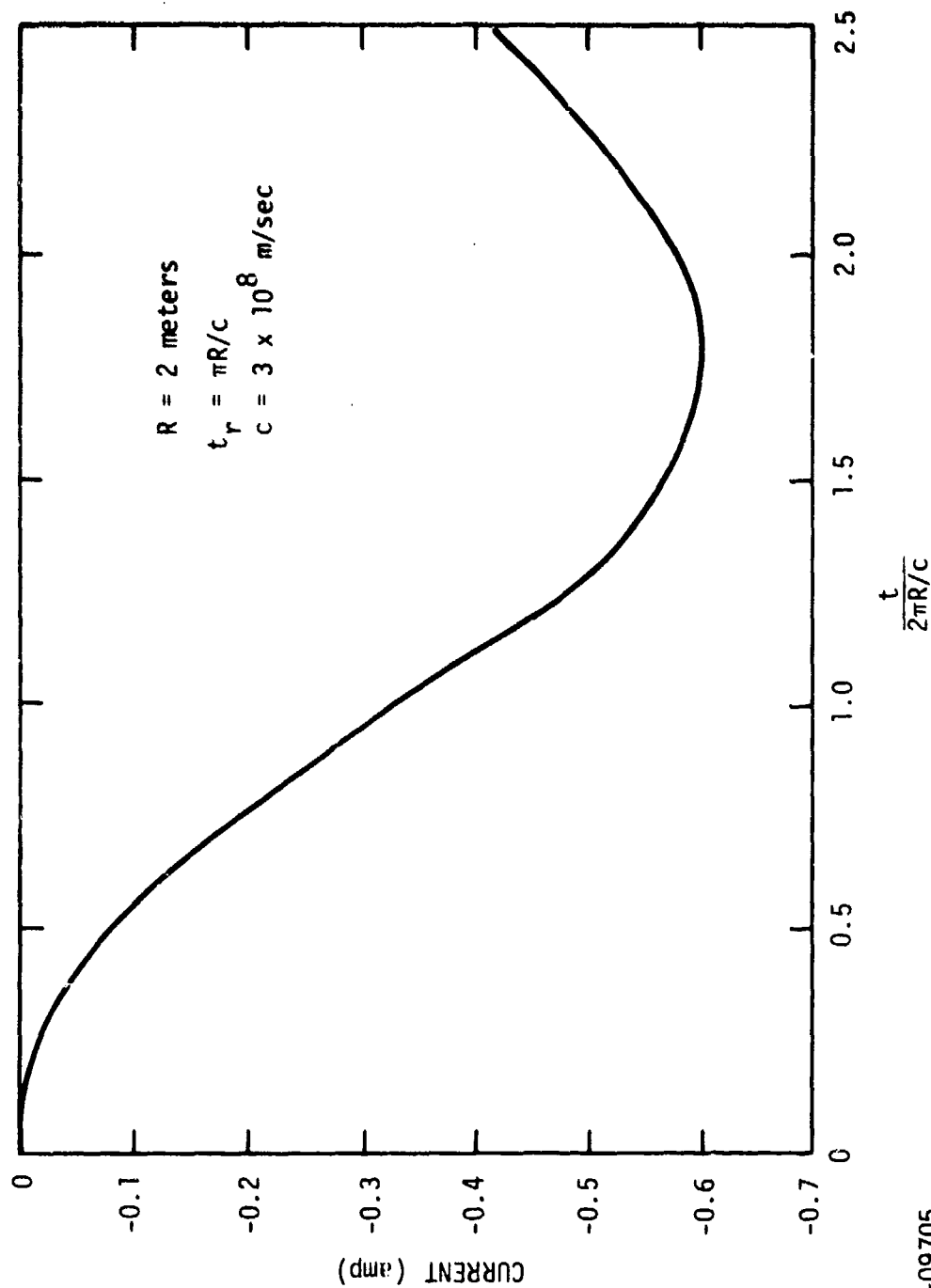
RT-09703

Figure A-1 Angular magnetic field strength at spherical surface ( $\theta = 90^\circ$ ) for the two low-emission cases of Table A-3. Electron emission is sufficiently low that the problem is linear. Excitation pulse rise time  $t_r$  is  $\pi R/c$ .



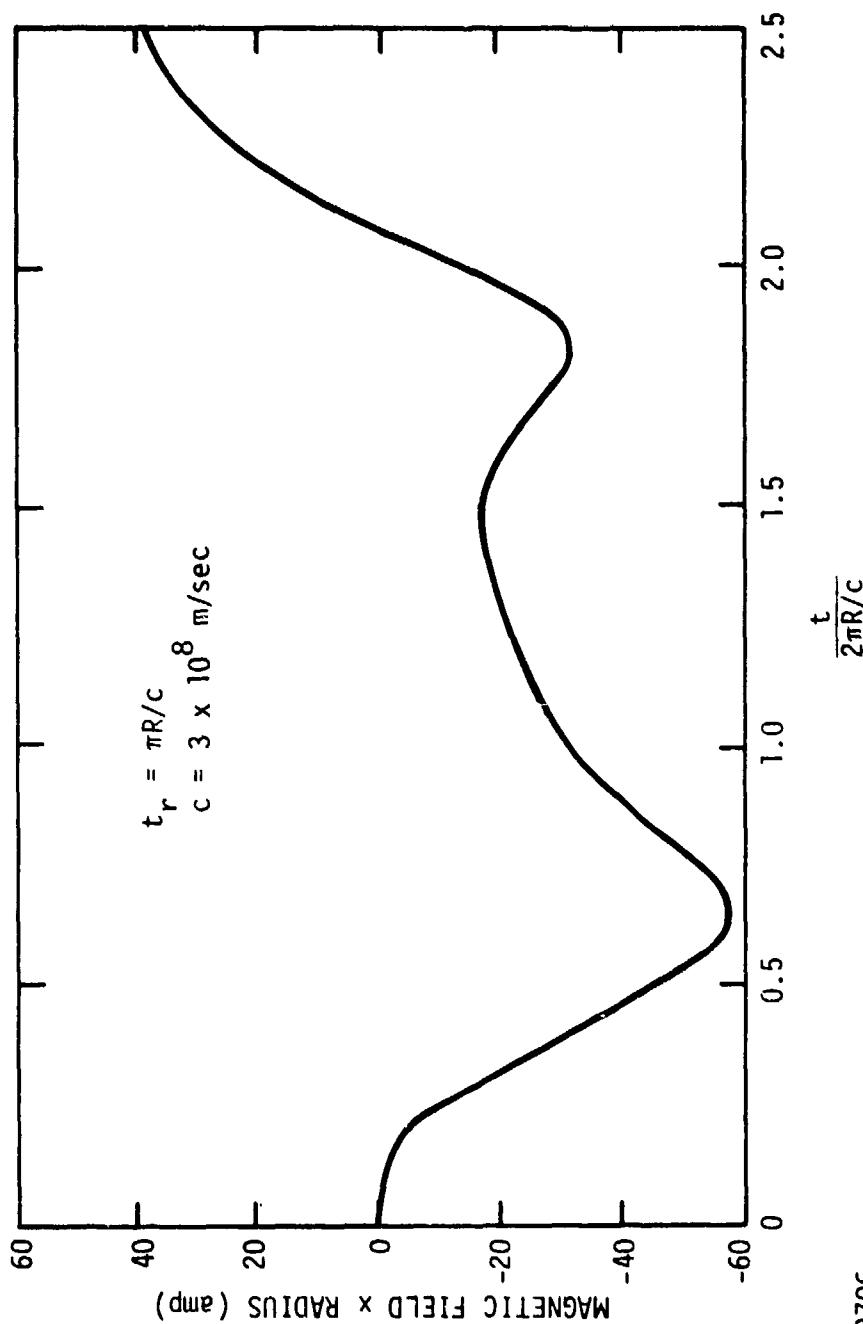
RT-09704

Figure A-2 Radial electric field at the spherical surface ( $\theta = 90^\circ$ ) for the two low-emission cases. Electron emission is sufficiently low that the problem is linear. Excitation pulse rise time  $t_r$  is  $\pi R/c$ .



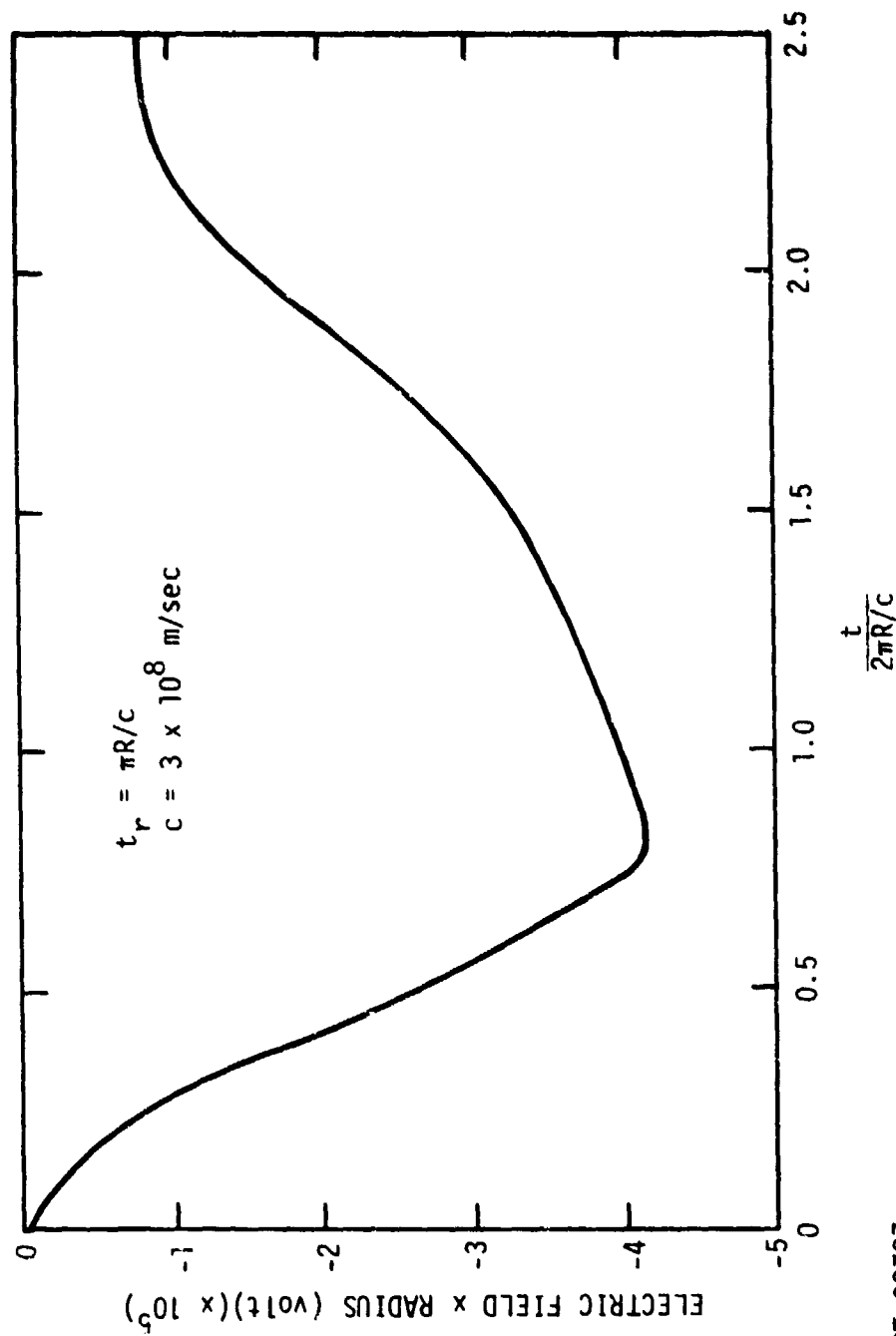
RI-09705

Figure A-3 Surface current passing through a plane located at  $\theta = 90^\circ$  for the two low-emission cases. Electron emission is sufficiently low that the problem is linear. Excitation pulse rise time  $t_r$  is  $\pi R/c$ .



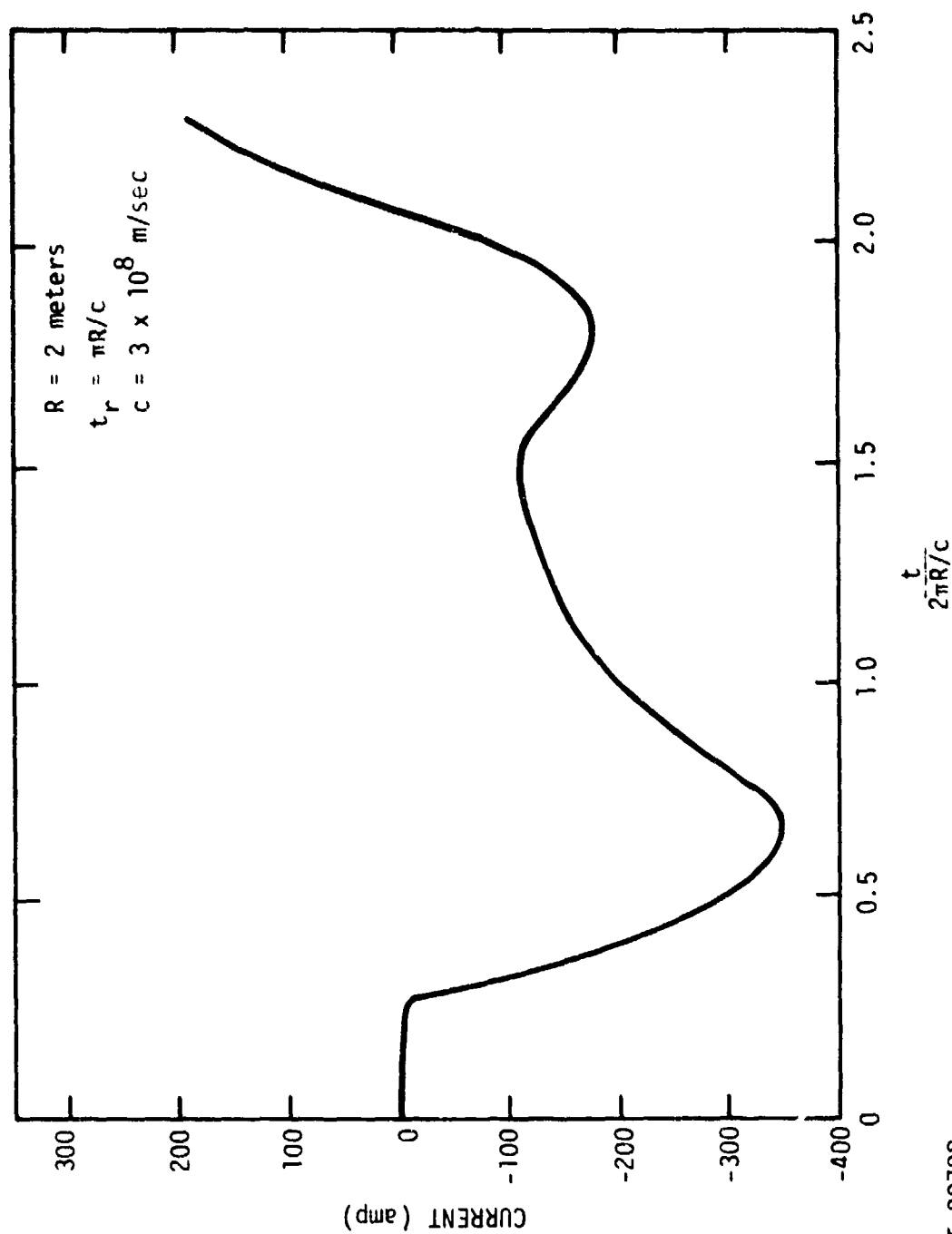
RT-09706

Figure A-4 Angular magnetic field strength at the spherical surface ( $\theta = 90^\circ$ ) for the two high-emission cases. Electron emission is sufficiently high that the problem is nonlinear. Excitation pulse rise time  $t_r$  is  $\pi R/c$ .



RT-09707

Figure A-5 Radial electric field at the spherical surface ( $\theta = 90^\circ$ ) for the two high-emission cases. Electron emission is sufficiently high that the problem is nonlinear. Excitation pulse rise time  $t_r$  is  $\pi R/c$ .



RT-09708

Figure A-6 Surface emission passing through a plane located at  $\theta = 90^\circ$  for the two high-emission cases. Electron emission is sufficiently high that the problem is nonlinear. Excitation pulse rise time  $t_r$  is  $\pi R/c$ .

## 5. SUMMARY

Of the many variables available to the SGENP experimenter, the ones of most interest are the object dimension, the pulse time history, the incident fluence, and the incident photon energy spectrum (or the emitted electron velocity distribution). In this note we have explored the possibility of changing one or more of these parameters to values more convenient to the experimenter, while retaining the essential features and results corresponding to the original parameter values.

First, we find that one cannot change the electron velocity and hope to scale the solutions. A simple "Gedanken" experiment illustrates the problem. Consider a pillbox with steady current flowing from one face to the other. The magnetic field within the cavity is proportional to the emitted current density and is independent of the velocity. On the other hand, the electric field is proportional to the charge density which, in turn, is inversely proportional to the electron velocity. Thus, the magnetic and electric field ratios change as a function of electron velocity, and the solutions cannot scale.

Next, we find that the dimensions and pulse time must scale by the same factor. This scaling is required to keep the ratio of excitation wavelength to object wavelength constant. It is also required to ensure that the electron reaches the scaled distance from the object at the correct scaled time.

Finally, we find the total charge emitted must be changed by the inverse factor used for pulse and object dimension if we are to retain the same potential at the scaled coordinate. For nonlinear problems in which space-charge limiting is important, it is essential to have the potential difference between two scaled points equal to that between two unscaled points (along the same path).

We therefore conclude that the essential features of a problem are unchanged if

1. the electron velocity is constant,
2. the pulse time history is scaled by  $\alpha$ ,

3. the object dimension is scaled by  $\alpha$ ,
4. the incident fluence is scaled by  $1/\alpha$ .

Such a scaling will result in the following changes in field values, assuming electron motion in free space in the presence of perfectly conducting boundaries.

$t' = t/\alpha$	$\rho' = \alpha^2 \rho$
$r' = r/\alpha$	$E' = \alpha E$
$\Gamma' = \alpha \Gamma$	$H' = \alpha H$
$v' = v$	$\Delta V' = \Delta V$
$J' = \alpha^2 J$	$I' = I$

By scaling time, we mean that all features of the incident photon pulse/emitted electrons change by the factor  $\alpha$ : the pulse is essentially expanded or compressed by the factor  $\alpha$ .

Scaling problems associated with the electron velocity are of particular concern because of the wide variety of photon sources currently available or under consideration. The results of this note indicate that, strictly speaking, one cannot modify other variables such as object dimensions, machine output, time history, etc., to offset changes in electron velocity. Therefore, one cannot directly extrapolate results from one photon energy range to another. However, we note that the electron velocity has a square-root dependence on energy, and therefore, the results are not extremely sensitive to changes in the energy distribution.

It should be noted that decreasing an object size by the factor  $\alpha$  requires a corresponding decrease in the pulse time history by the factor  $\alpha$ ; however, the photon fluence need not be increased by a corresponding factor  $\alpha$  if the problem is in the linear regime where space-charge limiting is unimportant.

## APPENDIX B

### DYNASPHERE

This appendix contains a mathematical description of the code DYNASPHERE, which has been developed to numerically evaluate electron motion and electromagnetic field generation in a region bounded by two concentric spheres. The spheres are taken to be perfectly conducting, and the problem characteristics are taken to be rotationally symmetric, reducing the problem to two dimensions. The electromagnetic fields are calculated from the full set of Maxwell's equations in this simplified geometry, and the electric fields are used to influence the electron motion.

Electron emission from the inner sphere is the source term for driving the problem. Currents and fields between the two spheres are the quantities which result from the calculation. The electron emission must be specified in space and time. For example, in the case where the emission is due to photon interaction with materials, the photon energy and time spectrum determines the emission characteristics of the electrons. (Particles are used to represent large numbers of electrons.) The quantities calculated directly include the currents in the region between the boundaries as well as the electric and magnetic fields in that region. Applying Maxwell's equations properly at the boundaries gives surface currents and charge densities.

The remainder of this appendix outlines the method of solving the field equations, the conversion of particle motion into currents useful for driving these equations, and the method of calculating the particle motion. Since the first two of these procedures is given for a generalized coordinate system, their description is given initially. The specialization to the particular coordinate scheme used here is then discussed, and the particle motion is treated in these coordinates.

The numerical solution of Maxwell's equations is straightforward in a region enclosed by perfectly conducting surfaces, such as the region considered in DYNASPHERE. The initial conditions are that all fields and charge densities are zero. The currents, as calculated from the motion of the charged particles injected into the region (see below),

are the quantities which drive the time evolution of the fields. Thus, for a medium with the permittivity ( $\epsilon_0$ ) and permeability ( $\mu_0$ ) of free space, Maxwell's equations reduce to

$$\epsilon_0 \frac{\partial \vec{E}}{\partial t} = -\vec{J} + \vec{\nabla} \times \vec{H} ,$$

$$\mu_0 \frac{\partial \vec{H}}{\partial t} = -\vec{\nabla} \times \vec{E} ,$$

with the initial conditions

$$\vec{E} = 0 \quad \text{at } t = 0 ,$$

$$\vec{H} = 0 \quad \text{at } t = 0 ,$$

$$\vec{E} \times \vec{n} = 0 \quad \text{where } \vec{n} \text{ is the normal to the bounding surface .}$$

Putting these equations into numerical form for solution is also straightforward, and may be carried out directly in two dimensions. However, by performing the task in three dimensions, one is forced naturally into a symmetry which is very convenient and not obvious in the two-dimensional case.

To complete the geometrical generality (and permit a simple method of varying zone spacing), the space under consideration is taken to be metrized by the generalized orthogonal coordinates ( $q_1, q_2, q_3$ ) where the order is such that the coordinate system is right-handed. Using the notation of Margenau and Murphy,<sup>\*</sup> displacements in real space,  $ds$ , may be related to displacements in  $q$  space by the functions  $Q$ , where

$$ds = Q_i dq_i .$$

Using this definition and the definition of the curl,  $\nabla \times$ , as the path integral of a quantity in the left-hand direction (Cauchy rule) around a closed path divided by the area of the enclosed surface, Maxwell's equations in finite-difference form can be represented by

---

<sup>\*</sup>H. Margenau and G. M. Murphy, "The Mathematics of Physics and Chemistry," Princeton, D. van Nostrand Company, Inc. (1956).

$$\begin{aligned}
E_1^{n+1}(i+\frac{1}{2}, j, k) = & E_1^n(i+\frac{1}{2}, j, k) - \frac{\Delta t^{n+\frac{1}{2}}}{\epsilon_0} J_1^{n+\frac{1}{2}}(i+\frac{1}{2}, j, k) \\
& + \left\{ \frac{\Delta t^{n+\frac{1}{2}}}{\epsilon_0 Q_2(i+\frac{1}{2}, j, k) \Delta q_2 Q_3(i+\frac{1}{2}, j, k) \Delta q_3} \right\} \\
& \times \left\{ \left[ H_3^{n+\frac{1}{2}}(i+\frac{1}{2}, j+\frac{1}{2}, k) Q_3(i+\frac{1}{2}, j+\frac{1}{2}, k) \Delta q_3 - H_3^{n+\frac{1}{2}}(i+\frac{1}{2}, j-\frac{1}{2}, k) Q_3(i+\frac{1}{2}, j-\frac{1}{2}, k) \Delta q_3 \right] \right. \\
& \left. - \left[ H_2^{n+\frac{1}{2}}(i+\frac{1}{2}, j, k+\frac{1}{2}) Q_2(i+\frac{1}{2}, j, k+\frac{1}{2}) \Delta q_2 - H_2^{n+\frac{1}{2}}(i+\frac{1}{2}, j, k-\frac{1}{2}) Q_2(i+\frac{1}{2}, j, k-\frac{1}{2}) \Delta q_2 \right] \right\}
\end{aligned}$$

and

$$\begin{aligned}
H_1^{n+3/2}(i, j+\frac{1}{2}, k+\frac{1}{2}) = & H_1^{n+\frac{1}{2}}(i, j+\frac{1}{2}, k+\frac{1}{2}) \\
& - \left\{ \frac{\Delta t^{n+1}}{\mu_0 Q_2(i, j+\frac{1}{2}, k+\frac{1}{2}) \Delta q_2 Q_3(i, j+\frac{1}{2}, k+\frac{1}{2}) \Delta q_3} \right\} \\
& \times \left\{ \left[ E_3^{n+1}(i, j+\frac{1}{2}, k+\frac{1}{2}) Q_3(i, j+\frac{1}{2}, k+\frac{1}{2}) \Delta q_3 - E_3^{n+1}(i, j, k+\frac{1}{2}) Q_3(i, j, k+\frac{1}{2}) \Delta q_3 \right] \right. \\
& \left. - \left[ E_2^{n+1}(i, j+\frac{1}{2}, k+\frac{1}{2}) Q_2(i, j+\frac{1}{2}, k+\frac{1}{2}) \Delta q_2 - E_2^{n+1}(i, j+\frac{1}{2}, k) Q_2(i, j+\frac{1}{2}, k) \Delta q_2 \right] \right\}
\end{aligned}$$

with the continuity equation (not essential to determining the fields, but of interest for itself and for converting particle motion into equivalent currents) represented by

$$\begin{aligned}
\rho^{n+1}(i, j, k) = & \rho^n(i, j, k) \\
& - \left\{ \frac{\Delta t^{n+\frac{1}{2}}}{Q_1(i, j, k) \Delta q_1 Q_2(i, j, k) \Delta q_2 Q_3(i, j, k) \Delta q_3} \right\} \\
& \times \left\{ \left[ J_1^{n+\frac{1}{2}}(i+\frac{1}{2}, j, k) Q_2(i+\frac{1}{2}, j, k) \Delta q_2 Q_3(i+\frac{1}{2}, j, k) \Delta q_3 \right. \right. \\
& \quad \left. \left. - J_1^{n+\frac{1}{2}}(i-\frac{1}{2}, j, k) Q_2(i-\frac{1}{2}, j, k) \Delta q_2 Q_3(i-\frac{1}{2}, j, k) \Delta q_3 \right] \right. \\
& \quad \left. + \left[ J_2^{n+\frac{1}{2}}(i, j+\frac{1}{2}, k) Q_1(i, j+\frac{1}{2}, k) \Delta q_1 Q_3(i, j+\frac{1}{2}, k) \Delta q_3 \right. \right. \\
& \quad \left. \left. - J_2^{n+\frac{1}{2}}(i, j-\frac{1}{2}, k) Q_1(i, j-\frac{1}{2}, k) \Delta q_1 Q_3(i, j-\frac{1}{2}, k) \Delta q_3 \right] \right\} \dots
\end{aligned}$$

$$+ \left\{ J_3^{n+1/2} (i, j, k+1/2) Q_1 (i, j, k+1/2) \Delta q_1 Q_2 (i, j, k+1/2) \Delta q_2 \right. \\ \left. - J_3^{n+1/2} (i, j, k-1/2) Q_1 (i, j, k-1/2) \Delta q_1 Q_2 (i, j, k-1/2) \Delta q_2 \right\} .$$

The notation used in these equations requires some comment. The superscript refers to the time step. Thus, some quantities are centered in time and some are at boundaries in time. Corresponding to this, there are two time steps: the time step connecting quantities centered in time,  $\Delta t^n$ , and the time step connecting quantities at boundaries in time,  $\Delta t^{n+1/2}$ .

Subscripts refer to directions in the generalized coordinate space. Thus,  $E_1$  is the component of the electric field along the direction of a displacement in space given by a displacement in  $q_1$  at the spatial point in question. The quantities in parentheses refer to the position in space. Thus,  $E_1(\alpha, \beta, \gamma)$  is evaluated at the point in space determined by the coordinates

$$q_1 = \alpha \Delta q_1 + q_{1(MIN)} ,$$

$$q_2 = \beta \Delta q_2 + q_{2(MIN)}$$

$$q_3 = \gamma \Delta q_3 + q_{3(MIN)} ,$$

where the minimum value of the coordinate is specified for convenience, allowing the spatial boundaries to be other than zero in the  $q$  space.

It will be noted that the grid spacing in  $q$  space is uniform. Further, if one of the  $Q$ 's is zero at a point of interest, the procedure fails. In fact, at such points the coordinate system does not metrize real space. The failure is that many points in  $q$  space correspond to one point in real space. Such cases must be treated specially.

The equations for the other components of the electric and magnetic fields are obtained by cyclically permuting the integer subscripts and the corresponding coordinates  $\alpha$ ,  $\beta$ , and  $\gamma$ .

#### Description of Charged-Particle Motion by Currents

In the numerical solution of Maxwell's equations, currents are evaluated at discrete points in space and time. Particles, representing

electrons, move in a generalized coordinate system in time. An interpolation scheme must be constructed to translate the continuous motion of the particles into a set of discrete currents. The scheme chosen is such that the residual charge, as calculated from the time integral of the divergence of the current, is zero after a particle has passed into and then out of a region. (This does not hold for boundary zones since currents outside the region of interest are not considered.)

In the present zoning, currents are evaluated at zone centers in their own direction and zone boundaries in perpendicular directions. The current is time-centered. Accordingly, as forced by the continuity equation, the charge densities are at zone boundaries in space and time.

The present objective is, then, to take a particle from point

$$(q_1^a, q_2^a, q_3^a, t^a)$$

to the point

$$(q_1^b, q_2^b, q_3^b, t^b)$$

where  $t^b = t^a + \Delta t$ . That is, the currents representing such a translation must be generated.

Since the grid spacing is uniform in the  $q$ 's, linear interpolation can be performed in the transverse coordinates. This can be seen from the formulation

$$J_1(i+1/2, j, k, t^a + \frac{\Delta t}{2}) = Q_p \left[ \frac{q_1^b - q_1^a}{\Delta t} Q_1(i+1/2, j, k) \right] \\ \left[ Q_1(i+1/2, j, k) \Delta q_1 Q_2(i+1/2, j, k) \Delta q_2 Q_3(i+1/2, j, k) \Delta q_3 \right] \\ \int_{t_1}^{t_2} \left[ 1 - \left| \frac{q_2^a - q_2(j) + (q_2^b - q_2^a)(t - t^a)/\Delta t}{\Delta q_2} \right| \right] \\ \left[ 1 - \left| \frac{q_3^a - q_3(k) + (q_3^b - q_3^a)(t - t^a)/\Delta t}{\Delta q_3} \right| \right] \frac{dt}{\Delta t}$$

for point  $(q_1, q_2, q_3) = [(i+1/2)\Delta q_1, j\Delta q_2, k\Delta q_3]$ , particle of charge  $Q_p$ . Here,  $J_1$  is the current in the  $q_1$  direction.

The first bracket contains the real-space particle velocity in the  $q_1$  direction. The second bracket contains the real-space volume element. The integral represents the time-average fractional distance from the point of interest in the transverse directions. It can be seen that the particle is treated as a volume element in  $q$  space of dimensions  $\Delta q_1, \Delta q_2, \Delta q_3$ , and the integral represents the transverse area overlapping the zone of interest.

The time limits are such that they are within the range of interest  $t^b, t^a$ , and the particle is within one zone of the point of interest in its linear traversal:

$$q_1 = \left[ q_1^a + (q_1^b - q_1^a) \frac{(t - t^a)}{\Delta t} \right]$$

$$q_2 = \dots$$

$$q_3 = \dots$$

from point a to point b.

In practice, a particle is tracked from point a to point b in intervals of zone crossings so that the appropriate values of  $i, j$ , and  $k$  are easily established. The treatment for  $J_2$  and  $J_3$  is related to that of  $J_1$  by the same symmetry as mentioned in the discussion of the field calculation.

#### Restriction to Two-Dimensional Spherical Coordinates

Here the application to the special case, where the coordinates are radius  $r$  and polar angle  $\theta$ , is considered. Azimuthal velocities of electrons are not considered. This simplifying assumption has been checked in cylindrical geometry using the DYNACYL code on an evacuated cylinder with differences in the electric field near the cylinder axis of around 50%. There should be even less effect in the spherical case because the shape of the emitting surface causes less charge to be directed toward the axis of the problem.

To have the capability of varying the zone spacing in the  $r$  coordinate, the generalized coordinate  $q_1$  is related to  $r$  by

$$r = f(q_1) ,$$

and the other coordinates are

$$\theta = q_2 ,$$

$$\phi = q_3 .$$

The restriction to two dimensions gives the line element as

$$Q_3 \Delta q_3 = 2\pi r \sin \theta .$$

In the other direction, the line element is

$$Q_1 \Delta q_1 = f\left(q_1 + \frac{\Delta q_1}{2}\right) - f\left(q_1 - \frac{\Delta q_1}{2}\right) .$$

In the  $\theta$  direction, the line element is

$$Q_2 \Delta q_2 = f(q_1) .$$

For the particular case where  $\theta = 0$ , we take  $\theta = \frac{\Delta \theta}{2}$  .

The particle motion is calculated in this coordinate scheme using the relativistic generalization of Newton's law:

$$\vec{F} = \frac{d\vec{p}}{dt}$$

where  $\vec{p}$  is the particle momentum.

$$\vec{p} = \gamma m \vec{v} ,$$

$$\gamma = \frac{1}{\sqrt{1 - \left(\frac{v}{c}\right)^2}}$$

In spherical coordinates with azimuthal symmetry, the force equations become

$$qE_r = m\dot{Y}_r - \frac{Y_\theta^2}{r} m$$

and

$$qE_\theta = m\dot{Y}_\theta + \frac{mY_r Y_\theta}{r} ,$$

where

$$Y_r, Y_\theta = \gamma v_r, \gamma v_\theta, \text{ respectively ,}$$

$q$  = particle charge,

$m$  = particle mass

$r$  = particle radial position,

$v_r, v_\theta$  = particle velocities in  $r$  and  $\theta$  directions, respectively.

Making the substitution  $\vec{r} = \gamma \vec{v}$  and integrating over one time step, assuming fields are constant over the step, results in

$$Y_r = Y_{r_0} + \frac{qE_r}{m} \Delta t + \frac{1}{2} \frac{Y_{\theta_0}^2 \Delta t}{r_0}$$

and

$$Y_\theta = Y_{\theta_0} + \frac{qE_\theta}{m} \Delta t - \frac{1}{2} \frac{Y_{r_0} Y_{\theta_0} \Delta t}{r_0},$$

where the subscript "0" indicates the value of the quantity at the earlier time.  $v_r$  and  $v_\theta$  are obtained from

$$v_r = Y_r / \gamma$$

and

$$v_\theta = Y_\theta / \gamma,$$

and are used to calculate the new particle position

$$r = r_0 + \frac{1}{2} (v_{r_0} + v_r) \Delta t,$$

$$\theta = \theta_0 + \frac{1}{2} (v_{\theta_0} + v_\theta) \Delta t / \bar{r},$$

where

$$\bar{r} = (r_0 + r) / 2.$$

This completes the mathematical description of the DYNASPHERE code.

## APPENDIX C

### UPPER LIMIT FOR SCEMP-INDUCED SURFACE CURRENT ON A SPHERE, IN TERMS OF THE EMISSION CURRENT, FOR LONG-PULSE-WIDTH EXCITATION

The surface current on a sphere is related to the sheet current  $K$  amp/m, which flows on the sphere surface. Application of the continuity equation to an element of surface area yields

$$\frac{\partial \sigma}{\partial t} + \nabla \cdot \vec{K} = J_{em} , \quad (1)$$

where  $\sigma$  is the surface charge per unit area,  $K$  is the sheet current (in amp/m), and  $J_{em}$  is the emission current density (in amp/m<sup>2</sup>).

Suppose that the emission current is varying slowly, such that significant variations in its amplitude occur slowly in relation to the time required for light to travel around the sphere. In this case,  $\sigma$  will be nearly uniform and equal to the net charge on the sphere divided by the sphere surface area ( $4\pi R^2$ ). The sheet current  $K$  will be a function of position on the sphere, but this spatial dependence will be nearly invariant in time for a slowly changing emission current. For these conditions, Eq. 1 can be simply integrated.

We define the surface current  $K$  about a perimeter  $2\pi R \sin \theta$ , as shown in Figure C-1. Since  $K(\theta)$  is constant about this perimeter,

$$I_s(\theta) = 2\pi R \sin \theta K(\theta) . \quad (2)$$

Integrating Eq. 1 over the sphere surface between  $\theta = 0$  and  $\theta = \theta_0$ , one easily finds

$$2\pi R^2 (1 - \cos \theta_0) \frac{\dot{Q}}{4\pi R^2} + K(\theta) 2\pi R \sin \theta = I_{em}(\theta_0) , \quad (3)$$

where  $\dot{Q}$  is equal to the total emission current and  $I_{em}(\theta_0)$  is the integral of the emission current density between  $\theta = 0$  and  $\theta = \theta_0$ . Therefore, using Eq. 2, Eq. 3 becomes

$$I_s(\theta_0) = I_{em}(\theta_0) \left[ \frac{1}{2} (1 + \cos \theta_0) \right] . \quad (4)$$

Note that  $I_s$  approaches zero for  $\theta_0 = 0$  and for  $\theta_0 = 180^\circ$ , as required by symmetry.

The relations of Eq. 4 may be slowly varying (overall) in time, but for the quasi-static conditions assumed, Eq. 4 holds during any short time interval.

Any spatial function may be postulated for the emission function  $I_{em}(\theta)$ . If  $\theta_0$  is large enough to include the entire photo-emitting area,

$$I_s(\theta_0) = \frac{1}{2} I_{em} (1 + \cos \theta_0) \quad (5)$$

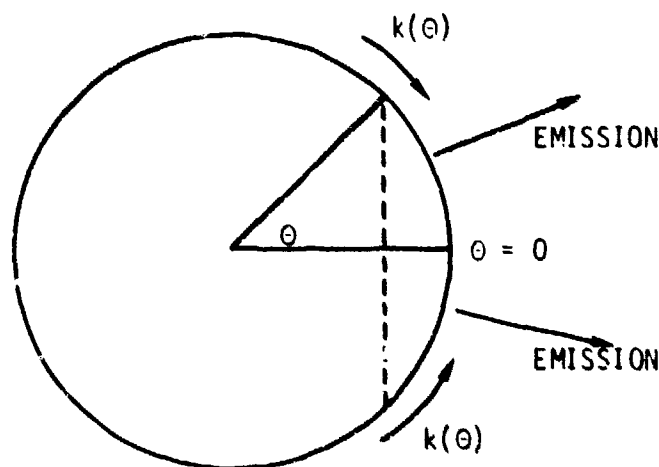
For half-sphere emission, Eq. 5 holds for  $\theta_0 \geq 90^\circ$ .

For uniform emission [ $I_{em}(\theta) = \text{const}$ ], the maximum surface current occurs at  $\theta = 90^\circ$ . For a cosine spatial distribution of the emission over a half-sphere, the maximum surface current occurs at a slightly smaller angle. For emission over less than a half-sphere surface, the maximum surface occurs near the edge of the emission area, and can approach the value of the emission current for the case of emission from a small spot near  $\theta = 0$ .

Returning to the case of half-sphere emission, with a uniform spatial distribution of the emission, it is simple to show, from Eq. 4, that

$$I_s(\theta_0) \leq \frac{1}{2} I_{em}$$

and that the peak value occurs at  $\theta = 90^\circ$ .



$$I_s(\theta) = k(\theta) 2\pi R \sin \theta$$

RT-09936

Figure C-1. Schematic illustration for definition of surface current in amperes

## APPENDIX D

### DESCRIPTION OF THE PHYSICS AND MODELING USED IN THE CALCULATION OF THE ELECTRIC AND MAGNETIC FIELDS IN THE DYNACYL COMPUTER CODE

Passage of photon-induced electrons through a gas generates electromagnetic fields, ionizes the gas, and (through the action of the fields) causes currents to flow in this partially ionized gas. The method of calculating these fields and currents is described here, assuming that the motion of the photon-generated electrons (referred to as primary electrons), as well as the ionization rate due to these electrons, is known. Of course, the treatment is equally valid if electrons are injected directly into the region of interest, in which case these injected electrons are called primary electrons.

The two aspects of the problem considered here are the generation of the fields, and the generation and behavior of the ionized gas. The fields are calculated for a cylindrically symmetric region enclosed in a perfectly conducting can. The laws governing the generation of the fields are Maxwell's equations. Motion of the primary electrons ionizes the background gas by generating electron ion-pairs. The latter electrons are referred to as secondary electrons. The motion of the secondary electrons can cause further ionization. The motion of the secondary electrons is described by an empirical drift velocity and the rate of ionization by these electrons is also empirical.

Maxwell's equations are solved in cylindrical coordinates. We assume rotational symmetry about the cylinder axis. The rotational symmetry is tantamount to saying that all derivatives with respect to azimuthal angle are zero. However, this still leaves the possibility

of currents in the azimuthal direction (toroidal currents). The assumption that there is no preferred direction of rotation eliminates this possibility. The form of the reduced equations is

$$\frac{\partial \epsilon_0 E_r}{\partial t} = -\frac{\partial H_\phi}{\partial z} - J_r,$$

$$\frac{\partial \epsilon_0 E_z}{\partial t} = \frac{1}{r} \frac{\partial (r H_\phi)}{\partial r} - J_z,$$

and

$$\frac{\partial \mu_0 H_\phi}{\partial t} = \frac{\partial E_z}{\partial r} - \frac{\partial E_r}{\partial z}.$$

These are the equations to be solved for the radial and axial components of the electric field ( $E_r$  and  $E_z$ ) and the azimuthal magnetic field ( $H_\phi$ ) written in MKS units. The medium in which the fields are generated is such that the medium has the same permittivity and permeability as a vacuum. The region of interest is surrounded by a perfectly conducting can. It is assumed that all fields are initially zero, so that the three equations above imply the divergence equations

$$\nabla \cdot \epsilon_0 \mathbf{E} = \rho$$

and

$$\nabla \cdot \mu_0 \mathbf{H} = 0$$

if the charge density,  $\rho$ , is determined by

$$\frac{\partial \rho}{\partial t} = -\frac{1}{r} \frac{\partial (r J_r)}{\partial r} - \frac{\partial J_z}{\partial z}.$$

From the form of the equations, it is clear that they represent the time evolution of the fields driven by the current. Thus, it is the current which must be specified to determine the fields. The current is due to the motion of the electrons; ions are considered to be stationary on time scales of interest here. Those electrons which are moving inertially are classified

as primary electrons and those whose motion is better described as drifting through the background gas are classified as secondary electrons.

The partially ionized background gas (air) is treated as a conductor. The conductivity is equal to the current density divided by the electric field, here considered a scalar. Since the current density is the charge on an electron multiplied by the product of the electron density and the electron drift velocity, the latter two quantities must be known.

The secondary electron density must be calculated by integrating in time the continuity equation

$$\frac{\partial N_e}{\partial t} + \nabla \cdot N_e v = S,$$

where  $N_e$  is the secondary electron density,  $v$  is the electron velocity, and  $S$  is a source term (there is no sink for the electrons considered here).

The source term has two contributions. The first is the ionization rate due to the primary electrons which is calculated while integrating the equations of motion of the primary electrons. The second contribution is due to the ionization by the secondaries themselves. For the rate coefficient for this last process, we approximate the experimental results of Reference 1 by

$$\text{Rate for ionization by secondaries} = \frac{1.62 \times 10^{-13} \text{ m}^3/\text{sec}}{\left[ 3.58 \left( 10^{17} E/N \right) + \exp \left( \frac{0.8}{\sqrt{10^{17} E/N}} \right) \right]},$$

where  $E$  is the magnitude of the electric field and  $N$  is the neutral number density in MKS units.

Although the results are for the hydrogen molecule, in the region of interest there should not be considerable difference between hydrogen molecules and nitrogen molecules, the prime constituent of air. For low  $E/N$  ratios, the approximation is somewhat low compared to the experimental results for nitrogen molecules given in Reference 2.

The experimental data for the drift velocity are presented in Reference 2, and approximated by the expression

$$\text{Drift velocity} = \frac{1.2 \times 10^{26} (E/N)}{\left\{ 1 + 8 \times 10^5 (E/N)^2 \exp \left[ \frac{-1.75 \times 10^{-11}}{\sqrt{E/N}} \right] \right\}} \quad (\text{m/sec})$$

This is the last bit of information needed to describe the background gas. The conductivity,  $\sigma$ , is thus determined.

The motion of the primary electrons is treated separately from the pressure effects and Maxwell's equations. This separate treatment provides both the primary current,  $J_p$ , and the rate at which the primary electrons are ionizing the gas to provide the secondary electrons. The primary electrons are considered as high energy (greater than 10 rydbergs) and, thus, the Bethe form of the energy loss of a particle can be used (References 3 and 4) to derive the ionization cross section if one assumes 3 rydbergs are lost per ionization. The cross section for nitrogen molecule is

$$\sigma_{\text{ionization}} = \frac{16\pi}{3\beta^2} \left( \frac{\hbar}{mc} \right)^2 Z^2 \ln \left( \frac{4\beta^2}{Z\alpha^2} \right),$$

where  $Z$  is the atomic number, taken to be 7 for air,  $\hbar/mc$  is the Compton wavelength (divided by  $2\pi$ ),  $\alpha$  is the fine structure constant, and  $\beta$  is the electron velocity divided by the speed of light. The expression is non-relativistic. Of course, the above cross section can be used to calculate the rate of slowing of the primary electrons.

The total current is then

$$J = J_p + nE.$$

This fully determines the solution and it remains to describe the treatment of the numerical procedure and the boundary conditions.

The centering in time and space is summarized below.

	Coordinate		
	z	r	t
$H_\phi$	b	c	b
$E_r$	c	c	c
$E_z$	b	b	c
$J_r$	c	c	b
$J_z$	b	b	b
$\rho$	c	c	c

The term b indicates evaluation at a boundary and c indicates evaluation at a center in the appropriate coordinate. This centering scheme is somewhat unfortunate in that it lacks symmetry in the coordinates and causes undue difficulty in the boundary conditions. However, these difficulties have been overcome. Actually, the above centering is not precisely true for the current since the conduction current is calculated using the new value of the electric field. This implicit scheme insures numerical stability.

For a perfectly conducting can, the boundary conditions require that the electric fields are normal to the can and the magnetic field is parallel to the can at the boundaries. The electric field in the z direction is thus zero at the radius of the can. However, due to the centering used here, the radial electric field is not evaluated on the top and bottom of the can, but is evaluated half a zone inside the can. Thus, a field equal and opposite is assumed to exist half a zone outside the can, and this is used to calculate the time derivative of the magnetic field at the ends of the can. The fact that  $H_\phi$  is the only nonzero magnetic field automatically fulfills the boundary condition on the magnetic field.

A further difficulty occurs at the axis where the radius is zero. To evaluate the curl of the magnetic field there, resort must be made to

the definition of the curl which is the line integral around the boundary of the surface divided by the area of the surface. This provides the necessary quantity.

Surface currents and charges are secondary quantities in that they are derived from other fields and currents. Surface currents are calculated by requiring them to be such as to make the magnetic fields zero outside the can.

This completes the summary of the treatment of the background gas for pressure effects and the calculation of the electromagnetic fields. The numerical treatment is straightforward and stable as long as the time step is chosen so that light cannot travel across more than half a zone in one time step.

#### REFERENCES

1. Buffa, A., Malesani, G., and Nalesso, G.F., "Measurement of Ionization Growth Rates in  $H_2$  at High E/p," Phys. Rev. A 3, 955, 1971.
2. Engelhardt, A.G. and Phelps, A.V., and Risk, C.G., "Determination of Momentum Transfer and inelastic Collision Cross Sections for Electrons in Nitrogen Using Transport Coefficients," Phys. Rev. 135, A1566, 1964.
3. Bethe, H.A., Ann. Phys. (Leipzig), 5, 325, 1930.
4. Dalgarno, A., Atomic and Molecular Processes, ed. Bates, D.R., (New York: Academic Press), 1962.

APPENDIX E  
DESCRIPTION OF PHYSICS AND MODELING USED IN FIELDS  
AND CURRENTS IN THE TSPHERE COMPUTER CODE

This appendix describes the physics and modeling employed in the TSPHERE computer code to obtain charge distributions, electric fields, and surface currents. Charge distributions are obtained by following individual "particles" of charge which were emitted by the inner sphere. Electric fields are calculated from the charge distribution employing a Green's function which is integrated over the distribution each time step. Surface currents are obtained from the electric field at the inner sphere boundary employing the continuity equation which relates the spatial gradient of the surface current to the time rate of change of the normal electric field at the surface. Each of these methods is described in detail in the following.

The charge density is obtained in TSPHERE by following individual particles of charge. These particles are acted on by the electric fields through the appropriate force equations. Their positions are updated each time step. The particles are then collected into the different spatial cells to obtain the spatial distribution of the charge density. The calculation is self-consistent in that the particles move consistently in fields which were calculated from the charge distribution of the previous time step.

Relativistic effects are included in the particle position updating scheme used in TSPHERE. The equations are obtained by integrating the equations

$$\vec{F} = \frac{d \vec{p}}{dt}$$

where  $\vec{p}$  is the particle momentum.

$$\vec{p} = \gamma m \vec{v}$$

$$\gamma = \frac{1}{\sqrt{1 - \left(\frac{v}{c}\right)^2}}$$

In spherical coordinates with azimuthal symmetry, the force equations become

$$qE_r = m \dot{v}_r - \frac{v_\theta^2}{r} m$$

and

$$qE_\theta = m \dot{v}_\theta + \frac{mv_r v_\theta}{r}$$

where

$q$  = particle charge ,

$m$  = particle mass,

$r$  = particle radial position,

$v_r, v_\theta$  = particle velocities in  $r$  and  $\theta$  directions, respectively.

Making the substitution  $\vec{Y} = \gamma \vec{v}$  and integrating over one time step, assuming fields are constant over the step, results in

$$Y_r = Y_{r0} + \frac{qE_r}{m} \Delta t + \frac{1}{2} \frac{Y_{\theta0}^2 \Delta t}{r_0}$$

and

$$Y_\theta = Y_{\theta0} + \frac{qE_\theta}{m} \Delta t - \frac{1}{2} \frac{Y_{r0} Y_{\theta0} \Delta t}{r_0} ,$$

where the subscript "0" indicates the value of the quantity at the earlier time.  $v_r$  and  $v_\theta$  are obtained from

$$v_r = Y_r / \gamma$$

and

$$v_\theta = Y_\theta / \gamma ,$$

and are used to calculate the new particle position

$$r = r_0 + \frac{1}{2} (v_{r_0} + v_r) \Delta t ,$$

$$\theta = \theta_0 + \frac{1}{2} (v_{\theta_0} + v_\theta) \Delta t / \bar{r} ,$$

where

$$\bar{r} = (r_0 + r)/2 .$$

Electric fields are obtained in TSPHERE by solving Poisson's equation each time step:

$$\nabla^2 \phi = - \rho / \epsilon_0 \quad (\text{mks units}) \quad (\text{E.1})$$

where  $\phi$  = electric potential

$\rho$  = charge density .

The Green's function technique is used for the solution. The space between the spheres is broken into radial and angular zones. Each resulting cell is actually a donut-like shape when it is rotated about the axis of symmetry.  $\phi$  is obtained analytically from Eq. E.1 for individual rings of infinitesimal thickness at the locations of every zone in the mesh by solving the equation

$$\nabla^2 \phi = - \delta(r - c) \delta(\theta - \alpha) . \quad (\text{E.2})$$

The terms  $r, \theta$  is the field point and  $c, \alpha$  is the source point.

The solution to Eq. E.2 is in terms of an infinite series. The series is differentiated in each direction term by term to obtain expressions for the electric fields. The resulting expressions are:

$$G_{r_{ijkl}} = \frac{1}{4\pi\epsilon_0} \sum_{n=1}^{\infty} \left\{ \frac{\left[ nr_i^{n-1} + (n+1) \frac{a^{2n+1}}{r_i^{n+2}} \right]}{\left[ 1 - \left( \frac{a}{b} \right)^{2n+1} \right]} \left( \frac{1}{c_k^{n+1}} - \frac{c_k^n}{b^{2n+1}} \right) \right. \\ \left. \times P_n(\cos \theta_j) P_n(\cos \alpha_\ell) \right\}$$

$$G_{\theta_{ijkl}} = \frac{1}{4\pi\epsilon_0} \sum_{n=1}^{\infty} \left( \frac{r_i^n - \frac{a^{2n+1}}{r_i^{n+1}}}{\left[ 1 - \left( \frac{a}{b} \right)^{2n+1} \right]} \right) \left( \frac{1}{c_k^{n+1}} - \frac{c_k^n}{b^{2n+1}} \right) \\ \times P_n(\cos \alpha_\ell) P'_n(\cos \theta_j)$$

In the above expressions, the following definitions apply.

$G_{r_{ijkl}}, G_{\theta_{ijkl}}$	=	Green's functions relating source points $c_k, \alpha_\ell$ , to field points $r_i, \theta_j$ , for radial and electric fields, respectively angular
$r_i, \theta_j$	=	field points
$c_k, \alpha_\ell$	=	source points
$a, b$	=	inner and outer sphere radii
$P_n$	=	Legendre polynomial of order $n$

These expressions are then integrated term by term over each zone volume to obtain Green's functions consistent with our particle-in-cell method for obtaining the charge distribution. The electric fields are then obtained from the Green's functions by

$$E_{rij} = \sum_{k,l} G_{rijkl} \rho_{kl} - \frac{Q_s}{4\pi\epsilon_0 r_i^2}$$

$$E_{\theta ij} = \sum_{k,l} G_{\theta i j k l} \rho_{kl}$$

where

$E_{rij}, E_{\theta ij}$  = radial and axial electric fields at field point  $r_i, \theta_j$

$\rho_{kl}$  = charge density at source point  $c_k, a_l$

$Q_s$  = net charge on inner sphere

The surface current on the inner sphere is obtained from the net current and normal electric field there. It is obtained by integrating Ampere's law:

$$\nabla \times H = J + \epsilon_0 \frac{\partial E}{\partial t}$$

both in space and time. Remembering that the tangential component of  $H$  at the boundary is equal to the skin current there (in units of current per unit length), we obtain:

$$I = 2\pi R^2 \left[ \int_0^\theta J \sin\theta d\theta + \epsilon_0 \int_0^\theta \frac{\partial E_r}{\partial t} \sin\theta d\theta \right]$$

Refer to Figure 3-3 in Section 3 for definitions of the coordinates.

$J$  is the net current at the position  $\theta$  on the inner sphere  $E_r$  is the normal electric field there.  $I$  is the surface current at  $\theta$  in amps.

In the code, the quantities for the net current  $J$  and the time derivative of the normal electric field  $\frac{\partial E_r}{\partial t}$  are averaged over a number of time steps in order to produce smoothly varying surface currents. This

step is necessary at higher fluences because of the particle nature of the code. In a given time step, many particles might pass through a small area about the position,  $\theta$ . The next step there might be very few. The result is that the quantity  $J$  can oscillate in time. At high fluences, the two terms in the integral for  $I$  are large and their sum small so large oscillations in either term can render the sum completely useless unless appropriate steps such as just described are taken.